AALBORG UNVERSITY
Department of Chemistry and Bioscience

MASTER THESIS (60 ECTS)

SELECTED PROCESS SAFETY SYSTEMS ANALYSED USING DYNAMIC SIMULATIONS

A study of the Flare and the High Integrity Pressure Protection Systems

Master in Oil and Gas Technology

Ana Xiao Outomuro Somozas

June 2020

(This page is left intentionally blank)

Abstract

The relevancy of dynamic simulations is investigated through the modelling of two process safety systems in Aspen HYSYS Dynamics V9. On the one hand, the design of flare systems is conventionally made according to steady-state simulations, which even though is conservative, in turn leads to oversizing of the system beyond feasibility. API Standard 521 suggests that an improvement in the design can be achieved by using dynamic models to account the dynamic nature of the operation. The emergency depressurization of the flare system of three different facilities (in terms of system size, flare design rate, network pipe dimensions, and total hold-up volume) have been modelled, and results have been benchmarked against the steady-state design. It is found that the larger the flare system, the larger the hidden potential for debottlenecking, i.e. larger difference between the steady-state design rate and the dynamic peak flare rate. On the other hand, the process response time available for the valve closure of the High Integrity Pressure Protection System (HIPPS) is analysed, and the relation between robustness of the model and sensitiveness of the results is investigated. It is observed that a more conservative prediction can be achieved when using the pipe flow correlation Tulsa Unified Model.

Keywords: dynamic simulation, Aspen HYSYS, flare network, emergency depressurization, debottlenecking, HIPPS, response time, safety

Preface

This Master Thesis concludes the education in Oil and Gas Technology at Aalborg University Esbjerg. The work was carried out during the academic year of September 2019 / June 2020, and was conducted in collaboration with Rambøll Oil & Gas.

I would like to thank Marco Maschietti and Rudi P. Nielsen, my supervisors, who have supported me through this year. I am really grateful for their time and feedback.

I would also like to express my most sincere gratitude to Anders Andreasen, Technical Manager at the Process and Technical Safety Department of Rambøll Oil & Gas, for sharing his expertise with me, and for his strong support and guidance during the course of the thesis. Also, I am grateful for the opportunity I was given to conduct the second part of the thesis work at the Rambøll office, and I would like to thank all the people at his department for their kindness and for making me feel so comfortable.

Finally, I want to thank my family for their continuous support and love. Also, to Cezar, for making Denmark a bit sunnier and to my little sister, Eva, for inspiring me with her dedication and hard-work. Special thanks to my mother, who always had faith in me, and has always taught me to put the heart in all the things I do. Without her love, strength, and effort, I would have never gotten to this point... And as she has always told me *'Hace más el que quiere que el que puede'*.

Ana Xiao Outomuro Somozas in Esbjerg, Denmark, as of June 2020

Contents

Abstract **ii**

Preface **iii**

List of Figures **vii**

List of Tables **ix**

List of Abbreviations **x**

1 Introduction **1**
1.1 The Offshore Oil and Gas Industry 1
1.2 Relevancy of dynamic simulators 3
1.3 Initiating problem 4

2 Theoretical Background **5**
2.1 Process Safety Philosophy 5
2.2 Overpressure event 6
2.2.1 Detectable abnormal condition and consequences 6
2.2.2 Causes of overpressure 7
2.2.3 API Recommended Practice 7
2.3 Flare system 8
2.3.1 Depressurization and blowdown operations 9
2.3.2 Current design of flare systems 10
2.4 High Integrity Pressure Protection System 12
2.4.1 Applications of HIPPS 13
2.4.2 Benefits of HIPPS 13
2.4.3 HIPPS versus ESDV 14
2.4.4 Dynamic simulations of HIPPS 15
2.5 Thermodynamic modelling 15
2.5.1 Type of reservoir fluids 16
2.5.2 Equation of State model 17

3 Problem Formulation **19**
3.1 Objectives of Part I 19
3.2 Objectives of Part II 19
3.3 Problem Delimitation 20

4 Methodology Part I: The flare system **21**
4.1 Aspen HYSYS V9 21
4.1.1 Fluid characterization 21
4.1.2 Modelling the flare network 22
4.1.3 Plant emergency depressurization 23
4.1.4 Limitations on the model 23
4.1.5 Boundary stream specifications 24
4.2 Simulated Case Studies (Part I) 25
4.2.1 Facility A 25
4.2.2 Facility B 25
4.2.3 Facility C 27

5 Methodology Part II: The High Integrity Pressure Protection System **32**
5.1 Description of the HIPPS layout 32
5.2 Aspen HYSYS V9 33
5.2.1 Fluid characterization 33
5.2.2 HIPPS Flowsheet 34
5.2.3 Overpressure scenario 36
5.2.4 Process Safety Time 36
5.2.5 ESD and HIPPS settings 38
5.2.6 Boundary stream conditions 38
5.2.7 Pipe flow correlations 38
5.3 Simulated Case Studies (Part II) 39
5.3.1 Evaluation of mass flow 40
5.3.2 Evaluation of the piping layout 40

6 Results and Discussion Part I: The flare system **41**
6.1 Facility A 41
6.2 Facility B 43
6.3 Facility C 44
6.4 Discussion of results 45

7 Results and Discussion Part II: The High Integrity Pressure Protection System **49**
7.1 Evaluation of mass flow 49
7.2 Evaluation of the piping layout 54
7.3 Discussion of results 54

8 Conclusions **56**

Bibliography **58**

A Appendix A: Revealing hidden debottlenecking potential in flare systems on offshore facilities using dynamic simulations – A preliminary investigation **63**

B Appendix B: Aspen HYSYS Simulation Models **64**

C Appendix C: Additional graphs to support HIPPS results **70**
C.1 150,000 kg/h 70
C.2 180,000 kg/h 71
C.3 PST calculated for different mass flows 72

List of Figures

1.1 A schematic of a typical oil and gas production facility with two-stages separation train. Adapted from [3, 5]. 2

2.1 Typical flare system layout for an offshore production facility. PCVs/spill-over valves not shown. 9
2.2 Representation of the expected flow rate results at the flare when using both steady-state and dynamic approaches. 12
2.3 Electronic safety loop of HIPPS comprising 2oo3 initiators. 13
2.4 Block diagram comprising the sequence of events occurring in case of over-pressure. 14
2.5 Phase envelope of various types of reservoir fluids [59]. 16

4.1 Example of blowdown segment modelled in HYSYS, and specifications required for the model 22
4.2 Configuration of the flare system model for facility A. PSVs and PCVs sources (inactive) are not illustrated. 29
4.3 Configuration of the flare system model for facility B. PSVs and PCVs sources (inactive) are not illustrated. 30
4.4 Configuration of the flare system model for facility C. PSVs and PCVs sources (inactive) are not illustrated. 31

5.1 Typical wellhead and manifold layout on offshore production facility, including HIPPS. The Auxiliary Control Valve (XCV) is not represented. 32
5.2 Aspen HYSYS Flowsheet set-up. 35
5.3 Event Scheduler. Individual Action Specification: simulation of overpressure scenario. 37
5.4 Representation of pressure development in a pipeline over time, and calculation of Process Response Time (PST). 37

6.1 Comparison between calculated mass flow rate at the flare tip for Facility A, using steady state, dynamic simulations without dead ends, and dynamic simulations including dead ends. 41
6.2 Comparison between calculated backpressure in various places of the flare network for (A) steady-state and (B) dynamic simulations for facility A. . . . 42
6.3 Comparison between calculated mass flow rate at the flare tip for Facility B, using steady state, dynamic simulations without dead ends, and dynamic simulations including dead ends. 43

6.4 comparison between calculated backpressure in various places of the flare network for (A) steady-state and (B) dynamic simulations for facility B. . . . 44
6.5 Comparison between calculated mass flow rate at the flare tip for Facility C, using steady state, dynamic simulations without dead ends, and dynamic simulations including dead ends. 45
6.6 comparison between calculated backpressure in various places of the flare network for (A) steady-state and (B) dynamic simulations for facility C. . . . 45
6.7 The hidden potential for debottlenecking as a function of steady-state design rate. Previous studies from Andreasen [45] and Wasnik et al. [23] 47

7.1 Pressure development in the system for a well-feed of 100,000 kg/h and blockage Scenario 2, considering Case 1 pipe correlation (Beggs & Brill (1973)). 50
7.2 Comparisson of pressure development in the manifold considering well feed of 100,000 kg/h for (A) Scenario 1, (B) Scenario 2, (C) Scenario 3 and (D) Scenario 4. 51
7.3 Comparisson of pressure development in the manifold considering well feed of 200,000 kg/h for (A) Scenario 1, (B) Scenario 2, (C) Scenario 3 and (D) Scenario 4. 52

B.1 Process simulation flowsheet for the flare system of Facility A as modelled in Aspen HYSYS (dead-ends not included). 65
B.2 Process simulation flowsheet for the flare system of Facility A as modelled in Aspen HYSYS (dead-ends included). 66
B.3 Process simulation flowsheet for the flare system of Facility B as modelled in Aspen HYSYS (dead-ends not included). 67
B.4 Process simulation flowsheet for the flare system of Facility B as modelled in Aspen HYSYS (dead-ends included). 68
B.5 Process simulation flowsheet for the flare system of Facility C as modelled in Aspen HYSYS (dead-ends not included). 69

C.1 Comparison of pressure development in the manifold considering well feed of 150,000 kg/h for (A) Scenario 1, (B) Scenario 2, (C) Scenario 3 and (D) Scenario 4. 70
C.2 Comparison of pressure development in the manifold considering well feed of 180,000 kg/h for (A) Scenario 1, (B) Scenario 2, (C) Scenario 3 and (D) Scenario 4. 71
C.3 Comparison of PST for (A) Scenario 1, (B) Scenario 2, (C) Scenario 3 and (D) Scenario 4. 72

List of Tables

1.1 Examples of utility systems in an offshore oil and gas facility [3] [6]. 2
1.2 Examples of dynamic events occurring in an oil and gas facility, and how dynamic simulations can model and provide a solution. 4

4.1 Boundary stream specifications in Aspen HYSYS Dynamics 24
4.2 Summary of investigated facilities. 25
4.3 Summary of specifications for blowdown segments of Facility A. Note that the conditions are for the initial system state prior to depressurization. . . . 26
4.4 Summary of specifications for blowdown segments of Facility B. Note that the conditions are for the initial system state prior to depressurization. . . . 26
4.5 Summary of specifications for blowdown segments of Facility C. Note that the conditions are for the initial system state prior to depressurization. . . . 28

5.1 Well fluid composition of Gas Condensate. 33
5.2 Properties of the lumped fractions of the Gas Condensate mixture. 34
5.3 Dimensions of pipe segments. 35
5.4 Scenarios locations of blockages. 36

6.1 Summary of model details and modelling results for all three investigated facilities. 46

7.1 Summary of scenarios and case studies considered in the evaluation of HIPPS. 49
7.2 Comparison of PST calculated for different blockage scenarios and well-feed mass flow rates. 53
7.3 Comparison of PST calculated for different blockage scenarios and V/H ratios. 54

List of Abbreviations

API	American Petroleum Institute
BDV	Blowdown Valve
CCP	Central Processing Platform
CFD	Computacional Fluid Dynamics
CM	Cooling Medium
Cv	Valve coefficient
CVA	Choke Valve
EOS	Equation Of State
ESD	Emergency Shutdown
ESDV	Emergency Shutdown Valve
FSA	Flare System Analyser
HIPPS	High Integrity Pressure Protection System
HP	High Pressure
HTFS	Heat Transfer and Fluid Flow Service
HVAC	Heating, Ventilation, and Air Conditioning
KO	Knock-out
LP	Low Pressure
MAWP	Maximum Allowable Working Pressure
MCV	Master Control Valve
MW	Molecular Weight
NIST	National Institute of Standards and Technology
PCS	Process Control System
PCV	Pressure Control Valve
PRD	Pressure Relief Device
PRT	Process Response Time
PST	Process Safety Time
PSV	Pressure Safety Valve
PVT	Pressure Volume Temperature
SIL	Safety Integrity Level
SIS	Safety Instrumented System
SS	Steady State
VLE	Vapor Liquid Equilibrium
WCV	Wing Control Valve
WHP	Wellhead Platform
XCV	Auxiliary Control Valve

Chapter 1

Introduction

Process safety is a key aspect in the offshore oil and gas industry, where extremely flammable and high-pressure fluids are to be handled, feed conditions are unsteady, and operations can often undergo changes, perturbations, or transient conditions. The design of the process control through the application of good design principles [1] and the implementation of accurate plans of prevention and mitigation, is crucial to overcome the hazards that can jeopardize life, safety, environment, infrastructure, or economy [2].

Over the past few years, the depletion of existing mature fields and the difficulties of finding new ones are posing a challenge to the growing energy demand. In addition, reducing the environmental footprint is becoming an important concern within the oil and gas industry. Therefore, optimizing the existing processes while continuously improving in process safety is becoming of great importance.

1.1 The Offshore Oil and Gas Industry

A substantial number of operations simultaneously occur in an offshore oil and gas facility, where oil, gas, and water coming from the wells are separated and processed to meet the required product specifications for the exportation onshore. An overview of a typical oil and gas production facility is illustrated in Figure 1.1. The main processing systems are briefly explained next:

- **Wellhead.** A wellhead is a system comprising of pipework, valves and assorted adapters that provide pressure control of a production well, connecting the surface facilities to the wellbore that leads down to the reservoir [3].

- **Manifold.** A manifold is an arrangement of pipework and valves that collects the reservoir fluids coming from different wellheads into a single flowline [4], wherefrom they are delivered to the topside structure via multiphase pipeline called a riser [3].

- **Separation train.** The pressure is gradually reduced in a number of stages (High Pressure (HP) separator, Low Pressure (LP) separator, etc.) from the well-effluent conditions down to atmospheric conditions to allow the separation of the reservoir fluids into gas, oil and water [5].

- **Gas compression train.** Gas from separators is recompressed to achieve the sufficient pressure to be transported onshore [5].
- **Storage, metering and export.** Stable products that can be safely transported are storage for further exportation onshore. The produced fluids are monitored via metering stations [3].

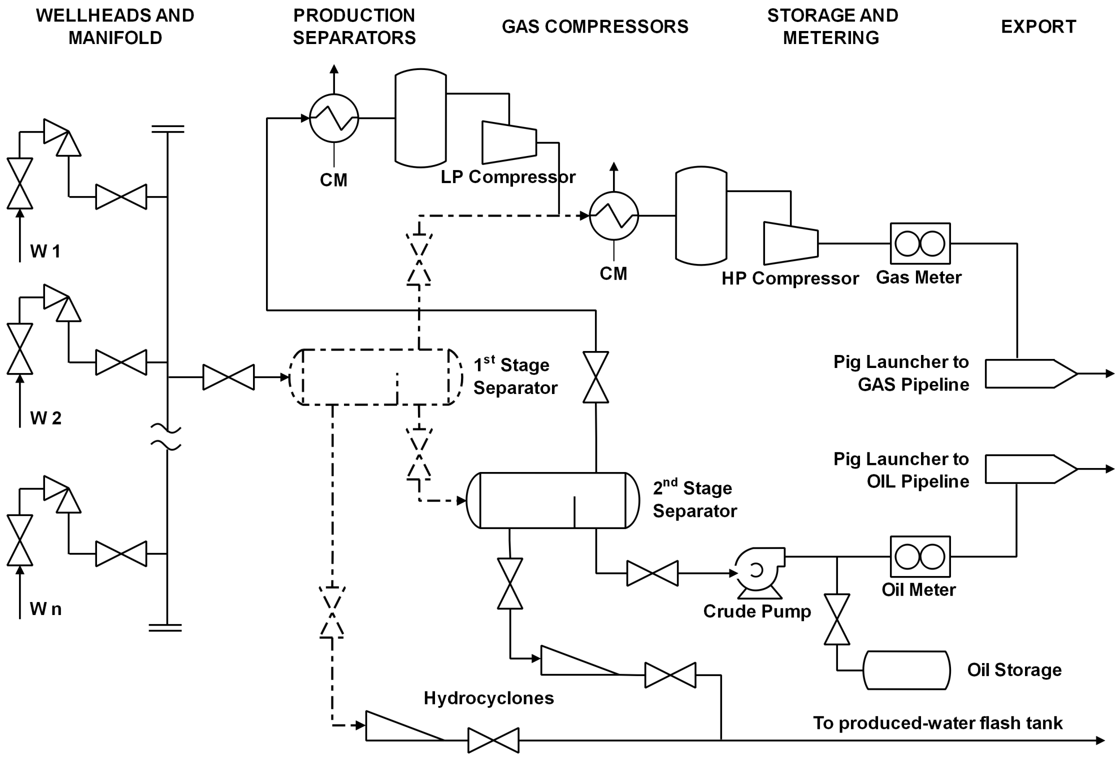

Figure 1.1: A schematic of a typical oil and gas production facility with two-stages separation train. Adapted from [3, 5].

In addition to the main hydrocarbon production processes explained above, several utility systems can be encountered in an oil and gas facility. These systems are essential to support the main process, as they involve operations related to safety and utilities supply, among others. Some examples of utility systems that can be found are listed in Table 1.1.

Table 1.1: Examples of utility systems in an offshore oil and gas facility [3] [6].

OperationsSafety	Utilities Supply	Personnel Safety	Miscellaneous
Firewater System Flare System Drain System	Instrument Air Process heating systems Cooling Medium Circuit	HVAC and Breathing Air Potable water system	Power generation Chemical Injection

1.2 Relevancy of dynamic simulators

Steady-state simulations are widely used in the modelling, design and optimization of process units within the oil and gas industry. On the contrary, dynamic simulations have been commonly applied in the context of control design analysis, being generally set aside from the plant design application due to less conservatism in the design and the level of detail and expertise that is required to run a reliable simulation. Some of the applications of dynamic simulations nowadays are:

- **Safety analysis.** The possibility of generating deviations from normal operating conditions allows the user to investigate the trajectory of the possible safety responses [7]. Therefore, it is possible to reduce the likelihood of incidents in the control or operability of the plant, or to develop new control strategies to resolve them easier, safer, or at an early stage of the operation [8].
- **Start-up and shutdown scenarios.** Verification of procedures [8].
- **Operator decision support.** The predictive capability of dynamic simulators allows the user to test a planned activity and evaluate the operational response in real time prior to implementing it on the process. This makes it possible to anticipate and counteract the occasion of an unsafe event before it is likely to happen [8]. Consequently, faster decision-making to the plant changes can be achieved, ensuring at the same time a safer operation at a lower cost [9].

From the perspective of process design, processes and systems are often exposed to transient conditions that the design using steady-state approaches does not account. Steady-state simulations represent an idealistic model in which operating conditions are stable, and the time-varying behaviour of the operations when they undergo changes, perturbations or unsteady conditions, is not taken into consideration [10]. For example, pipelines transmission systems are typically designed to withstand the most severe conditions during normal operation, based on steady-state simulations. The dimensions are sufficient when scenarios are relatively stable, but in case of excessive mass flow surges, the capability might be compromised due to dynamic effects (e.g. pressure surge, changes in volume along the pipeline, etc.) that were not considered in the steady-state design [11]. Therefore, the inherently dynamic nature of process safety events reveals the close connection between dynamic simulations and process design, thus meaning that a more realistic and improved design can be achieved [8].

Several software are available nowadays in the market, for example, Aspen HYSYS (AspenTech), UniSim (Honeywell), OLGA Dynamic Multiphase Flow Simulator (Schlumberger) or gPROMS (Process Systems Enterprise Ltd.), among others. A list comprising different examples of how dynamic simulations can be applied and what type of solution they can provide to different hazardous events is given in Table 1.2.

Table 1.2: Examples of dynamic events occurring in an oil and gas facility, and how dynamic simulations can model and provide a solution.

System	Hazardous Event	Dynamic concern	Solutions given by dynamic simulators	Ref.
Wellheads	Rapid shut-in in water injectors	Waterhammer	Water hammer sensitivity analysis considering different parameters	[12]
Manifold	Multiphase flow in the pipeline	Severe slugging	Analysis of pressure development to predict if control objectives can be achieved	[13]
	Sudden closure of valve upstream/ downstream	Overpressure	Investigating acceptable valve closure times to avoid over-pressure in piping/pipelines / Time for valve closure in High Integrity Pressure Protection Systems (HIPPS)	[14] [15] [7]
Separators	Overflow	Level Control	Study of the frequency of the hazardous event considering periodically inspection	[16]
	Vessels under Fire	Increase in pressure of internal fluids due to heat flowing	Analysis of pressure safety valves (PSV) for fire protection, for example validation of adequate PSV sizing	[17] [18] [19]
Compressors	Unscheduled discharg valve closure	Back pressure / Pressure surge	Analysis of gas dynamic flow to evaluate the compressor surge protection	[20]
Flare System	Event that results in overpressure scenario	Blowdown / Depressurization	Evaluation of the performance of the system during an emergency relief scenario / Debottlenecking of existing flare system	[21] [22] [23]
Firewater System	Deluge Start-up	Pressure surge due to air release and/or waterhammer	Improving sizing of air valve	[24]

1.3 Initiating problem

The use of steady-state simulations is universally accepted as they provide the required conservatism in the design, but this in turn has led to oversizing systems beyond feasibility or failing to understand the transient behaviour of the system when hazardous events occur. Accuracy in the design can be improved by accounting for the dynamic nature of the processes. This project aims to demonstrate the validity of the following statement:

'Dynamic simulations can revise the process design approach that has been traditionally made in accordance to steady-state simulations, respecting safety and ensuring an adequate level of conservatism.'

The author intends to assess the critical link that connects process design and process safety, and how dynamic simulations can enable this connection. Additionally, the level of detail and the robustness required in the models is also investigated.

Chapter 2

Theoretical Background

High-risk operations take place in offshore oil and gas platforms, where fire, explosion, and release of media are the three main events triggering disasters [25]. The correct design of the different protective devices and process safety systems is crucial to ensure safe operation in the facility [7]. The purpose of this section is to provide a general background of the main topics and concepts that could be required for a better understanding of the project.

2.1 Process Safety Philosophy

Process safety is a key aspect of the design and operation of a process plant in all industries. Several independent and successive protection layers are installed to control, prevent, and mitigate process risks [26]. In case one layer fails to bring the system back to a safe state, the next one takes on the action. In this way, the safest performance can be ensured by avoiding the possibility of two or more of the protection layers being disabled because of the same fatality [27, 28]. Safety is given by the effectiveness of these lines of defense. Seven independent layers of protection can be identified, and they are described next:

1. **Process design.** The proper equipment is selected according to good design principles. This results in a robust system that can prevent deviations in operation conditions, minimizing the likelihood of a scenario [28].

2. **Process Control System (PCS).** Basic control system and process alarms provide the required reliability. The objective of a control system is to monitor and maintain process conditions within safe operating limits, and to detect and prevent any undesirable event, ensuring the safest operation in the process during its operational time [3, 25].

3. **Operator intervention.** Safety is extended with manual prevention layers that includes the operator supervision and intervention after process alarm.

4. **Emergency Shutdown System (ESD).** A safety instrumented system (SIS) is installed to shut off and isolate the affected equipment, preventing the fatality [26].

5. **Active Protection.** A pressure relief system (e.g. Pressure Relief Valves (PSV), flare

system, etc.) is added to mitigate and prevent the escalation of an event (i.e. minimize the impact of the event) [22, 26].

6. **Passive protection.** To mitigate the fatality, bunds, barricades or dikes are built within the facility structure to act as a physical containment [28].

7. **Plant and Community Emergency response.** This layer involves the emergency plan that needs to be applied by plant personnel if the incident has grown beyond the facility and outside assistance of community representatives is required (e.g. the fire department, the ambulance rescue team, and related emergency response personnel) [28].

Among the process hazards that can take place in an offshore production facility, the API 14C on Analysis, Design, Installation, and Testing of Safety Systems for Offshore Production Platforms [29] proposes the major hazards to be fire, explosion, and release of media. Although many sources of these hazards can be found, overpressure is the most important in terms of severity as it can lead directly to all three. As a result of its hazard potential, very effective safety measures are required to ensure a low probability of an overpressure event occurring.

2.2 Overpressure event

An overpressure event refers to any hazardous scenario that can result in pressure development in a process component above the maximum allowable working pressure (MAWP) [29]. MAWP is the maximum pressure at which one equipment or piping can operate without its integrity being jeopardized. On the other hand, the design pressure refers to the pressure at which the equipment or piping is designed as specified with the vendor. The design pressure is selected in a way that can provide a suitable margin above the most severe pressure expected during normal operation. Therefore, the design pressure can be equal to or less than MAWP, depending on equipment and piping specifications [30].

2.2.1 Detectable abnormal condition and consequences

An abnormal operating condition refers to a process variable in a process component working outside the established normal operating limits [29]. With regards to an overpressure scenario, it is the increase in pressure in the system that indicates that overpressure may occur. If a higher pressure than normal operating pressure is detected in the system, then the control system will activate to mitigate this abnormal condition. If the control system fails to protect the process equipment against overpressure, the pressure will keep building up until it exceeds MAWP. Therefrom, the strength of the system will be downrated as pressure increases beyond safe levels, and once MAWP is exceeded, the material of the equipment or piping may fracture, hence releasing media or energy. This can result in catastrophic harm to personnel and the environment, as well as facility damage and relevant economic losses [29, 31].

2.2.2 Causes of overpressure

Several events can lead to the over-pressurization of equipment and piping. Some typical scenarios can be grouped under the following categories [29, 30, 32]:

1. Inflow exceeds outflow (e.g. Blocked or restricted outlet)
2. Direct pressure input from higher-pressure sources (e.g. Backflow occurring from a downstream source operating at higher pressure than MAWP of process component)
3. Pressure Control System failure (e.g. Check valve leakage or failure)
4. Equipment failure (e.g. Transient pressure surges, such as water hammer)
5. Abnormal heat input (e.g. Excess heat input given by the heating of component contents by an external fire)

2.2.3 API Recommended Practice

The process safety philosophy is divided in independent layers of protection to avoid any unsafe situation, as described in API 14C (refer to Section 2.1) [29]. In the situation of an overpressure scenario occurring and both the PCS (Layer 2) of the plant and the operator intervention (Layer 3) are not able to bring the system back to a safe state, the ESD system (Layer 4) acts as a first protection against overpressure. The ESD system will shut off and isolate the affected unit before the MAWP of the equipment is exceed [7, 29]. A secondary protection is added in case the ESD fails or is not fast enough. This secondary barrier is provided by a Pressure Relief Device (PRD), for example, a Pressure Safety Valve (PSV) (Layer 5). The PSV will open and allow the system to discharge the excess inflow by routing it to the flare system for flaring or venting it (i.e. depressurizing the system) [7].

The correct design of depressurization systems shall be made according to API 521 Standard on Pressure-relieving and Depressuring Systems [30], whereas methods for sizing the process relief devices shall generally follow the API Standard 520 on Sizing, Selection, and Installation of Pressure-relieving Devices [33].

The use of PRDs is preferred, but there are some applications where the installation of conventional PRDs is not feasible. In such cases, API Standard 521 considers the reliance on instrumented safeguards as a last resort [30], for example, a High Integrity Pressure Protection System (HIPPS). However, the installation of HIPPS shall fulfill the proper economic/technical analysis, rigorous design that gives justifiable reliability, testing, and maintenance requirements in accordance with API Standard 521 [30]. The following reasons can be considered for when the selection of HIPPS over PRDs is preferred [34]:

1. **PRD is not practical or possible:** Installing a PRD is impractical due to large size of PRD is required.
2. **PRD is not reliable:** Installing a PRD may not be reliable in applications such as corrosive media, or fluids that tend to freeze during depressurization.

3. **PRD requires excessive cost:** The installation of a new PRD to connect a new source to the flare system can give unproportionally large investments, since the revamping of the existing flare system might be needed to match the new required capacity.

The efforts of the following sections will be focused on giving a comprehensive overview of the aforementioned protection systems (HIPPS and PRD) in the context of an overpressure event.

2.3 Flare system

The flare system is a pivotal part of the safety system of any plant, but especially in an offshore oil and gas facility, where flammable hydrocarbons and other hazardous substances are being handled. In the event of pressure development in a process component above the MAWP (i.e. overpressure), the flare system acts as a last line of defence before rupture. The flare system relieves the excessive pressure by releasing the process media to the flare network . From there, the vented fluids are collected and safely disposed by converting them in less harmful compounds (CO_2 and H_2O) through controlled open flame combustion [22, 30].

The inventory of the units to be depressurized are collected via tail pipes in a network of subheaders and headers and routed to a Knock-Out (KO) drum, wherefrom they are delivered to the flare tip via flare stack [23, 35]. PSVs, Blowdown Valves (BDVs) and Pressure Control Valves (PCVs) for Start-up and spill-over Flaring are the PRDs acting as flare sources, opening in case of overpressure, and releasing the media to the flare piping network [23]. A typical flare system layout for an offshore production facility is shown in Figure 2.1.

The main components that can be found in a flare system are described next [23, 30, 36]:

- **Pressure Relieving Devices (PRDs):** Input sources to the flare system can be derived from PRDs such as PSVs, BDVs and/or BDVs. These valves comprise the active protection, acting as barriers between the process segments/equipment containing process fluids, and the subheaders and headers connected to the flare.

- **Subheaders and headers:** Subheaders and headers are the flare piping network where all flare loads comingle, and wherefrom the relief fluids are routed to the KO drum.

- **KO drum:** The KO drum is a two-phase separator designed to separate the liquid phase from the gas stream to be flared/vented, and to provide holding capacity for the separated liquids during the governing relief events.

- **Flare stack / Flare tip:** The flare stack is the pipe connected to the flare tip, which is the place where the combustion of the relief gases takes place.

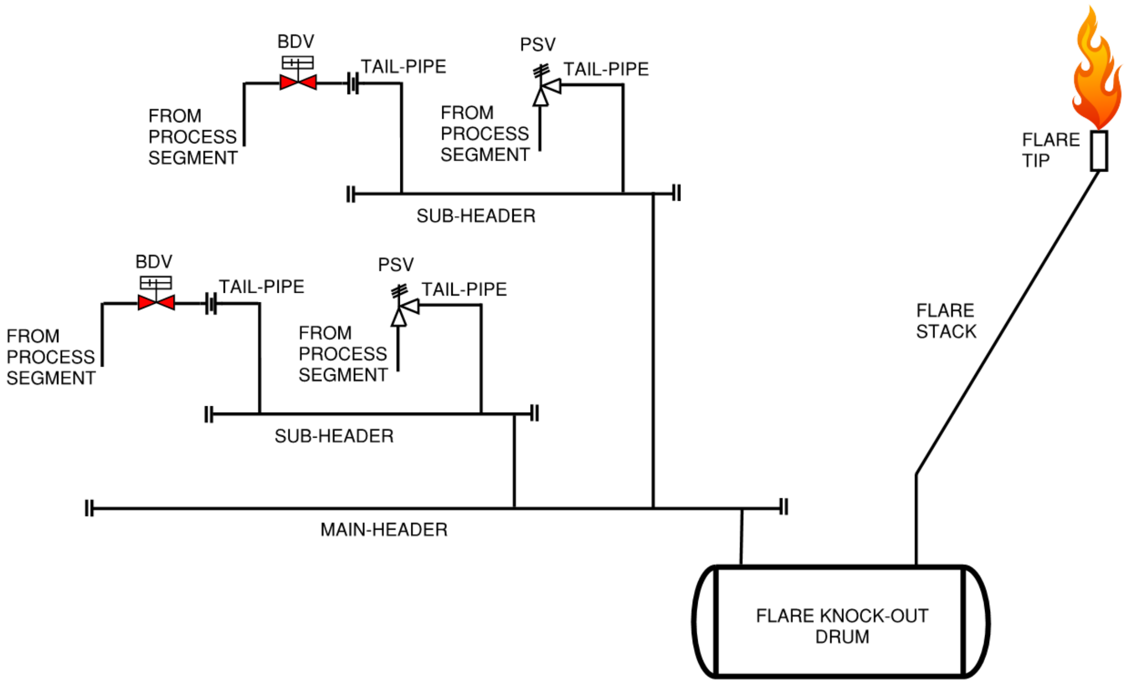

Figure 2.1: Typical flare system layout for an offshore production facility. PCVs/spill-over valves not shown.

As a summary, the main purposes of the flare system are outlined next:

1. Prevention of escalation of undesired events leading to an overpressure event (e.g. fire, outlet blockage that contributes to pressure built-up, etc.).

2. Protection of process equipment against rupture before pressure develops reaching MAWP.

3. Collection and safe disposal of hydrocarbon inventory (gases and liquids) from relief sources by flaring or venting it.

2.3.1 Depressurization and blowdown operations

Depressurization takes place when the ESD system fails to overcome the undesired events, thus leading to the possibility of pressure building up outside safety limits. Depressurization is a safety operation that aims to relieve the excess pressure of a plant or unit by relieving the inventory inside the affected process system [26, 30, 37]. In the same context, blowdown refers to the rapid depressurization of high-pressure vessels or pipework, thus considering also the removal of liquid contents inside the process equipment exposed to overpressure [37].

In the event of depressurization, the vapour phase is relieved and collected in the flare network via PRDs. The gas, which was confined in pressurized process equipment, expands while flowing through the valve without exchanging any heat with its environment. As a result, cooling over the valve occurs, and smaller amounts of condensation may form. This effect is called the Joule-Thomson effect [38]. Consequently, the process equipment may be exposed to very low temperatures. In the case the temperatures go below the ductile to brittle transition temperature of the material, the material may embrittle (loss of ductility of material), leading to brittle fracture of the equipment if they are also subjected to too high loads [30]. The material shall be selected in order to withstand the most severe temperature (lowest) that the flare system might be subjected to. The correct material selection (e.g. carbon steel, low-temperature carbon steel or stainless steel) is crucial to ensure a safe operation [39, 40]. The estimation of the lowest temperature that the equipment can undergo in the event of blowdown can be investigated using dynamic simulations.

Additionally, it shall be noted that the term 'venting' stands for the disposal of hydrocarbons and other hazardous compounds from the atmospheric vent lines directly into the atmosphere. In case of depressurization – considering sources from atmospheric vent lines and sufficient gas to run a flare – flaring shall be preferred over venting, as venting implies the release of unburned toxic gases [22, 37].

2.3.2 Current design of flare systems

Generally, the design of the flare system follows API 521 Standard recommended practice [30]. The sizing of the components has conventionally been made using steady-state simulations where the individual relieving rates from each of the PRDs sources are summed and considered to occur simultaneously, irrespective of their opening time [23]. In this way, it is guaranteed that the accumulated fluids will be discharged timely, and that the peak flare load can be safely relieved and disposed via flaring during a plant depressurization [17, 41]. Three main criteria are to be considered in the design of a flare system:

1. **Back pressure.** Back pressure is the pressure built up in the system as a result of the pressure in the discharge system [30]. The sizing of the relief discharge piping shall verify that the maximum back pressure coming from the flare can be handled.

2. **Momentum of the released fluid (ρv^2).** The momentum of the released fluid is calculated considering the fluid density (ρ) and the velocity to the power of 2 of the released fluid (v^2). This parameter considers the design load that the system can be subjected to.

3. **Mach number (Ma).** During depressurization, fluids relieved in the flare network are subjected to rapid changes in density and velocity. Therefore, they are rated as compressible fluids. The Mach number is introduced to account the compressibility effects (i.e. density changes) in the velocity of the fluid [35].

According to API Standard 521 [30], the Mach number is defined as the ratio between the fluid velocity and the sonic velocity (c), which is the velocity at which sound waves propagate through the fluid at the associated temperatures. The sonic velocity can be calculated as a relationship between the differences in pressure and density between the pipe inlet and pipe outlet [35]. The equation proposed by API Standard 521 [30] for the calculation of Mach Number is given in Equation 2.1.

$$Ma = 3.23 \cdot 10^{-5} \cdot \left(\frac{q_m}{P \cdot d^2}\right) \cdot \left(\frac{Z \cdot T}{M}\right)^{0.5} \tag{2.1}$$

Where q_m is the gas mass flow rate, P is the pipe outlet absolute pressure, d is the internal diameter of the pipe, Z is the gas compressibility factor, T is the absolute temperature, and M is the gas relative molecular mass.

According to NORSOK Standard P-002 on Process Safety Design [42], the flare lines shall be designed to keep the ρv^2 below a maximum value of 200,000 kg/ms^2. Higher values than 200,000 kg/ms^2 can lead to the risk of erosion and/or acoustic vibration problems. A maximum flowing velocity of 0.7 and 0.6 Mach Number is recommended for tail pipes and headers/subheaders, respectively.

Even though a steady-state approach is carried out to preserve the conservatism in the design, the oversizing of the flare network given by the prediction of an unrealistic peak flow rate, and the lack of prediction of the transient behaviour during depressurization, makes the use of dynamic simulations an appealing approach [22, 23, 35]. API Standard 521 states: *'Conventional methods for calculating relief loads are generally conservative and can lead to overly sized relief and flare systems designs. Dynamic simulation provides an alternative method to better define the relief load and improves the understanding of what happens during relief'* [30].

The interest in using dynamic simulations to describe the flare system relies on the possibility of accounting variations in system volumes and changes in compositions and conditions over time, thus resulting in a more realistic evaluation of the behaviour of the system during the pressure-relieving scenario. By applying dynamic simulations, the following effects can be analysed [22, 23, 35, 43]:

1. **Line packing.** The line packing effect accounts two facts occurring when the depressurization starts: (1) the relief fluids start gradually filling the flare network, and (2) initial accumulation of these fluids occurs due to empty volume being filled. Consequently, a certain time is required before the media reaches the flare tip, and the combustion of the process media from the relieving source does not occur all at once.

2. **Back pressure.** The back pressure built up in the flare network poses resistance to the flowing of the relief fluids towards the flare.

3. **Back flow.** Reverse flow (back flow) into inactive (non-flowing) pipelines of the flare network, or low-pressure tailpipes sources [43].

The consideration of these dynamic effects arises a more sensitive estimation of the rates and pressures in the different parts of the flare system, which in return can result in a peak at the flare tip lower than the predicted considering the sum of relieving rates from each of the PRDs sources occurring simultaneously (steady-state approach). An example of the expected flow rate at the flare tip considering both approaches is illustrated in Figure 2.2.

As shown in Figure 2.2, the steady-state approach is represented as a constant peak rate that continues independently of time, whereas the dynamic state considers a lower peak (due to the effects explained above) that decreases over time as the inventory is relieved. This realistic analysis of the capacity of the system provided by dynamic simulations can be applied to minimizing project execution costs and the associated risks in greenfield (new design) and brownfield projects (modifications on existing facilities). With regards to the brownfield projects, the hidden potential for debottlenecking (i.e. hidden capacity) of existing flare networks can be revealed, and consequently, unnecessary revamping or modifications of the systems can be avoided if the required capacity is met.

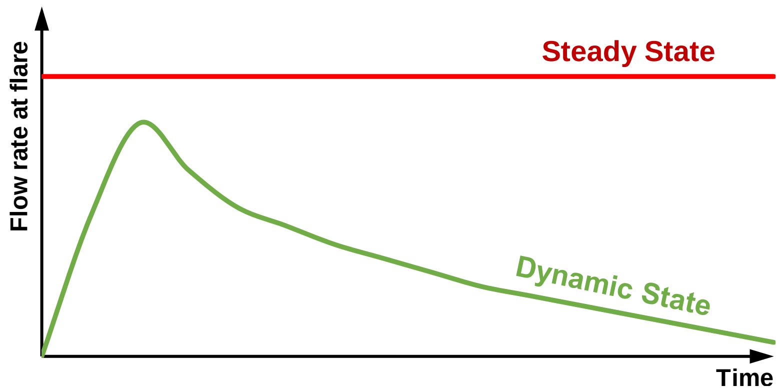

Figure 2.2: Representation of the expected flow rate results at the flare when using both steady-state and dynamic approaches.

The references found in the literature are limited. Several authors have used them to analyse individual relief loads from various scenarios [18, 41, 44, 21]. Andreasen [45] modelled a sub-part of a flare system on an existing offshore oil and gas production facility, and found a 12% reduction in the peak flare when benchmarking the dynamic model to the steady-state simulation. Wasnik et al. [23] studied the depressurization of an offshore platform with 14 depressurization sources and a total initial flow of 545 MMSCFD, and found a maximum peak flare of 447 MMSCFD (18% reduction) when modelling the system using dynamic simulations. Therefore, although the reported studies addressing the use of dynamic simulations in the design of the flare system are sparse, there are clear indications that reveal the advantages of this approach.

2.4 High Integrity Pressure Protection System

HIPPS is a safety instrumented system designed to protect vessels and piping systems against overpressure by rapidly shutting off the pipeline, stopping the inflow and containing it inside the system [30, 46]. HIPPS is a functional loop comprising of three main elements: field instruments (e.g. sensors, pressure transmitters), logic solving devices (e.g. high-integrity logic solver, relays, etc.), and final control elements (e.g. valves, switches, actuators, etc.) [29, 30].

The number of elements defining the functional safety loop of HIPPS will depend on the required Safety Integrity Level (SIL). According to IEC 61511 standard on Safety Instrumented Systems for the Process Industry Sector [47, 48], SIL is defined as the relative level of risk-reduction (i.e. level of protection) provided by the SIS. There are four SIL Levels (1-4), depending on the frequency and the severity of the hazard. According to API Standard 14C [29], HIPPS shall meet a minimum SIL of Level 2 (one final control element & voting

1oo2), but a SIL Level 3 (two final control elements & voting 2oo3) is often found based on the associated risk assessment [49].

An example of HIPPS with 2oo3 voting and two final elements is shown in Figure 2.3. The field instruments (illustrated as pressure transmitters (PT)) monitor the pipeline pressure during operation and compare it to the pre-defined set value. If the pressure stars building up, the PT will sense it and will send the information to the logic solver. The logic solver processes the signals from the initiators and performs a 'two out of three' (2oo3) voting logic to check whether the received signal is false or real. In case it is real, the logic solver activates the final control elements (represented as solenoids valves), which will force the actuators to close the block valves, isolating the high-pressure zone and protecting the low-pressure zone against overpressure [49].

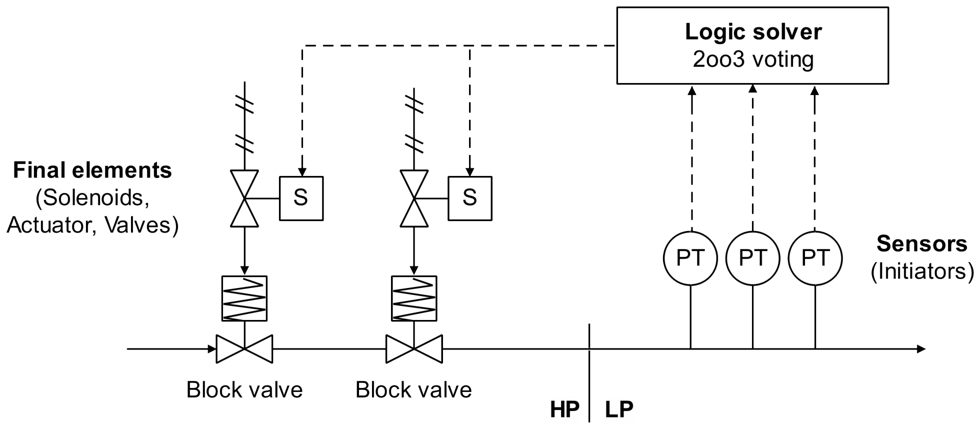

Figure 2.3: Electronic safety loop of HIPPS comprising 2oo3 initiators.

2.4.1 Applications of HIPPS

HIPPS can be implemented as a last resort when the installation of a PRD for secondary protection is not technically or economically viable, not reliable or requires excessive cost [30], as mentioned in Section 2.2.3. One example in which using HIPPS can be justified is when a new high-pressure production well is added and, as a result, the existing relief system cannot guarantee the required level of safety. Upgrading the existing relief/flare system can be costly or impractical due to weight and sizing factors. Then, it is possible to install HIPPS in concert with the existing relief system, eliminating the addition of extra weight and a large amount of capital that would be required if a new relief/flare system were added [29]. Additionally, HIPPS can also be installed to act as a barrier between high-pressure and low-pressure (HP/LP) sections.

2.4.2 Benefits of HIPPS

HIPPS is cost-effective and it incorporates appropriate levels of redundant instrumentation, with all components designed to be fail-safe. In addition, it can be designed to achieve a higher level of reliability than a mechanical relief device (i.e. PRD) if continuous maintenance, testing, and inspection during its operational life is provided [29, 30]:

1. To overcome the overpressure scenario, HIPPS does not need to flare or vent the excess inflow. Therefore, it is environmentally friendly as the release of media is avoided.

2. Lower purchase, installation, and maintenance costs.

3. HIPPS is not space-demanding and does not compromise the weight in the facility.

4. To avoid the upgrading of the existing relief/flare system in case a new high-pressure marginal field is tied-back to the existing infrastructure (i.e. HIPPS is cost-saving).

2.4.3 HIPPS versus ESDV

Even though both HIPPS and ESD systems are installed to shut off process equipment in case of overpressure, they are different from the perspective of functionality. On the one hand, an ESD is a safety instrumented system installed as a primary protection layer against overpressure that forces the shutdown of a unit process or plant in case of emergency [7]. On the other hand, HIPPS is installed as a backup of the ESD. It is added to the system to act as a secondary protection of the unit in case the ESD fails or is not fast enough. It is an active protection installed to mitigate the event when the installation of a PSV is not feasible [34]. Both systems are designed to be able to independently isolate the system. The sequential workflow of the safety protection barriers against overpressure is illustrated in Figure 2.4.

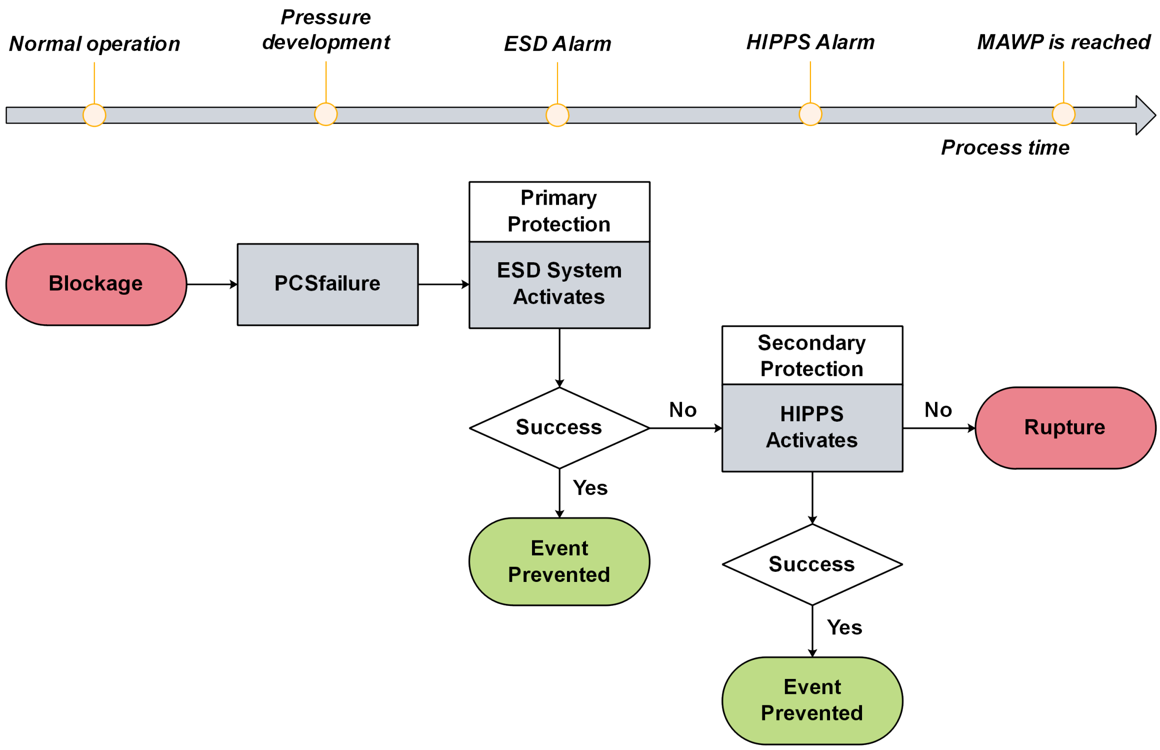

Figure 2.4: Block diagram comprising the sequence of events occurring in case of overpressure.

2.4.4 Dynamic simulations of HIPPS

An overpressure scenario is an inherent dynamic event in which pressure develops over time due to an undesired event. HIPPS – and in the main, all piping systems including pipes, fittings or valves – shall be designed to withstand the most severe pressure and temperature conditions that can be recorded during operation to ensure the safest operation [11]. Generally, the performance of a safety barrier can be defined based on effectiveness, reliability (level of confidence), and response time [50]. HIPPS shall be designed to ensure that the requirements of SIL Level [47, 48, 49] and speed of closure of the block valves [29] are fulfilled.

To evaluate the response capability of the HIPPS, a parameter called Process Safety Time (PST) has been used. PST is defined as the time from solicitation of the barrier (i.e. HIPPS activation / HIPPS Alarm) to the end of the response (i.e. 100% closure of HIPPS) [7, 47, 48, 50]. By calculating the PST parameter, it is possible to predict whether the available time for closure is sufficient to prevent escalation, or if the safe design limit of the process equipment (i.e. MAWT) has been surpassed before the HIPPS is fully closed.

Dynamic simulations are commonly conducted in the offshore oil and gas industry to periodically validate the PST and the performance of HIPPS under different transient conditions. The required PST of HIPPS in the industry is approximately set to 2 seconds closure [49]. Additionally, some authors have also addressed the interest in using dynamic simulations to verify the performance of HIPPS [51, 52, 53, 54].

The modelling of dynamic simulations demands a level of detail superior to the requirements to be specified in a steady-state model. Dynamic simulations use the volume in the system and the pressure drop across the units to solve the model [55]. Therefore, a physical description of the process equipment must be provided. This means that volume, dimensions, sizes, and location (i.e. elevation) of the pipes, vessels, valves, and other unit operations are required [56, 57]. However, even though the modelling of HIPPS using dynamic simulations is an accepted practice and it is commonly applied in the offshore oil and gas industry, the literature available and the know-how are limited. The requirements with regards to the level of detail to be specified when modelling the HIPPS in dynamic are not well-established, and the relation between the robustness of the model and sensitivity of the results is not clear.

2.5 Thermodynamic modelling

The analysis of hazardous events often implies variations in pressure and/or temperature of process fluids to undesired values. Furthermore, various types of petroleum fluids can be identified depending on the reservoir conditions and the composition of the well-mixture, thus different physico-chemical properties and phase behaviours can be expected from field to field [58, 59]. Therefore, the accurate selection of the thermodynamic model will allow the user to correctly describe the interactions and equilibrium within the mixture components at given conditions.

2.5.1 Type of reservoir fluids

Reservoir fluids are multicomponent mixtures that are primarily composed of hydrocarbons. In the process of extracting the well-mixtures from the reservoir, the reservoir temperature remains approximately constant, while on the contrary, pressure declines progressively [59, 60]. However, different multiphase behaviour is expected during reservoir depletion depending on the type of reservoir fluid under investigation. Fluids can be classified based on the composition of the well fluid and the position of the mixture's critical temperature relative to the reservoir temperature [59]. A typical phase envelope of each of the main reservoir fluids is illustrated in Figure 2.5.

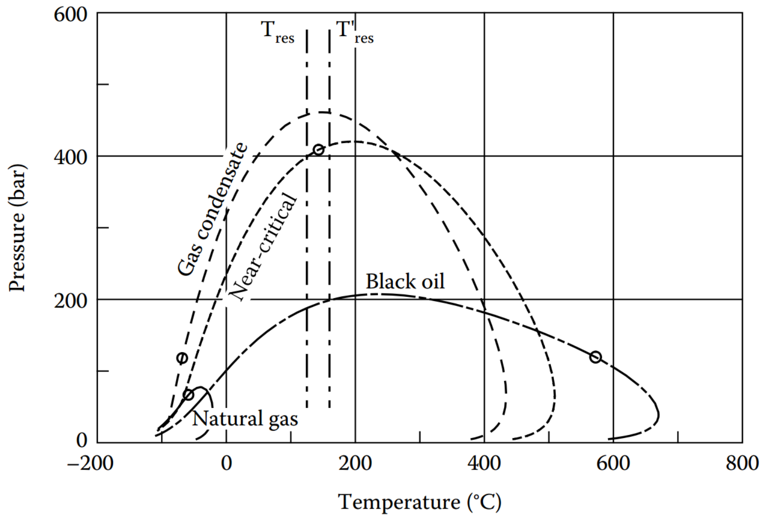

Figure 2.5: Phase envelope of various types of reservoir fluids [59].

The main types are briefly explained next [58, 59, 60]:

- **Black oil reservoir.** The critical point is much higher than the reservoir temperature. When the pressure falls below the bubble point branch, a gas phase will form.
- **Near-critical oil reservoir.** The critical temperature of the mixture is near to the reservoir temperature. In this type of reservoirs, a gas phase is liberated from the liquid phase when the pressure reaches the bubble point branch.
- **Gas condensate reservoir.** The critical temperature of the mixture is lower than the reservoir temperature. A liquid phase will be formed when the pressure meets the dew point at the reservoir temperature. This occurs as a result of gas condensate mixtures containing a relative amount of heavy hydrocarbons that condensate in the reservoir as pressure declines.
- **Gas reservoirs (dry).** The critical temperature of the mixture is much lower than the reservoir temperature. Gas expansion takes place, meaning that the gas phase remains as gas as pressure decreases.

2.5.2 Equation of State model

To describe the phase behaviour of a mixture (also referred to as Vapor Liquid Equilibrium (VLE)), it is required an Equation of State (EOS). An EOS estimates the Pressure-Volume-Temperature (PVT) relationship, which represents the volumetric behaviour of a fluid as a function of pressure and temperature [4, 59]. The Peng Robinson EOS is the most widely applied EOS in the oil and gas industry, since it can be applied to predict the behaviour of pure components and hydrocarbon mixtures under wide pressure and temperature ranges with proven satisfactory results in PVT estimations [61, 62, 63].

Pure compound application of Peng Robinson EOS

The Peng Robinson EOS for pure compound applications is given in Equation 2.2.

$$P = \frac{RT}{\underline{V_m} - b} - \frac{a(T)}{\underline{V_m} \cdot (\underline{V_m} + b) + b \cdot (\underline{V_m} - b)} \tag{2.2}$$

Where R is the universal gas constant, V_m is the molar volume, a(T) is the attractive constant related to the attractive central forces that molecules exchange, and b is the covolume. Both a(T) and b are fluid dependant parameters that are calculated as shown in Equation 2.3 and Equation 2.4, respectively. They depend on critical pressure (P_C) and critical temperature (T_C), which are properties of pure species that have been determined from the available PVT experimental data [61, 62, 63].

$$a(T) = 0.45724 \cdot \frac{R^2 \cdot T_c^2}{P_c} \cdot \alpha(T) \tag{2.3}$$

$$b = 0.07780 \cdot \frac{R \cdot T_c}{P_c} \tag{2.4}$$

α(T) can be calculated using Equation 2.5, where T_R denotes the reduced temperature and it defines the ratio between the absolute temperature and the critical temperature, and k represents the polynomial fit of the acentric factor (w). The acentric factor is a dimensionless parameter that was introduced to increase the accuracy of the EOS prediction, as it accounts the non-sphericity (acentricity) of the molecules [63].

$$\alpha(T) = [1 + k \cdot (1 - \sqrt{T_R}]^2 \tag{2.5}$$

$$k = 0.37464 + 1.54226 \cdot w - 0.26992 \cdot w^2 \tag{2.6}$$

Mixture application of Peng Robinson EOS

The Peng Robinson EOS for mixture applications is given in Equation 2.7.

$$P = \frac{RT}{\underline{V_m} - b_m} - \frac{a_m(T)}{\underline{V_m} \cdot (\underline{V_m} + b_m) + b_m \cdot (\underline{V_m} - b_m)} \tag{2.7}$$

Where the attractive constant a_m and covolume b_m of the mixture are calculated applying empirical mixing rules as it follows:

$$a_m = \sum_{i=1}^{c}\sum_{j=1}^{c} z_i z_j a_{ij} \quad \text{with} \quad a_{ii} = a_i \quad \text{and} \quad a_{ij} = \sqrt{a_i a_j} \cdot (1 - k_{ij})$$

$$b_m = \sum_{i=1}^{c}\sum_{j=1}^{c} z_i z_j b_{ij} \quad \text{with} \quad b_{ii} = b_i \quad \text{and} \quad b_{ij} = \frac{b_i + b_j}{2}$$

The composition is taken into consideration through the mole fraction of each of the components (z) in the mixture. k_{ij} is a parameter known as Binary Interaction Parameter (BIP). It is added to account the deviations from the non-ideality of the mixture in the value of the attractive constant. This parameter is regressed from the VLE experimental data of binary systems, i.e. every BIP correlates a binary pair of mixture [61, 64].

Chapter 3

Problem Formulation

This Master Thesis revolves around the existing connection between process safety and the use of dynamic simulations to improve the design or to evaluate the transient conditions of the different processes and systems within the offshore oil and gas industry. In order to address the statement presented in Section 1.3, the Master Thesis considers the analysis of two process safety systems:

- Part I: A study of debottlenecking on existing flare systems
- Part II: A study of the performance of a High Integrity Pressure Protection System

3.1 Objectives of Part I

The design of flare systems is conventionally made according to steady-state simulations, which even though is conservative, in turn, leads to oversizing of the flare system beyond feasibility. Part I of this Master Thesis aims to investigate if a better design of the systems can be obtained by using dynamic simulations. For that, the following objectives are outlined:

- To simulate the full plant emergency depressurization process in three different flare systems (in terms of flare size, flare system design load, and blowdown segments) from different oil and gas facilities using both steady state and dynamic simulations.
- To benchmark the results obtained from steady state and dynamic simulations.
- To analyse the level of detail required to model the operation. For that, the addition of PCV, PSV and dead ends to the model and the associated influence is studied.

3.2 Objectives of Part II

The use of dynamic simulations to verify the performance of HIPPS is a common practice in the industry, however, the available know-how is limited or reserved to the company rules. The available reported studies differ from each other in terms of the level of detail and correlations selected. Part II intends to investigate the minimum level of detail to be specified in the dynamic simulations, assessing the effort required in order to get reliable and conservative results. For that, the following objectives are outlined:

- To simulate the occasion of an overpressure scenario occurring in the subsea pipeline that connects the wellheads to the processing platform, and to evaluate the performance of HIPPS by calculating the PST.

- To investigate how important is the robustness of the dynamic model in the accuracy of the obtained results by comparing the PST when calculated for different flowrates, system volumes, overpressure scenarios, pipe configurations, and pipe flow correlations.

3.3 Problem Delimitation

Three facilities have been modelled to accomplish the objectives of Part I. Information used to build the dynamic models has been provided by Rambøll Oil & Gas. The contribution of the author was to create the steady-state and dynamic models in Aspen HYSYS V9 for the purpose of reproducing the performance of the plant under the emergency depressurization, and to evaluate the hidden debottlenecking potential in different flare systems. It shall be noted that the optimization of the pipe diameters (i.e. proposal of a new design of the flare network), or the heat transfer (e.g. depressurization of the system under fire, equipment undergoing low temperatures during blowdown) are not part of the scope of this Master Thesis.

With regards to Part II, a hypothetical oil and gas facility handling gas condensate fluids has been simulated using Aspen HYSYS V9. No real data has been used, so the calculated process response time of the HIPPS is not meant to be compared with any safety threshold. The main purpose of the author was to analyse the operability of the HIPPS when an overpressure scenario is occurring, and to evaluate the level of detail required to simulate this system. No heat transfer contribution has been considered in any of the case studies.

Chapter 4

Methodology Part I

A study of kPaottlenecking on existing flare systems

Part I of this Master Thesis aims to investigate the use of dynamic simulations to improve the design of flare systems. Chapter 4 intends to provide the reader with the necessary background to understand the methodology carried out in the simulation environment.

4.1 Aspen HYSYS V9

Aspen HYSYS is a process simulator widely used in both industry and academia. It offers the user the possibility of simulating several unit operations with a substantial database of pure chemical compounds, thus allowing the design, model, and optimization of a large number of industrial processes, or even full chemical plants. The software relies on chemical engineering calculations such as mass and energy balances, heat and mass transfer, chemical kinetics, or phase equilibrium, among others. It uses an extensive property database developed in collaboration with the National Institute of Standards and Technology (NIST).

Aspen HYSYS allows the user to conduct either steady state or dynamic simulations, as it incorporates a dynamic process simulator software called Aspen HYSYS Dynamics. By using this software, it is possible to switch the steady state simulation into a dynamic model where the transient nature of the process can be evaluated. The large number of possibilities that the software offers within the plant design and operation (e.g. evaluating the control system of a process or plant, simulating undesired events, performing start-up and shutdown scenarios, etc.), makes Aspen HYSYS Dynamics a relevant tool in the context of process safety [56].

4.1.1 Fluid characterization

The process fluids are modelled using the Peng Robinson EOS. With regards to the composition prior to depressurization, the heavy hydrocarbon fractions (fractions above $C7^{+}$) are modelled as hypotheticals/pseudo-components. A more detailed explanation on this matter will be given in Section 5.2.1.

4.1.2 Modelling the flare network

The flare network has been modelled considering a number of BDV sources that are routed into the flare tip via headers and subheaders, as represented in Figure 2.2. The BDV segments object of depressurization are selected considering all hydrocarbon-containing volumes at pressures above 690 kPa [30], and they are modelled as vessels in HYSYS with a vessel volume equivalent to the BDV rate to be relieved. The liquid inventory from the BDV sources is represented as the liquid volume in the vessel. Since the heat transfer is not part of the scope of this Thesis, the dimensions of the pseudo-vessels are irrelevant, as long as the volume is matched. If an abnormal heat input from an external heat source was to be considered (e.g. fire scenario), the dimensions of the pseudo-vessels and their geometry will be of concern, as the heat absorbed by the vessel is affected by the contact area between the heat source and the area of the vessel filled by the liquid volume (which is known as the wetted area) [65].

The BDV for each segment is modelled as a control valve that is 100% closed. The sizing of each of the valves has been made calibrating their valve coefficient (Cv), which represents the capacity of the valve orifice for the flow through it. To calibrate the Cv, the composition of the mixture prior to depressurization (i.e. Molecular Weight (MW) of the mixture), the inlet pressure to be relieved, and the initial BDV flow rate have been considered. The Cv is determined by the ANSI/ISA method [66, 67] using a semi-ideal Cp /Cv. An example of a blowdown segment (pseudo-vessel volume + BDV), together with the specifications required for the model is given in Figure 4.1.

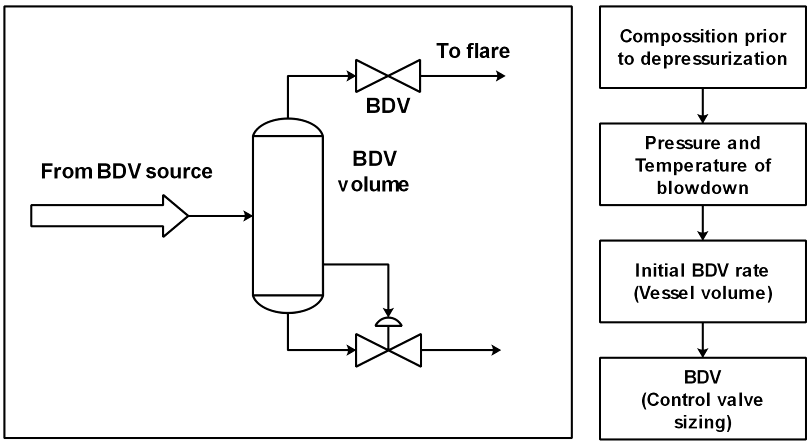

Figure 4.1: Example of blowdown segment modelled in HYSYS, and specifications required for the model

The composition of the mixture prior to depressurization of each of the blowdown segment is sourced from a corresponding steady-state process simulation of the plant. The initial conditions (i.e. pressure and temperature right before blowdown) are set according to the company blowdown and relief report. A unit operation from Aspen HYSYS called 'Pipe Segments' has been utilized to reproduce the layout and the level of detail (length, internal diameter, fittings, etc.) of existing Flare System Analyser (FSA) simulations that have been used to evaluate the system from a steady-state approach. Elevations of tail pipes, subheaders and headers are ignored, as it is assumed to have negligible influence in the results. The only contribution to the static pressure is made by the flare stack, whose elevation has been specified as stated in the FSA models. The flare is modelled as a control valve calibrated to withstand the maximum load expected during full plant depressurization (flow rate considering the sum of all individual relieving rates (steady-state approach)), and the associated pressure drop, in accordance to vendor data.

4.1.3 Plant emergency depressurization

The full plant emergency depressurization of three existing facilities has been simulated. All simulations have been conducted using Aspen HYSYS Dynamics. The start of the depressurization is simulated as the moment in which the BDVs – that were represented as a control valve that is 100% closed – open simultaneously, relieving the process fluids into the flare network. All BDVs are actuated at once. Although some of the blowdown segments may contain hydrocarbon liquid inventory, the liquid phase is contained in the pseudo-vessels whereas the vapour phase is relieved through the BDV. Thus, inflow to the BDV is vapour phase. Nevertheless, smaller amounts of condensation may occur downstream of the BDV due to Joule-Thomson cooling over the valve. In the case the flashing of the liquid occurs at the BDV, liquids will be stored in the KO drum, allowing the safe disposal of the vapor phase via flare. The backpressure in the flare network will be created by the pressure drop across the flare tip.

For vapour depressurization, API Standard 521 recommends: *'Depressuring to a gauge pressure of 690 kPa (100 psi) in 15 min is commonly considered when the depressuring system is designed to reduce the consequences from a vessel or failure'*. Therefore, all simulations have been conducted for a simulation time of 15 minutes. Time step of the simulation has been set to 0.01 seconds to ensure a sufficient residence time of the fluid in the pipe segment that enables realistic dynamic calculations of the pressure-flow solver incorporated in Aspen HYSYS Dynamics [68].

4.1.4 Limitations on the model

The pipe segment in Aspen HYSYS has some shortcomings in its modelling rigor. On the one hand, the phase slip effects cannot be modelled. The phase slip effect refers to the difference in velocity between the phases that are flowing through the pipe segment [68]. The pipe segment unit in Aspen HYSYS assumes that both liquid and vapor are flowing at the same velocity [69]. For the present study, where most part of all segments downstream the BDVs are filled with vapour, with only a minimum amount of condensates that might be formed due to Joule-Thomson cooling over the valve, phase slip effects can be ignored. On the other hand, the acceleration pressure drop is not included for pure gas flow. The Darcy-Weisbach is used for the pressure drop calculation, but it is better suited for incompressible flow with constant density. In the present study, compressible flow with varying density is considered, so the incorrect use of this correlation might lead to inaccurate results. To mitigate the modelling deficiencies that might appear with the use of the Darcy-Weisbach correlation, the pipe network of the flare is either broken down into a vast number of individual pipe segments or into a number of increments within each of the pipe segments. Consequently, pressure drop, energy balance, and mass balance calculations are performed in each of the smaller segments. Due to the discretization of the flare network, the fluid density can be considered constant over the length. Therefore, the use of pipe segments to model the flare network can be considered acceptable and fit for purpose.

4.1.5 Boundary stream specifications

Steady-state simulations consider the flow and the pressure independently, neglecting in some cases the pressure drop of the unit operation or allowing the user to set it without any consideration of the flow across the unit. On the contrary, a pressure flow solver is incorporated in Aspen HYSYS Dynamics, and it considers the relationship between pressure and flow to solve the model (i.e. pressure and flow cannot be set independently) [55]. In a dynamic simulation environment, it is needed to define the boundaries of pressure and flow occurring within the process to use them as pressure or flow controllers in case of a hazardous event. It shall be noted that internal streams do not require any dynamic specification, as their conditions are determined by the surrounding equipment based on the fixed operating boundaries. The two options for specifying the boundary streams are described in 4.1.

Table 4.1: Boundary stream specifications in Aspen HYSYS Dynamics

Dynamic Specification	Description	Applications
Flow Specification	Inlet (or outlet) flow is fixed, regardless downstream (or upstream) conditions	Evaluation of plant performance when an undesired event occurs. The inflow is constant, so variations in pressure due to transient conditions can be analysed
Pressure Specification	Inlet (or outlet) pressure is fixed, regardless downstream (or upstream) conditions.	Process / Plant start-up. The maximum flow entering the system can be calculated, as the flow needs to match the source pressure and the pressure drop within the system

With regards to the present study, the boundaries of the flare system are the BDVs sources (inlet) and the flare tip (outlet). Three dynamic simulations have been built for each of the facilities under study. The considerations for each of the simulations are the following:

1. **Steady State case.** The dynamic model built in Aspen HYSYS is benchmarked against the FSA model for validation. For that, a 'steady-state' dynamic simulation (steady-state approach) has been conducted fixing the pressure at sources (BDVs inlets) and flare outlet, i.e. using the initial peak flow from blowdown segments. Peak flare load, individual relieving rates from the BDVs, and pressure drop in the pipe segments are checked against the FSA model.

2. **Dynamics case.** Once the model is validated (i.e. can reproduce the FSA model), the dynamic simulation (dynamic approach) of the flare system is conducted. For that, a zero flow boundary is now selected for the inlet streams, whereas a pressure boundary is selected for the flare.

3. **Dead ends case.** Additionally, a third model with increased complexity is built considering inactive (non-flowing) pipelines of the flare network, such as dead-ends or PSVs and PCVs sources (inactive), and their associated tail pipes/subheaders. This model adds an extra level of detail to the Dynamic case, and it is also a dynamic simulation with inflow and pressure outlet boundaries.

The comparison between these three simulations for each of the facilities is shown in the Results section (Part I).

4.2 Simulated Case Studies (Part I)

Three different flare systems on different offshore facilities are analysed in the present study. A summary of key data describing the three systems is provided in Table 4.2. The design load of the facilities is sourced from the respective blowdown report.

Table 4.2: Summary of investigated facilities.

	Design Load			
Facility	**(kg/h)**	**(MMSCFD)**	**No. BDVs**	**No. Subheaders**
A	88,000	73	13	3
B	350,000	341	24	5
C	684,000	714	43	4

4.2.1 Facility A

Facility A is an integrated platform with wellheads and processing facilities on the same topside facility. This facility is designed for light crude with associated gas. The separation of oil, gas and water takes place in a two-stage separation train with final polishing of crude export in an electrostatic coalescer (final dewatering and desalting). A compression system boots the gas pressure from the separators for wet gas export/injection and gas lift.

The flare system receives relieving fluids from 13 BDV sources, and it is rated to a maximum rate design capacity of 73 MMSCFD (88,000 kg/h), considering the sum of all individual relieving rates discharging simultaneously upon depressurization (i.e. a steady-state approach was used in the design). The specifications for blowdown segments, considering initial conditions prior to depressurization, are given in Table 4.3. Three subheaders of 12" (Subheader 1), 14" (Subheader 3), and 4-6" (Subheader 5) collect the fluids and send them to the KO drum (ID 3 m by T/T 10 m) via 16-18" main header, wherefrom they are disposed at the flare. A representation of the flare system as modelled in the Aspen HYSYS V9 is illustrated in Figure 4.2.

4.2.2 Facility B

Facility B is a gas-condensate integrated processing platform, with two-stage condensate knock-out and booster compression of flash gas from the 2nd stage separator. Before export, the gas is dehydrated, and dew point controlled (hydrocarbons).

The flare system has 24 BDVs discharging into the flare network upon depressurization, and it is rated to a maximum rate design capacity of 341 MMSCFD (350,000 kg/h). The specifications for blowdown segments are given in Table 4.4. Five subheaders collect the fluids and send them to the KO drum (ID 3 m by T/T 7.2 m) via 20" main header, wherefrom they are disposed at the flare. The platform has two separated flare systems (LP and HP), but only the HP flare is modelled in the present study. A representation of the flare system as modelled in the Aspen HYSYS V9 is illustrated in Figure 4.3.

Table 4.3: Summary of specifications for blowdown segments of Facility A. Note that the conditions are for the initial system state prior to depressurization.

BDV No.	Pressure (bar)	Temperature (°C)	Total volume (m^3)	Liquid Volume (m^3)	Initial BDV rate (kg/h)	Initial BDV rate (MMSCFD)	Gas MW
1	36.0	93.4	101.0	70.9	26,836	22.36	23.8
2	63.4	64.8	1.8	0.7	4,610	3.97	21.8
3	68.6	64.8	4.6	1.8	9,140	7.87	21.8
4	2.5	80.0	113.1	67.7	11,656	5.85	40.0
5	36.0	93.4	49.8	31.3	19,578	16.48	23.8
6	180.0	111.9	0.4	0.0	1,391	1.14	24.5
7	4.9	38.0	15.2	1.9	3,996	1.74	38.0
8	13.2	45.0	5.6	0.9	3,319	0.96	34.0
9	34.0	93.4	3.6	0.2	1,561	1.35	24.0
10	125.0	115.0	1.9	0.0	3,044	2.49	24.5
11	40.6	40.0	1.3	0.0	6,544	5.16	24.3
12	130.9	75.0	3.7	1.1	10,209	8.34	24.5
13	31	93.4	3.6	0.2	500	0.43	24.0

Table 4.4: Summary of specifications for blowdown segments of Facility B. Note that the conditions are for the initial system state prior to depressurization.

BDV No.	Pressure (bar)	Temperature (°C)	Total volume (m^3)	Liquid Volume (m^3)	Initial BDV rate (kg/h)	Initial BDV rate (MMSCFD)	Gas MW
1	87.9	68.2	0.3	0.1	627	0.6	20.3
2	55.0	88.1	0.3	0.1	375	0.4	20.6
3	41.5	47.7	0.6	0.1	524	0.5	20.4
4	41.2	69.0	0.5	0.1	537	0.5	20.7
5	42.4	85.7	0.6	0.0	528	0.5	20.8
6	41.6	72.8	0.9	0.0	531	0.5	20.7
7	40.9	67.7	30.9	1.4	15,943	15.5	21.7
8	40.0	58.1	3.7	2.5	1.797	1.8	20.4
9	89.9	84.8	22.3	3.6	26,717	25.2	21.2
10	24.0	30.7	105.7	58.5	23,721	22.5	21.0
11	56.2	35.0	7.4	0.0	4,674	4.7	19.7
12	22.3	30.6	7.9	7.4	20,035	18.8	21.8
13	56.4	35.0	8.5	0.0	9,609	9.8	19.7
14	76.5	39.5	82.3	34.9	99,998	95.9	20.2
15	40.7	52.1	6.7	0.1	2,207	2.1	21.0
16	75.0	19.0	41.3	7.3	41,878	40.4	20.5
17	56.6	-9.1	59.6	17.7	51,306	54.1	20.0
18	65.4	39.2	5.3	0.0	3,872	3.9	19.7
19	14.0	45.4	2.4	0.0	235	0.2	19.7
20	95.2	49.5	10.9	3.4	13,520	13.2	20.5
21	101.4	75.7	0.4	0.1	1,642	1.6	21.1
22	58.7	33.8	1.1	0.0	1,039	1.0	20.9
23	67.0	45.4	3.9	0.0	8,617	8.3	20.9
24	25.9	30.7	1.5	1.5	19,901	18.9	21.3

4.2.3 Facility C

Facility C is a Central Processing Platform (CCP) handling production from a number of bridge-connected platforms including tie-backs from remote/unmanned facilities. Separation of oil/gas/water, as well as gas compression, dehydration and hydrocarbon dew-pointing takes place in the CCP. The CCP exports gas to shore as well as it provides gas lift to wells required artificial lift.

The flare system has 43 BDVs disposing into the flare network upon depressurization, and it is rated to a maximum rate design capacity of 714 MMSCFD (684,000 kg/h). The specifications for blowdown segments are given in Table 4.5. The flare system has three separated 18" main headers terminating at the flare KO drum (ID 3.55 m by T/T 10.6 m). The flare stack of 24" to the flare tip. A representation of the flare system as modelled in the Aspen HYSYS V9 is illustrated in Figure 4.4.

Table 4.5: Summary of specifications for blowdown segments of Facility C. Note that the conditions are for the initial system state prior to depressurization.

BDV No.	Pressure (bar)	Temperature (°C)	Total volume (m^3)	Liquid Volume (m^3)	Initial BDV rate (kg/h)	Gas MW
1	50.0	31.0	41.0	13.3	16,260	18.9
2	23.8	48.2	56.6	3.6	10,230	19.2
3	55.0	55.0	47.2	2.6	18,507	19.3
4	72.0	30.0	67.2	9.1	41,714	19.3
5	62.6	6.5	17.5	1.7	13,375	18.9
6	62.6	6.5	17.5	1.7	13,375	18.9
7	137.6	49.0	8.5	0.0	14,075	19.2
8	114.6	48.8	15.8	0.0	19,137	18.5
9	50.0	15.9	4.1	1.9	13,798	20.0
10	138.0	45.0	16.7	0.0	27,107	18.5
11	15.0	55.0	155.5	155.5	15,329	23.1
12	9.7	75.1	9.0	0.5	0	34.5
13	9.7	75.1	9.0	0.5	0	34.5
14	72.0	26.0	9.5	0.0	6,893	19.2
15	50.0	28.2	8.6	0.1	4,087	19.3
16	63.0	24.2	20.8	0.0	11,488	18.5
17	72.0	25.0	67.5	6.1	58,678	19.7
18	50.0	31.7	62.3	37.8	101,354	18.6
19	50.0	31.7	14.3	9.3	22,285	18.6
20	50.0	31.7	5.4	5.4	104,121	26.4
21	50.0	31.7	32.4	32.4	8,466	26.4
22	50.0	28.2	74.2	0.7	29,908	18.8
23	50.0	28.2	3.7	0.0	1,476	18.8
24	50.0	28.2	3.7	0.0	1,373	18.8
25	50.0	28.2	10.7	0.1	4,325	18.8
26	50.0	36.1	51.6	1.3	21,989	18.6
27	50.0	36.1	4.4	0.1	2,008	18.6
28	138.0	44.7	28.9	0.0	47,256	18.5
29	138.0	44.7	17.3	0.0	28,254	18.5
30	72.0	-7.8	0.2	0.2	3,914	20.0
31	72.0	-7.8	1.3	1.3	12,185	18.5
32	72.0	1.4	61.2	6.1	59,171	18.4
33	125.0	1.4	1.8	0.0	4,096	19.1
34	80.0	1.4	0.9	0.0	954	18.5
35	170.0	28.5	9.1	0.0	24,445	19.2
36	192.0	36.9	0.6	0.0	1,793	19.2
37	138.0	44.7	26.5	0.0	48,273	18.5
38	138.0	44.7	13.3	0.0	24,304	18.5
39	138.0	44.7	35.6	0.0	70,405	18.5
40	192.0	36.9	9.5	0.0	29,933	19.2
41	192.0	36.9	0.7	0.0	2,121	19.2
42	192.0	36.9	0.7	0.0	2,274	19.2
43	97.1	52.6	7.9	0.0	7,956	18.5

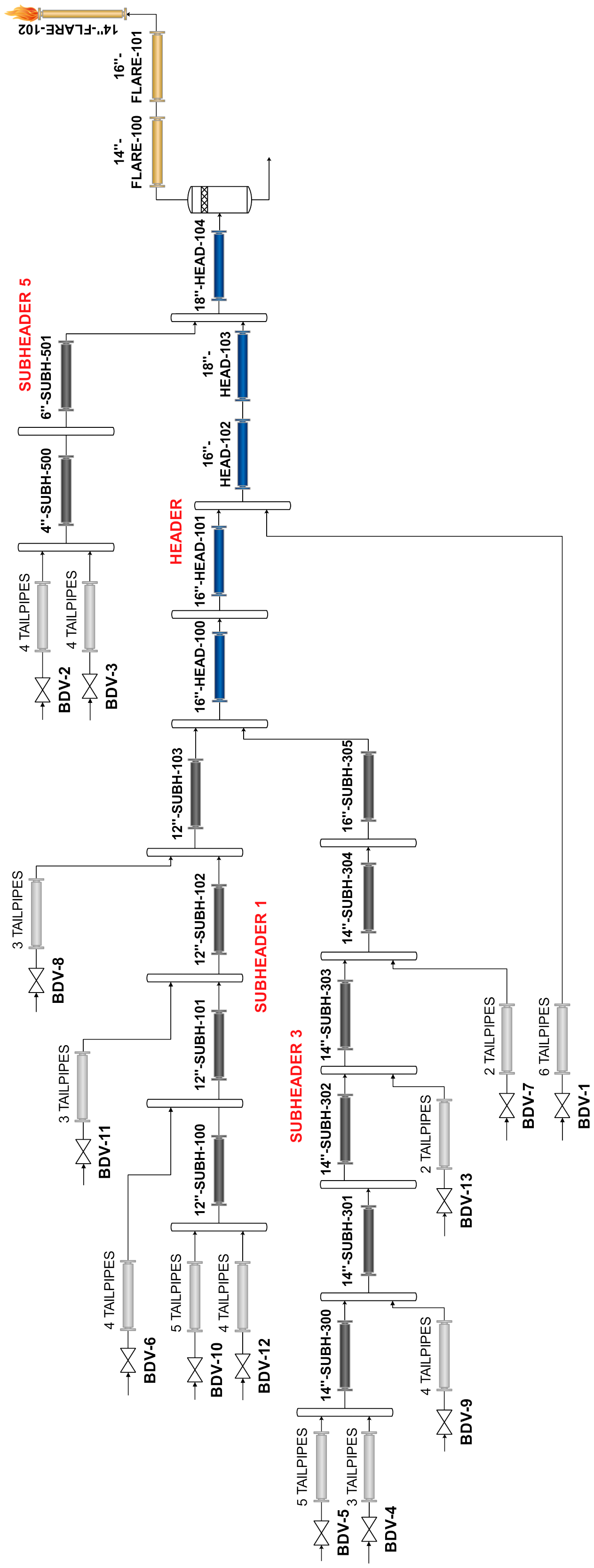

Figure 4.2: Configuration of the flare system model for facility A. PSVs and PCVs sources (inactive) are not illustrated.

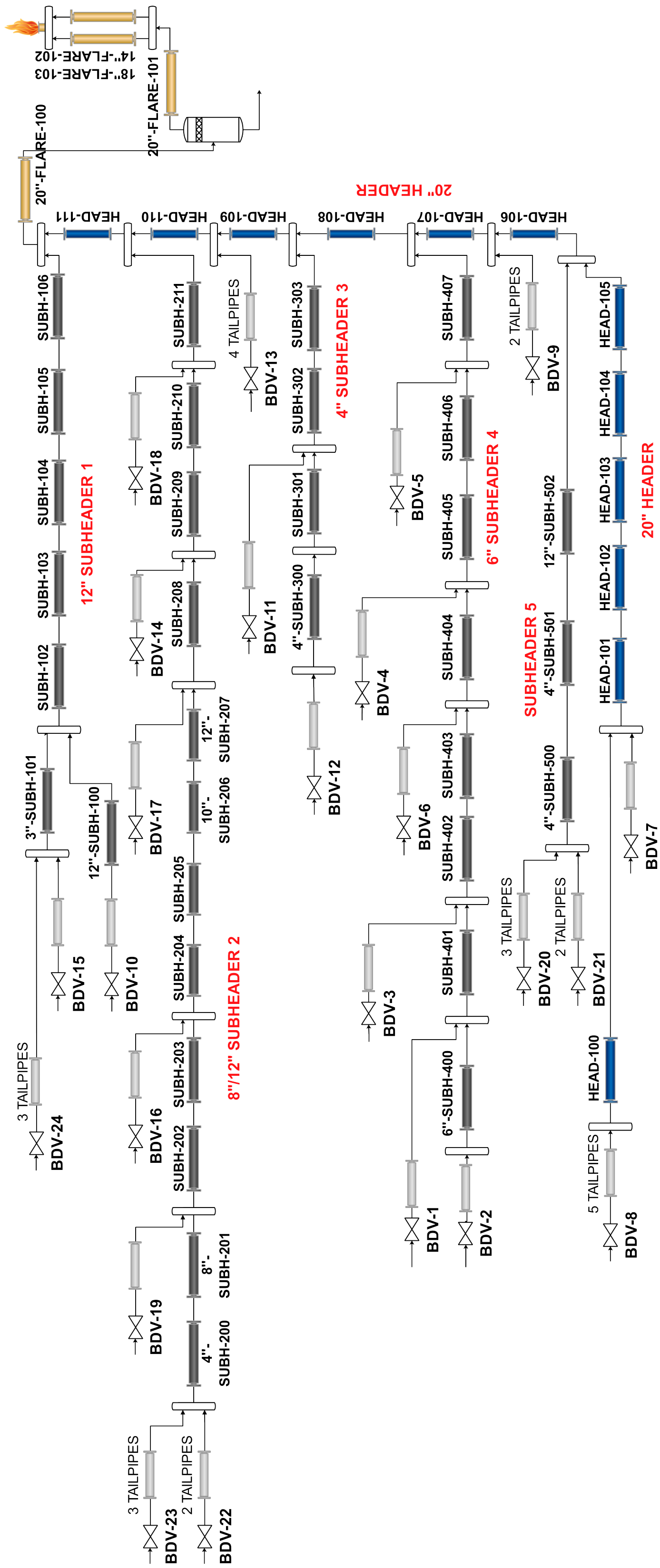

Figure 4.3: Configuration of the flare system model for facility B. PSVs and PCVs sources (inactive) are not illustrated.

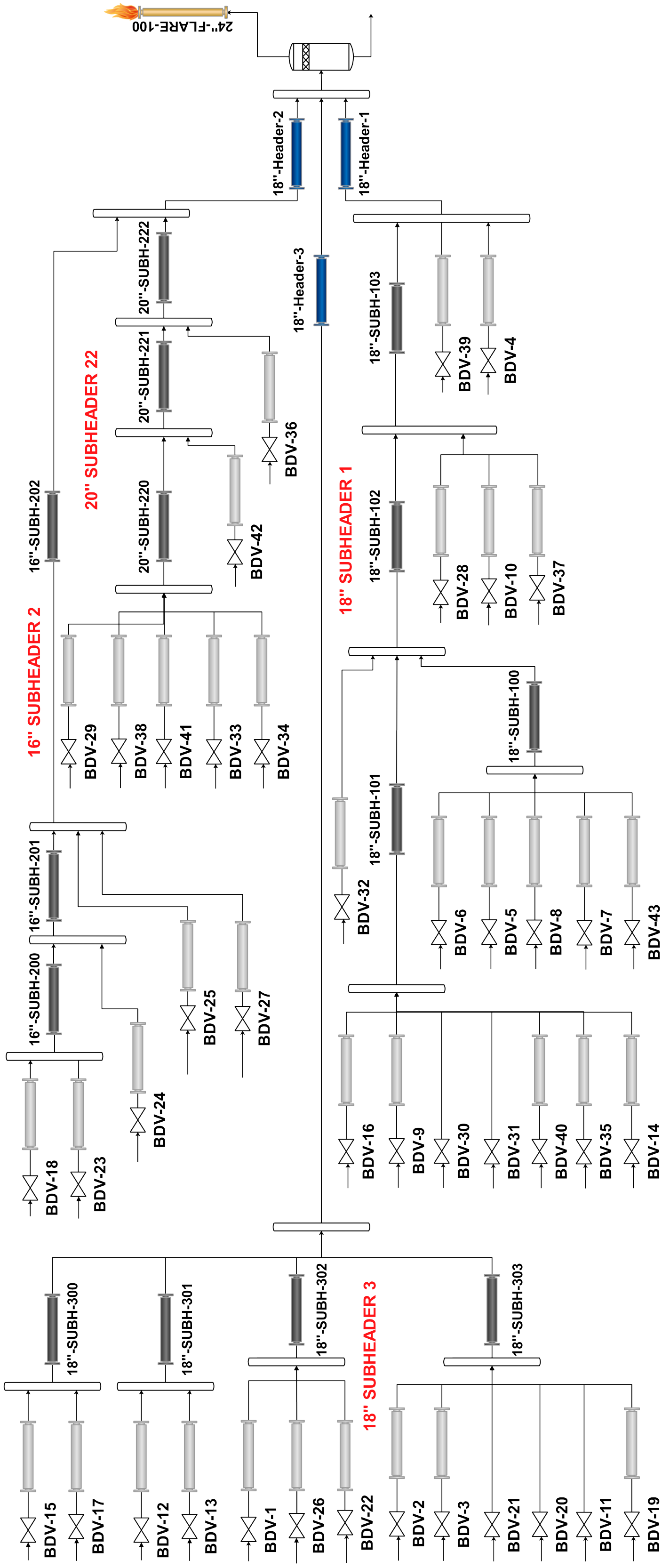

Figure 4.4: Configuration of the flare system model for facility C. PSVs and PCVs sources (inactive) are not illustrated.

Chapter 5

Methodology Part II

A study of the performance of a High Integrity Pressure Protection System

Part II of this Master Thesis aims to analyse the performance of a hypothetical HIPPS as a safety barrier against overpressure. For that purpose, a dynamic model considering different operational conditions has been built using Aspen HYSYS V9, and the analysis concerning the level of detail required to model the HIPPS environment is investigated. Chapter 5 intends to provide the reader with the necessary background to understand the methodology carried out in the simulation environment.

5.1 Description of the HIPPS layout

For the purpose of evaluating HIPPS, its performance when located in between the wellheads and topside processing facility (i.e. manifold) has been analysed. The wellheads are on a Wellhead Platform (WHP), which is a remote unmanned facility located several kilometers away from the Central Processing Platform (CCP). The WHP does not have a flare system. A sketch illustrating the layout of the system is given in Figure 5.1.

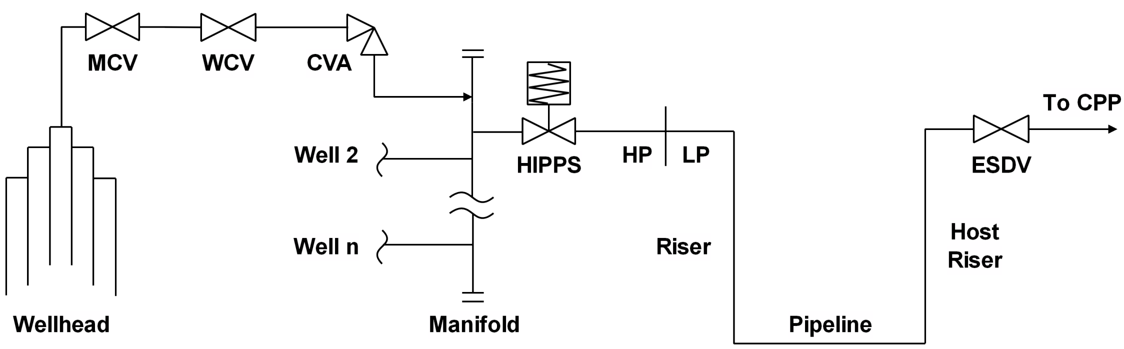

Figure 5.1: Typical wellhead and manifold layout on offshore production facility, including HIPPS. The Auxiliary Control Valve (XCV) is not represented.

The wellhead provides pressure control of the production well. It connects the surface facilities to the wellbore and serves as a point to suspend the production tubing. The production tubing is an assembly of pipework, valves, choke, and connecting fittings that regulates the flow from the reservoir during the operation of the well [4]. A brief explanation of the safety valves that can be found in a production tubing is described next [70]:

- **MCV.** The Master Control Valve (MCV) is the primary safety valve. It is the primary means of shutting in the flow of a well.
- **WCV.** Wing Control Valve (WCV) is the secondary safety valve. It acts as a secondary barrier when MCV fails to shut in the flow or is not fast enough.
- **CVA.** Choke Valve (CVA) is a control valve that regulates the production rate. It is typically a hydraulic-actuated valve that restricts the fluid flow through a bean or orifice.
- **XCV.** Auxiliary Control Valve (XCV) is a valve that isolates the inlet of utilities that are often injected in the well (e.g. gas lift or water injection).

5.2 Aspen HYSYS V9

5.2.1 Fluid characterization

The hypothetical facility that has been modelled in Aspen HYSYS is a gas-condensate processing platform with reservoir fluids coming from three wells. The wellheads are operating at 60°C and 300 bar (steady-state conditions). The composition of the gas condensate under study is given in Table 5.1. These compositions have been selected based on the available literature references [4, 59].

Table 5.1: Well fluid composition of Gas Condensate.

Component	Mole Fraction (%)
N2	0.12
CO2	2.49
C1	76.43
C2	7.46
C3	3.12
iC4	0.59
nC4	1.21
iC5	0.5
nC5	0.59
C6	0.79
C7-C10	3.4
C11-C16	1.94
C17-C80	1.36

Fractions above $C7^+$ have been lumped together as pseudo-component mixtures [59]. Aspen HYSYS allows the user to introduce these fraction loops in the simulator as hypothetical components. For that, it is required to provide the following parameters for each of the lumped groups: Normal Boiling Point, Molecular Weight, Liquid Density, and Critical properties (T_C, P_C, and w). The accuracy of these properties for the hydrocarbon mixtures will influence the prediction of the behaviour of the pseudo-components in the simulation. The properties of the lumped fractions of the Gas Condensate are given in Table 5.2.

Table 5.2: Properties of the lumped fractions of the Gas Condensate mixture.

Fractions	**MW**	**Density kg/m^3**	**T_C (K)**	**P_C (bar)**	w
C7-C10	109.92	753.87	286.31	28.02	0.513
C11-C16	179.88	801.17	374.10	18.56	0.707
C17-C80	327.23	860.22	520.40	13.93	1.055

The critical properties of the lumped fractions (Tc mix, Pc mix, and ω mix) depend on the critical properties of the pure components and the mole fraction of each in the pseudo-component mixture. They have been estimated by using the mixing rules given in Equation 5.1, Equation 5.2, and Equation 5.3 [63].

$$T_{c_{mix}} = \sum z_i \cdot T_{c_i} \tag{5.1}$$

$$P_{c_{mix}} = \sum z_i \cdot P_{c_i} \tag{5.2}$$

$$w_{c_{mix}} = \sum z_i \cdot w_{c_i} \tag{5.3}$$

Peng Robinson EOS has been utilized to predict the phase equilibrium of the mixture because (1) it has been proved that it can describe with accuracy the behaviour of hydrocarbon mixtures, and (2) no water is considered in the analysis [61, 62, 63].

5.2.2 HIPPS Flowsheet

The simulations have been performed based on variations of the HYSYS flowsheet shown in Figure 5.2. This model considers a hypothetical facility with three wells, as described in Section 5.1 (refer to Figure 5.1). Dimensions of the piping system depends on the number of wells, production rate, type of reservoir fluid, etc., but most common sizes and lengths have been taken from available literature to model the pipe segments [4, 59].

Three wells have been considered (Well 3, Well 5, Well 7). The wells connecting the reservoir to the topside facility are represented by pipe segments 6''-PIPE-300, 6''-PIPE-500, and 6''-PIPE-700. The length and size of these well pipelines are 2 km and 6 inches (outside diameter is 168.3 mm), respectively. The valves from the production tubing are represented by MCV, WCV, XCV and CVA, and the connecting pipes between valves are 10 m and 6 inches. The manifold is simulated as two pipe segments 10''-PIPE-100, 10''-PIPE-101. Dimensions are 10 and 100 m, respectively, and both segments are sized to 10 inches

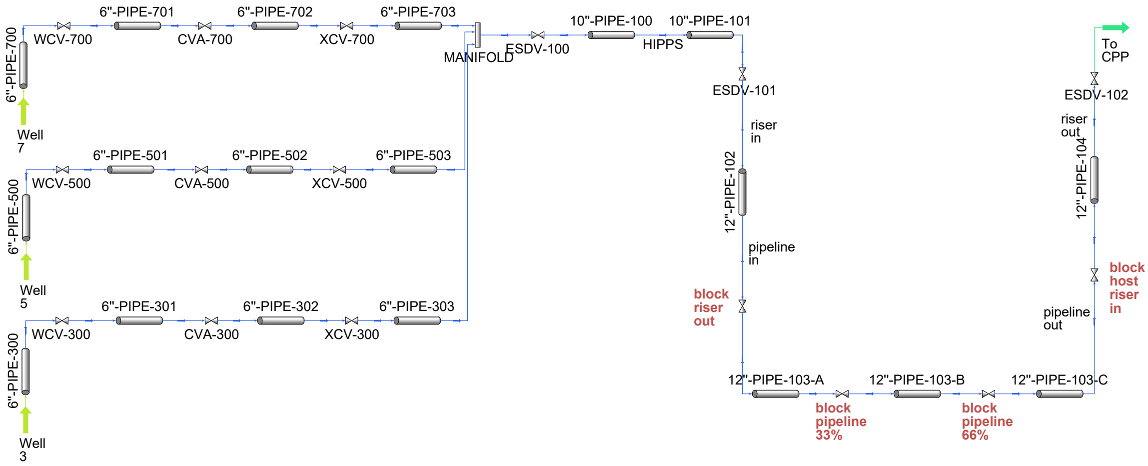

Figure 5.2: Aspen HYSYS Flowsheet set-up.

(outside diameter is 273 mm). The riser 12 inches (outside diameter is 323.8 mm), and it is represented by a vertical pipe of 70 m (12"-PIPE-102) carrying the fluids down to the bottom of the riser. The pipeline on the sea bed is a horizontal pipe of 9 km (12"-PIPE-103 A/B/C), wherefrom the host riser of 70 m routes the fluids up to the processing facility (12"-PIPE-104). Protection of the system is given by the illustrated ESD valves (ESDV), whereas the location of the HIPPS is represented by the stream called HIPPS. A summary of the dimensions of the modelled pipe segments is given in Table 5.3.

Table 5.3: Dimensions of pipe segments.

Location	Simulation name	Length (m)	Elevation (m)	Outer Diameter (mm)
Wellhead 3	6"-PIPE-300	2,000	2,000	168.3
	6"-PIPE-301	10	-	168.3
	6"-PIPE-302	10	-	168.3
	6"-PIPE-303	10	-	168.3
Wellhead 5	6"-PIPE-500	2,000	2,000	168.3
	6"-PIPE-501	10	-	168.3
	6"-PIPE-502	10	-	168.3
	6"-PIPE-503	10	-	168.3
Wellhead 7	6"-PIPE-700	2,000	2,000	168.3
	6"-PIPE-701	10	-	168.3
	6"-PIPE-702	10	-	168.3
	6"-PIPE-703	10	-	168.3
Manifold	10"-PIPE-100	10	-	273
	10"-PIPE-101	100	-	273
Riser	12"-PIPE-102	70	-70	323.8
	12"-PIPE-103 A/B/C	9,000	0	323.8
	12"-PIPE-104	70	70	323.8

5.2.3 Overpressure scenario

To evaluate the performance of HIPPS, the blockage of a pipe segment has been modelled. The blockage is represented as a valve that is 100% open during normal operation, so it does not restrict the flow along the pipeline. When the incident is simulated, the valve closes, leading to the over-pressurization of the process equipment upstream of the blockage. Four locations have been considered, as described in Table 5.4 and Figure 5.2.

Table 5.4: Scenarios locations of blockages.

Scenario	Simulation name	Description
S1	block riser out	Blockage occurs at the end of riser (i.e. inlet of seabed pipeline)
S2	block pipeline 33%	Blockage occurs at 1/3 of pipeline length
S3	block pipeline 66%	Blockage occurs at 2/3 of pipeline length
S4	block host riser in	Blockage occurs at the beggining of host riser (i.e. outlet of seabed pipeline)

The closure of the valve corresponding to the blockage in the line has been modelled using the Event Scheduler. The Event Scheduler is a tool implemented in Aspen HYSYS that allows the user to define and 'schedule' hazardous events at a desired simulation time. Figure 5.3 shows an example of how the blockage at the inlet of the bottom riser has been specified in the Event Scheduler tool.

Once the event is started by the user, the pressure will start to build-up. Even though the ESDVs are modelled in the flowsheet (see Figure 5.2), it is considered that they fail to activate and, consequently, the pressure keeps developing in the system. When the pressure in the system gets at the HIPPS alarm, there is a limited time that the HIPPS can utilize for closing its blocked valves before MAWP is reached, i.e. the PST.

5.2.4 Process Safety Time

The dynamic model for the assessment of HIPPS simulates a blockage in the pipeline, and records how the internal pressure develops accordingly if no safety barrier is added. The ESD and HIPPS alarms, as well as the MAWP, are fixed to a specific pressure value selected by the user. The time to arrive at those values of pressure is noted. Based on that, the PST can be calculated as the difference between the time at which the pressure of HIPPS alarm is reached (t HIPPS) (i.e. HIPPS is initiated), and the available time of the HIPPS for closing the block valves before MAWP (t MAWP), according to Equation 5.4 [48]. A representation of how the PST is calculated is illustrated in Figure 5.4.

$$PST = t_{MAWP} - t_{HIPPS} \tag{5.4}$$

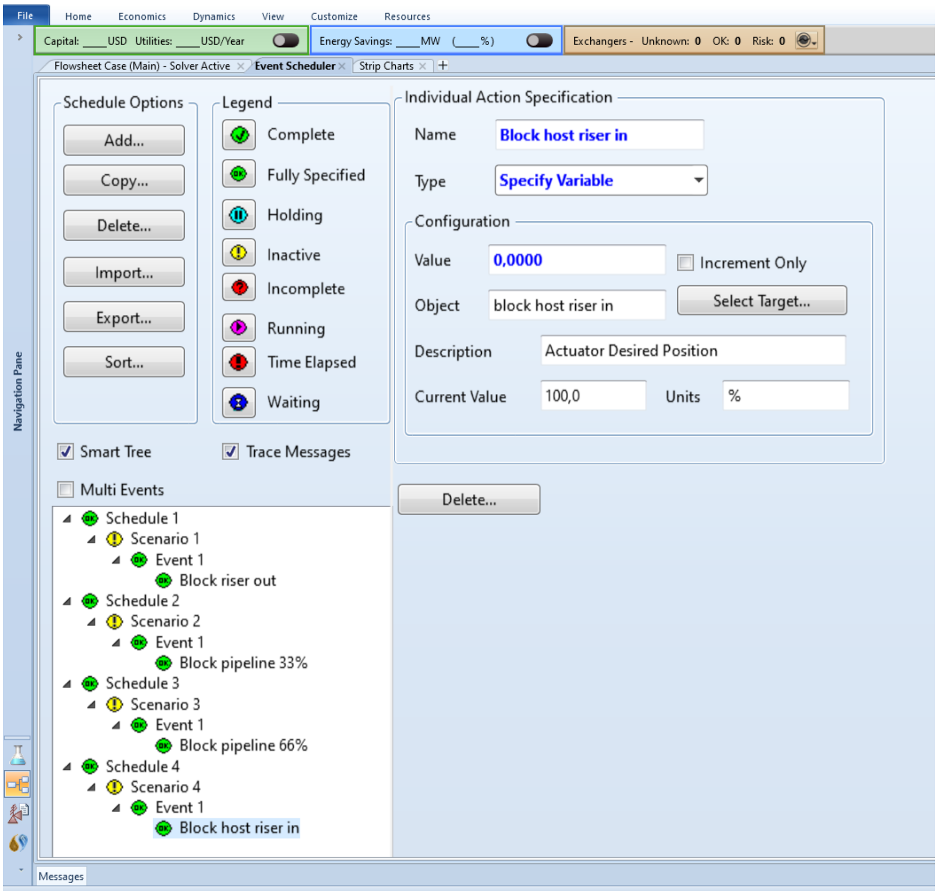

Figure 5.3: Event Scheduler. Individual Action Specification: simulation of overpressure scenario.

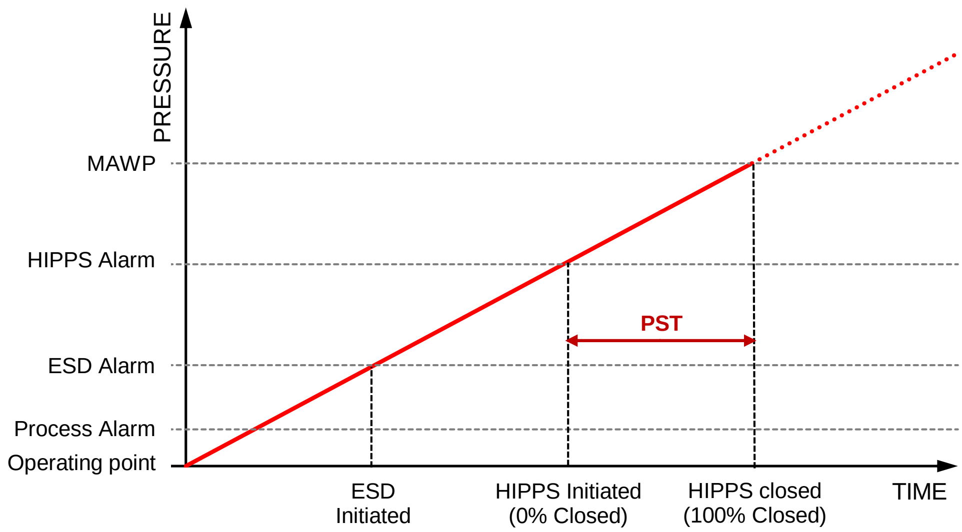

Figure 5.4: Representation of pressure development in a pipeline over time, and calculation of Process Response Time (PST).

5.2.5 ESD and HIPPS settings

For the modelled system, the following pressure settings have been specified:

- ESD alarm is set to 140 bar
- HIPPS alarm is set to 155 bar
- Design pressure of the equipment (MAWP) is set to 170 bar

5.2.6 Boundary stream conditions

The boundaries of the system are the three well inlets (*Well 3*, *Well 5*, and *Well 7*) and the outlet stream (*To CPP*), as can be seen in Figure 5.2. When running the dynamic simulations, the boundary stream specifications are to be defined. The explanation behind the selected dynamic specifications is given next.

- The inlets are specified as fixed flow sources. It is the purpose of the model to investigate the pressure development in the system when an overpressure scenario is occurring. By fixing the flow sources, a constant mass rate throughout the system will be simulated. Therefore, no unsteady inflow will influence the pressure development in the system.
- The outlet is specified as fixed pressure sources. When a blockage occurs, the pressure starts to build up in the process equipment located upstream of the obstruction. In order to avoid the possible pressure surges coming from an upstream condition, a pressure boundary is set for the outlet stream.

5.2.7 Pipe flow correlations

The interest in using dynamic simulations to describe the consequences derived from an overpressure scenario relies on the possibility of modelling the process piping in such a way that variations in system volumes and pressure development over time can be accounted. Water (aqueous phase) is not part of the scope of the present study, so a two-phase flow (vapor and liquid) can be found in the modelled HIPPS network. A large number of two-phase flow correlations for estimating the pressure drop across the pipe segment are found in Aspen HYSYS. Therefore, it is also part of the scope of Part II, the evaluation of the influence of the prediction of flow correlations in the time response of HIPPS. Since both vertical and horizontal flows are considered in the pipe segments of the HIPPS model, four pipe flow correlations will be investigated: Beggs & Brill (1973), Beggs & Brill (1979), Heat Transfer and Fluid Flow Service (HTFS), and Tulsa Unified Model.

Case 1. Beggs & Brill (1973)

Beggs & Brill is an empirical correlation that predicts the pressure gradient by considering two factors: two-phase friction factor and liquid holdup. These parameters are estimated based on pressure drop correlations associated with the type of flow of the mixture across the pipe, which is based on the liquid content and the Froude number [71, 72]. Additionally, it allows the user to calculate the acceleration pressure drop in the segment. This correlation provides more sensitive results when considering inclined pipes [73].

Case 2. Beggs & Brill (1979)

Beggs & Brill (1979) is an improvement of Beggs & Brill (1973) correlation. It now takes into consideration the Frictional Pressure drop correction for rough pipes and the Liquid holdup correction for uphill and downhill pipes developed by Payne et al. [74]. Due to simplicity, Beggs & Brill (1979) is the default method in the pipe segment unit operation in Aspen HYSYS. However, experimental results have proven that Beggs & Brill (1979) tends to over-predict the pressure gradient, even though the estimation of the liquid hold-up has been improved [73].

Case 3. HTFS Homogeneous

Heat Transfer and Fluid Flow Service (HTFS) Homogeneous is a mechanistic correlation that has proven to give good estimations of pressure gradient and liquid holdup, but considers the process fluid as a homogeneous phase [72].

Case 4. Tulsa Unified Model

The Tulsa Unified Model is a mechanistic correlation that can predict the pressure gradient and liquid holdup by taking into account the phase distribution and flow patterns of the mixture [75]. This model has been tested in more than two thousand wells covering a wide range of field data and geometries with very accurate results [72, 73].

Case 5. Simplified Pipe Friction Model

The use of simplified pipe friction models, such as full range Churchill or turbulent models, instead of robust pipe flow correlations (as shown in Cases 1 to 4), is convenient from the simulation convergence and computing time points of view. Simplified pipe friction model can predict the pressure gradient as a function of Reynolds number and shear stress on the pipe wall [76].

5.3 Simulated Case Studies (Part II)

The importance of the choices made when building the simulations, in terms of flow correlation/pipe models and level of detail (i.e. pipe elevations, fittings, etc.) is now assessed. The target is to be able to build an effective model, as simple as possible (less prone to errors), that can provide the reliable results of the time response for valve closure (PST). For that, the following would be the desired results:

1. The same PST is found on whether full details of the piping system are implemented or not. Consequently, the need for specifying the elevation, fittings, etc. as given in isometrics can be eluded.
2. All flow correlation/pipe models give the same or similar prediction despite the consideration of different flow rates, operating conditions or compositions, etc.

For that, the system volumes and piping configurations are analysed as explained in Section 5.3.1 and Section 5.3.2, respectively.

5.3.1 Evaluation of mass flow

The flow through the wellheads is evaluated considering mass flows ranging from 100,000 to 200,000 kg/h. This part of the study aims to evaluate the influence of different flow loads in the performance of HIPPS. For that, the PST is calculated for the 4 locations of blockage and the 5 pipe models described in Section 5.2.3 and Section 5.2.7, respectively, and results are compared. All simulations have been performed using Aspen HYSYS Dynamics, based on variations of the HYSYS flowsheet illustrated in Figure 5.2.

5.3.2 Evaluation of the piping layout

When building a model comprising pipe segments, data such as elevations/inclination or fittings sourced from the piping isometrics can be specified. The configuration of the piping layout and its influence in the response of HIPPS is now assessed. This evaluation is a sensitivity analysis of the level of specification required in the simulation, meaning that the author aims to analyse the need of specifying all elevations in the piping segments even though there is no change in static pressure. The pipe segment of the manifold 10"-PIPE-101 – which is 100 meters long – is now broken down in 10 internal segments, where different vertical to horizontal (V/H) ratios are considered, always keeping the static pressure within the pipe equal to 0. For example, a V/H ratio of 20% would be specifying 10 meters of pipe flowing upwards + 10 meters of pipe flowing downwards, with 80 meters being horizontal flow.

The PST is calculated for the 4 locations of blockage and the 5 pipe models described in Section 5.2.3 and Section 5.2.7, respectively, and results are compared. All simulations have been performed using Aspen HYSYS Dynamics, based on variations of the HYSYS flowsheet illustrated in Figure 5.2.

Chapter 6

Results and Discussion Part I

A study of debottlenecking on existing flare systems

The results obtained for the full plant emergency depressurization of the flare system of three facilities are presented and discussed in this chapter. The results correspond to the paper prepared during the course of the Master Thesis (see Appendix A).

6.1 Facility A

The full plant emergency depressurization of Facility A is modelled as shown in Figure 4.2. Three simulations are conducted considering the three cases exposed in Section 4.1.5: Steady state, Dynamics (without dead ends), and Dead ends. Additionally, the process simulation flowsheets for Facility A as modelled in Aspen HYSYS are illustrated in Figure B.1 and Figure B.2 from Appendix B. A comparison of the results for the mass flow at the flare tip is given in Figure 6.1, where time 0 represents the initiation of the depressurization operation.

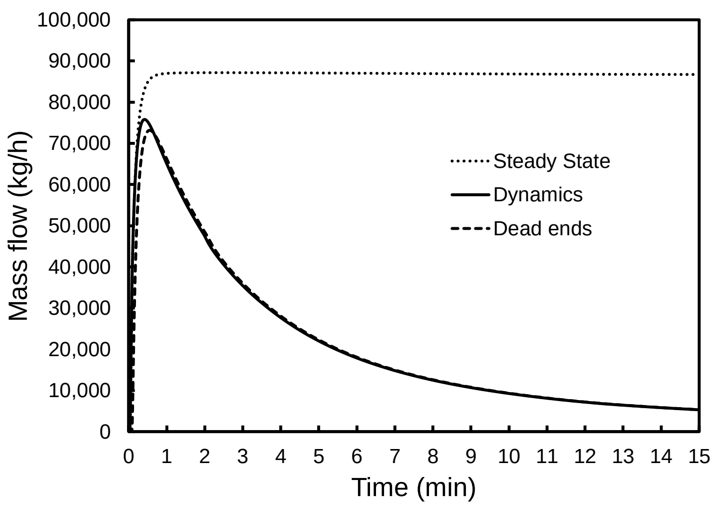

Figure 6.1: Comparison between calculated mass flow rate at the flare tip for Facility A, using steady state, dynamic simulations without dead ends, and dynamic simulations including dead ends.

On the one hand, according to Figure 6.1, results of the steady-state simulation represent the conventional steady-state approach that has been traditionally imposed, where the maximum design rate at the flare tip is calculated as the sum of all pressure-relieving sources disposing simultaneously. The steady-state value for the maximum mass flow at the flare tip is 87,165 kg/h (72.8 MMSCFD). On the other hand, the results of the dynamic approach (both without and with dead ends) show how the mass flow at the flare tip increases rapidly to a maximum value at a time between 0.5-1 min. Then, the flow reaching declines as the inventory is disposed via flare. The peak mass flow is reduced to 75,795 kg/h (63.2 MMSCFD). The differences in the peak mass flow can be explained by the line packing effect occurring in the flare network. The same behaviour was reported in previous studies made by Andreasen [45] and Wasnik et al. [23].

When adding an extra level of complexity to the model given by the addition of PSVs, PCVs and dead-ends (i.e. Dead ends case), the volume hold-up of the modelled piping increases to 7.8 m^3 (from 19.2 m^3 to 27 m^3). It is noted that the peak mass flow is reduced to 73,171 kg/h (61.1 MSCFD). The reason behind this is the contribution to a bigger line-packing potential given by the increased hold-up volume. In relative numbers, a reduction of 13% and 16.1% can be obtained when benchmarking the steady-state simulation with the dynamic and dead-ends simulations, respectively.

The backpressure in various places of the flare network, calculated by the steady state and the dynamic state models, is shown in Figure 6.2. The backpressure of the dead-ends case is not presented, as results are expected to be the same as the obtained for the dynamic simulation (see Figure 6.2(B)).

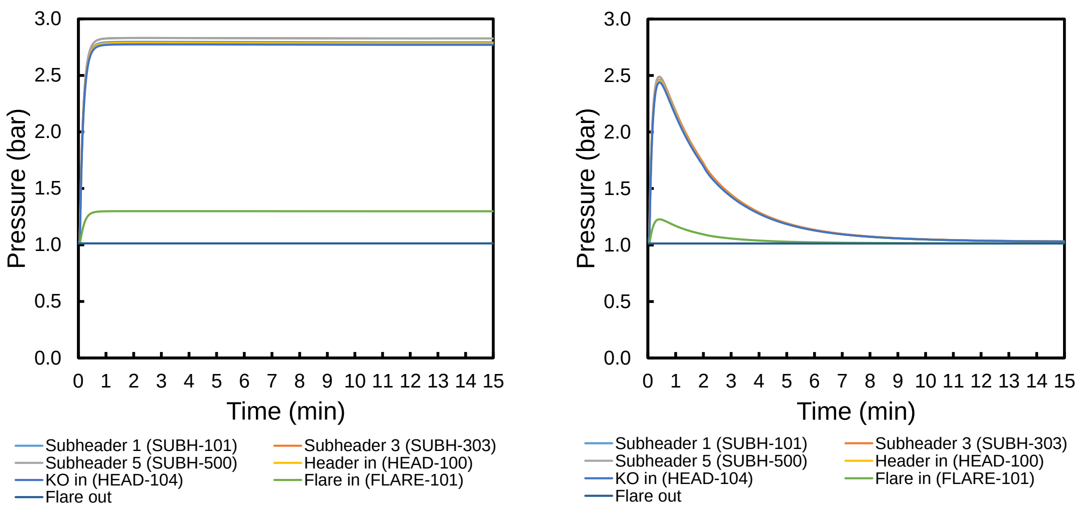

(A) **(B)**

Figure 6.2: Comparison between calculated backpressure in various places of the flare network for (A) steady-state and (B) dynamic simulations for facility A.

Backpressure is created in the system as a result of the pressure drop existing in the flare tip. Therefore, since the selected places represented in Figure 6.2 are subheaders, headers, and the flare header, the influence of the dead ends in the backpressure for the selected places are negligible. As seen in 6.2, the peak backpressure is lower than the corresponding steady-state value. For the subheaders and headers, it is reduced from a maximum of 2.85 bar to 2.50 bar (approx. 12% reduction). This reduction in peak backpressure given by the dynamic approach was reported before by Wasnik et al. [23].

6.2 Facility B

The full plant emergency depressurization of Facility B is modelled as shown in Figure 4.3. Three simulations are conducted considering the three cases exposed in Section 4.1.5: Steady state, Dynamics (without dead ends), and Dead ends. Additionally, the process simulation flowsheets for Facility B as modelled in Aspen HYSYS are illustrated in Figure B.3 and Figure B.4 from Appendix B.

A comparison of the results for the mass flow at the flare tip is given in Figure 6.3, where time 0 represents the initiation of the depressurization operation. The steady-state value for the maximum mass flow at the flare tip is 308,640 kg/h (303.1 MMSCFD). Again, the results of the dynamic approach (both without and with dead ends) show how the mass flow at the flare tip increases rapidly to a maximum value at a time between 0.5-1 min. The calculated peak mass flow is 266,970 kg/h (262.2 MMSCFD) and 264,311 kg/h (259.5 MSCFD) for the dynamic and dead ends simulations, respectively. The increase in volume hold-up due to the addition of PSVs, PCVs and dead ends has increased to 24 m^3 (from 126 m^3 to 150 m^3). In relative numbers, a reduction of 13.5% and 14.4% can be obtained when benchmarking the steady-state simulation with the dynamic and dead-ends simulations, respectively. The same reasoning as the given for the Facility A applies.

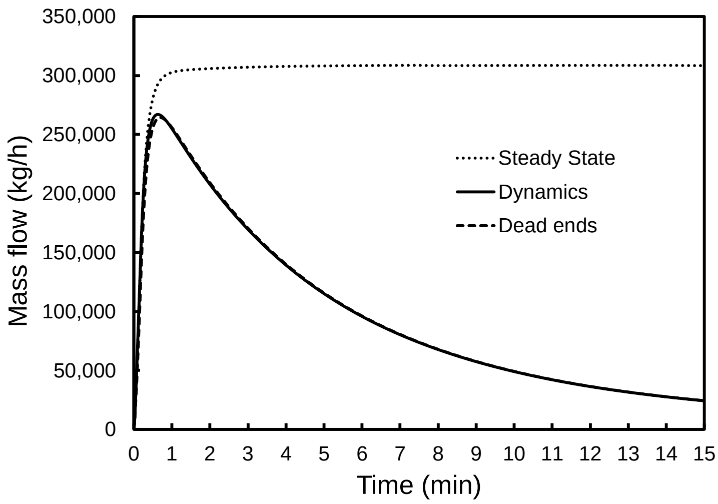

Figure 6.3: Comparison between calculated mass flow rate at the flare tip for Facility B, using steady state, dynamic simulations without dead ends, and dynamic simulations including dead ends.

The backpressure in various places of the flare network, calculated by the steady state and the dynamic state models, is shown in Figure 6.4. Again, the peak backpressure is lower than the corresponding steady-state value. The maximum backpressure is found in Subheader 2 (SUBH-207) and Subheader 5 (SUBH-501). For the Subheader 2, the peak backpressure is reduced from 10.96 bar to 9.85 bar (10% reduction), whereas for Subheader 5, it is found a 11.3% reduction (from 7.15 bar to 6.35 bar).

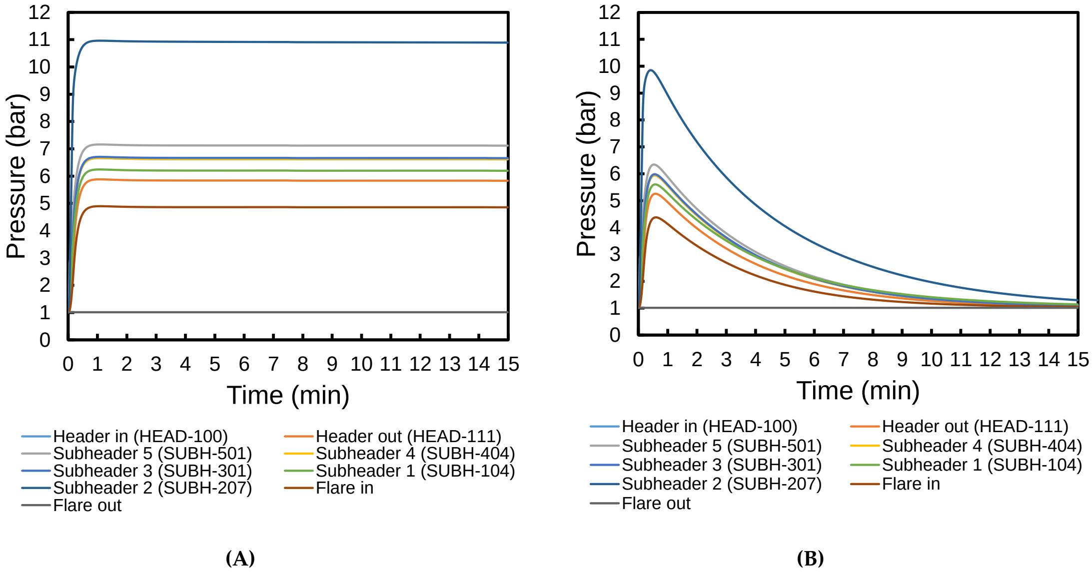

Figure 6.4: comparison between calculated backpressure in various places of the flare network for (A) steady-state and (B) dynamic simulations for facility B.

6.3 Facility C

The full plant emergency depressurization of Facility C is modelled as shown in Figure 4.4. The steady-state simulation is benchmarked against the dynamic simulation. The details available for Facility C has not allowed an analysis of the effect of dead-ends. Additionally, the process simulation flowsheet for Facility C as modelled in Aspen HYSYS is illustrated in Figure B.5 from Appendix B.

A comparison of the results for the mass flow at the flare tip is given in Figure 6.5, where the depressurization operation is started at 30 seconds. The mass flow at the flare tip increases rapidly to a maximum value within 0.5-1 min for the dynamic simulation. The results also show a reduction in peak mass flow at the flare tip when considering a dynamic approach. The mass peak flow for the steady state and dynamic simulations are 676,473 kg/h (303.1 MMSCFD) and 511,989 kg/h (262.2 MMSCFD), respectively, which corresponds to a reduction of 24.3%. The same reasoning as the given for the Facility A applies.

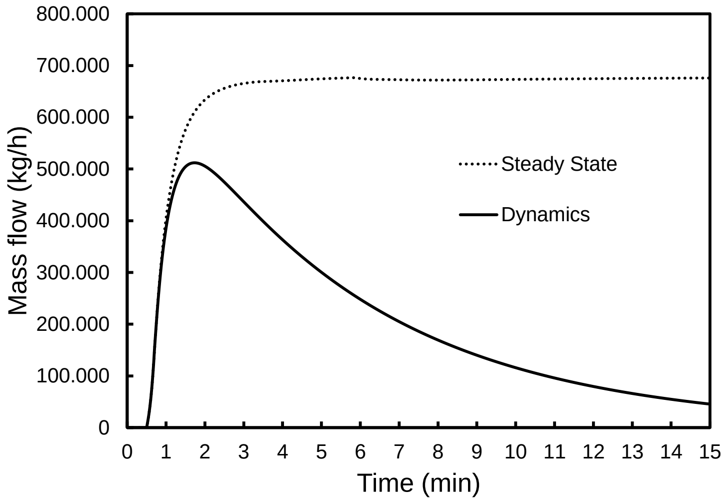

Figure 6.5: Comparison between calculated mass flow rate at the flare tip for Facility C, using steady state, dynamic simulations without dead ends, and dynamic simulations including dead ends.

The backpressure in various places of the flare network, calculated by the steady state and the dynamic state models, is shown in Figure 6.6. Again, the peak backpressure is lower than the corresponding steady-state value. For example, for the Header-1, it is reduced from bar 14 bar to 10.5 bar (25% reduction).

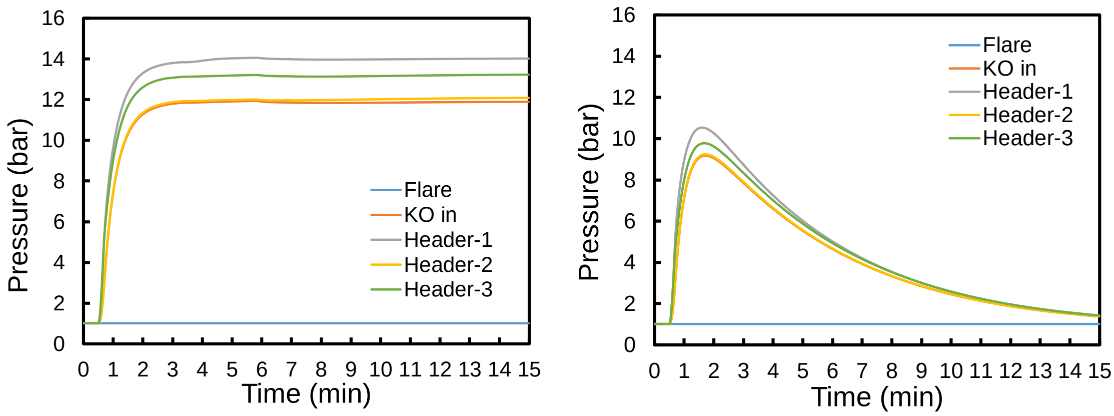

(A) **(B)**

Figure 6.6: comparison between calculated backpressure in various places of the flare network for (A) steady-state and (B) dynamic simulations for facility C.

6.4 Discussion of results

The results from the analysis of all three facilities are summarized in Table 6.1, where the main result is the hidden potential for debottlenecking, calculated as the relative difference in capacity found between the steady state (SS) and the dynamic simulations (Dyn.). In addition, the dimensions of the three simulated flare networks, with and without dead-ends, are also included. Parameters such as the total length (L_{net}) and the average diameter

(D_{mean}) of flare network piping and the total hold-up volume of the system (V_{tot}) are presented in 6.1. The average diameter is found from a weighted average with individual piping diameters weighted by their corresponding pipe length, whereas the total hold-up volume is calculated as the sum of the hold-up volume (V_{pipe}) of the modelled piping and the hold-up volume of the KO drum (V_{KO}).

Table 6.1: Summary of model details and modelling results for all three investigated facilities.

		Model dimensions					**Peak flare rate**		**Hidden potential**	
Facility	Dead end	L_{net} (m)	V pipe (m^3)	V_{KO} (m^3)	V_{tot} (m^3)	D_{mean} (inch)	SS (MMSCFD)	Dyn. (MMSCFD)	(MMSCFD)	(%)
A	no	288	19.2	79.4	98.6	10.5	72.8	63.2	9.5	13.0
	yes	497	27.0	79.4	106.4	9.3	72.8	61.1	11.7	16.1
B	no	1,457	126.0	50.5	176.6	11.7	303.1	262.2	40.9	13.5
	yes	2,034	150.0	50.5	200.5	10.7	303.1	259.5	43.5	14.4
C	no	2,686	359.6	103.3	462.9	15.3	733.2	555.0	178.2	24.3

Comparison of all modelled facilities

The three investigated flare systems are different from each other in terms of number of blowdown segments, dimensions, and system design load. The flare systems of Facility A, Facility B, and Facility C have 13, 24, and 43 BDVs discharging inventory upon depressurization, respectively. In this study, there is a direct relationship between the number of BDV segments and the size of the facility. A higher number of BDV sources involves a larger flare design rate, which in turn also involves a larger facility in terms of volume of the system. The increase in volume piping can be also seen from the point of view of a larger average piping diameter and longer piping being required in the system. Therefore, in terms of capacity and total volume of the system, the order of the facilities is the following: A < B < C.

The results of the simulations show that a higher potential for debottlenecking can be found when considering a larger flare design rate (steady-state design value), especially considering the absolute value of the hidden potential. The main reason behind this trend is the contribution to a bigger line-packing potential given by the increased hold-up volume. In relative terms, results for Facility A and Facility B are similar and exhibit hidden potential of the same ranges of approx. 13% and 16%, depending on whether dead ends are included or not. Conversely, Facility C displays a higher relative reduction of approx. 24.3% in flare rate.

With regards to backpressure, higher backpressures translate into more resistance for the flowing of the relieving fluids towards the flare. The highest backpressure can be found in Facility C (see Figure 6.6), whereas the lowest backpressure is observed in Facility A (See Figure 6.2). As a result of the line packing effects in the hold-up volume of the flare systems, a reduction in backpressure can also be observed for all investigated facilities.

Influence of dead ends in the model

Facility A and Facility B are modelled considering also the inclusion of PSVs, PCVs and dead ends (inactive sources) in the model. The available data for Facility C has not allowed the analysis of the effects of dead-ends.

According to the simulation results, Facility A is designed for a design load of 72.8 MMSCFD (87,165 kg/h) (steady-state value), whereas Facility B is designed for a higher design rate of 303.1 MMSCFD (308,640 kg/h). For both facilities, a higher hidden potential is found when considering the dead-ends in the model: 2.2 MMSCFD and 2.6 MMSCFD are revealed for Facility A and Facility B, respectively. This can be justified by the effect of pressure-relieving fluids flowing back into the inactive tailpipes of the PSVs, PCVs or deade ends (i.e. reverse flow effect). Therefore, a higher capacity of the system can be revealed if the simulation model is built considering all system volumes. However, using a less complex model is conservative.

From another perspective, even though a higher reduction in flare rate is found in Facility B given by the higher design rate and larger system volume, the comparison of the reduction in flare rate is less significant in relative numbers. The addition of dead ends for the Facility A results in a reveling potential of 16.1% for an extra volume of 7.8 m^3, whereas for Facility B is 14.4% for an increase in volume of 24 m^3. Although not conclusive, this might suggest that a more accurate and detailed model is more important for a smaller facility.

Synthesis of results

The hidden potential for debottlenecking (i.e. difference between the steady-state design rate and the dynamic mass peak flow calculated using a dynamic approach) is represented in Figure 6.7 as a function of the steady-state design rate, for all three investigated facilities (with and without ends).

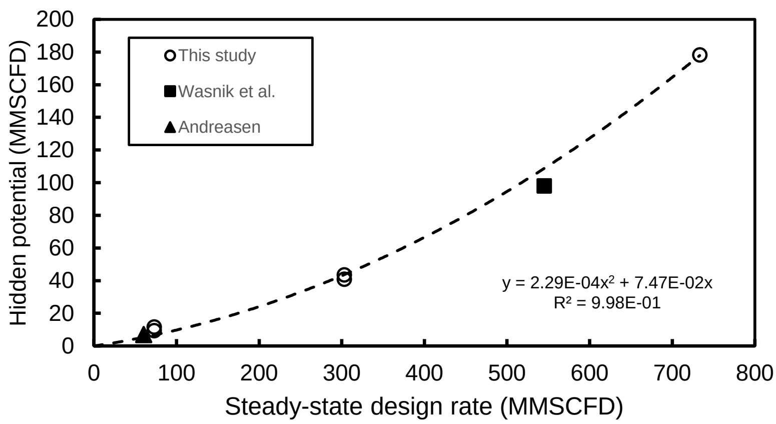

Figure 6.7: The hidden potential for debottlenecking as a function of steady-state design rate. Previous studies from Andreasen [45] and Wasnik et al. [23]

The data has been fitted using a second-order polynomial regression with a forced intercept at zero. Additionally, it has also been included previous studies reporting flare rate reductions from using dynamic approaches conducted by Andreasen [45] and Wasnik et al. [23] for comparison. Note that these two previous studies are included for benchmarking of the proposed relationship, and they are not included in the regression analysis.

As observed in Figure 6.7, the reduction in peak flow at the flare tip can be related to a quadratic relationship between the flare system design rate and the corresponding debottlenecking potential. Future studies on the subject should be conducted to confirm this quadratic trend.

Chapter 7

Results and Discussion Part II

A study of the performance of a High Integrity Pressure Protection System

The results obtained for the dynamic simulations of HIPPS valve closing times are presented and discussed in this chapter. Four locations of blockage (refer to Section 5.2.3) and five pipe models (see Section 5.2.7) are considered, and they are summarized in Table 7.1.

Table 7.1: Summary of scenarios and case studies considered in the evaluation of HIPPS.

Scenario	Short description
S1	block riser out
S2	block pipeline 33%
S3	block pipeline 66%
S4	block host riser in

Case	Pipe correlation/model
Case 1	Beggs & Brill (1973)
Case 2	Beggs & Brill (1979)
Case 3	HTFS Homogeneous
Case 4	Tulsa Unified Model
Case 5	Simplified Pipe Friction Model

7.1 Evaluation of mass flow

The flow through the wellheads is evaluated considering different inflows of 100,000 kg/h, 150,000 kg/h, 180,000 kg/h, and 200,000 kg/h in each of the well inlets. The blockages occur at different lengths of the seabed pipeline that connects the manifold with the CPP (see Figure 5.2).

An example of the simulation results

An example to introduce the results is shown in Figure 7.1, which considers the case of mass flow inlet fixed to 100,000 kg/h per well and a blockage occurring at 33% of the seabed pipeline (Scenario 2). Figure 7.1 shows the results of pressure developed in the system when no safety barrier is added. The pressure drop in the system is calculated using the pipe flow correlation Beggs & Brill (1973) (Case 1). Time 0 refers to the time when the blockage starts. As expected, pressure starts to build up upstream the blockage (*Well inlet* and *Manifold*) as a result of the flow being obstructed and the possible occurrence of reverse flow. Given that the HIPPS valve is located in the manifold, before entering the riser, the PST is calculated considering the difference between the time when HIPPS is triggered (155 barg) and the time when MAWP is reached (170 barg). For the given case, the PST is 56 seconds. All other cases of mass flow and blockage scenarios have been computed similarly.

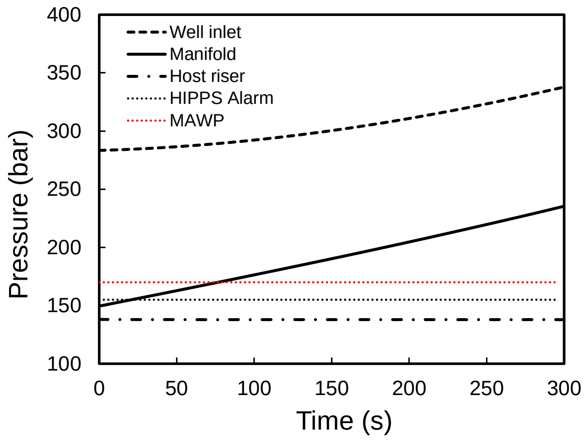

Figure 7.1: Pressure development in the system for a well-feed of 100,000 kg/h and blockage Scenario 2, considering Case 1 pipe correlation (Beggs & Brill (1973)).

Analysis 1: 100,00 kg/h

The results for the pressure development in the manifold for a well-feed of 100,000 kg/h are shown in Figure 7.2. Note that the example presented in Figure 7.1 corresponds to Case 1 of Figure 7.2(B).

As it can be seen in Figure 7.2, the dynamic simulations show that the pressure builds up at an almost constant rate for all cases. Additionally, near similar pressure development trends are found when considering different pipe correlations (Case 1–4) and the simplified pipe friction model (Case 5) for the different evaluated scenarios. Slight differences between the pipe models appear only when blockage locations are further from the manifold (i.e. as the distance between manifold and blockage becomes larger). This is because a larger pipe length is to be considered and each of the pipe models will estimate a different pressure drop across the pipe.

With regard to the time for HIPPS closure, the pressure development over time is much faster in Scenario 1 (see Picture 7.2(A)). Even though the same mass inflow (100,000 kg/h per well) is considered, a slower pressure build up is found when the blockage occurs at a longer distance from the manifold. This translates into a longer response time, and it can be attributed to a buffer volume effect given by the gas phase in the pipeline counter-acting and delaying the reverse flow towards the manifold.

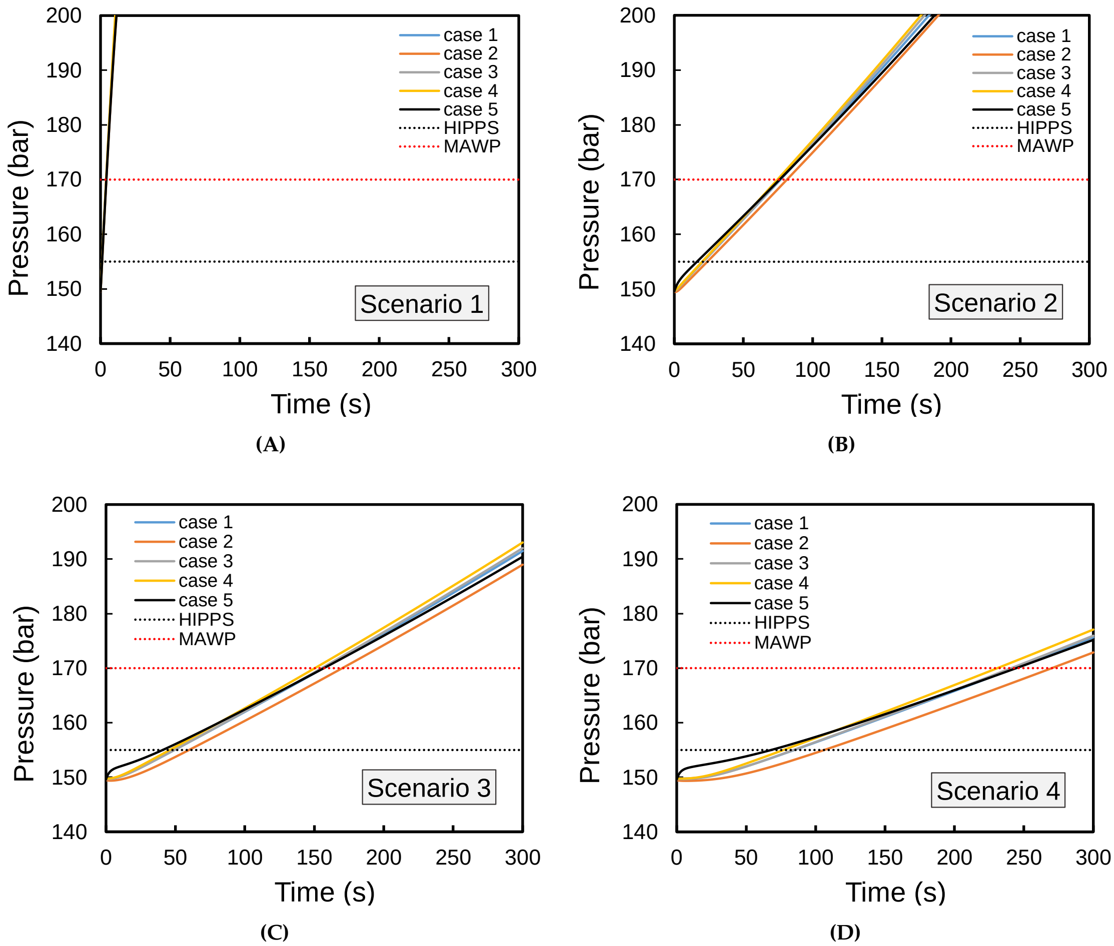

Figure 7.2: Comparisson of pressure development in the manifold considering well feed of 100,000 kg/h for (A) Scenario 1, (B) Scenario 2, (C) Scenario 3 and (D) Scenario 4.

Analysis 4: 200,00 kg/h

The results considering a mass flow of 200,000 kg/h are given in Figure 7.3. The results for the cases of 150,000 kg/h (Analysis 2) and 180,000 kg/h (Analysis 3) are presented in Appendix C. A higher volume in the system results in less time available for HIPPS closure. This can be observed in Figure 7.3, where lines are more pronounced than in the case of 100,000 kg/h (see 7.2). When comparing the results from the case of 100,00 kg/h (see Figure 7.2) and 200,000 kg/h, it is observed a larger degree of deviation between pipe models as larger system volumes are considered. This can be explained considering that a higher volume in the system will result in a higher pressure drop across the pipe segments, and each of the pipe models will calculate it differently.

As observed in Figure 7.3, the trend now diverges from linearity for all pipe flow correlations (Case 1–4) investigated, i.e. the pressure does not start developing right after the blockage, in fact, either no slope or a smaller slope is found before the pressure starts increasing at a constant rate. The simplified pipe friction model (Case 5) does not follow the same trend. Case 5 uses the Reynolds number and the friction factor to calculate the pressure gradient in the system. Therefore, it does not account for the type of flow inside the pipe segment or the volume holdup, so the predictions using Case 5 might not be representing the actual fluid behaviour inside the pipe.

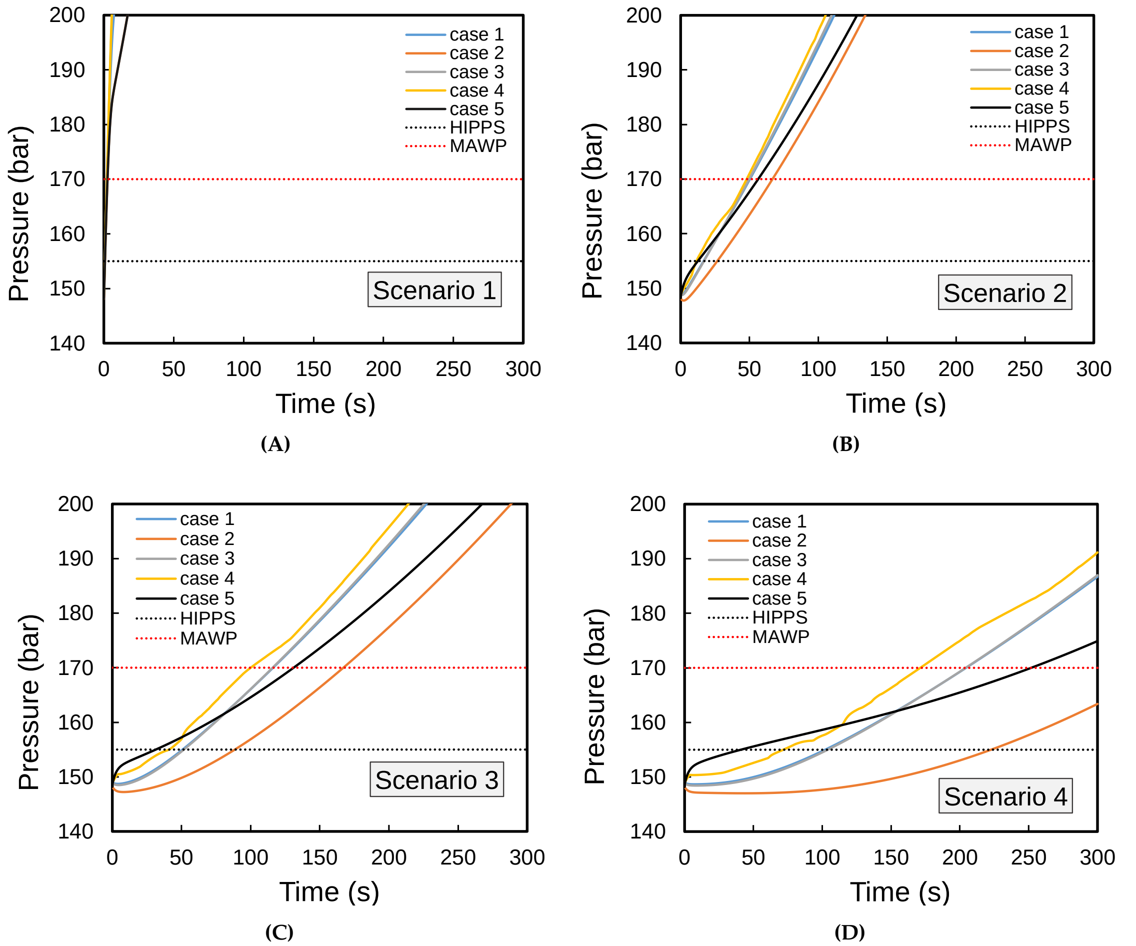

Figure 7.3: Comparisson of pressure development in the manifold considering well feed of 200,000 kg/h for (A) Scenario 1, (B) Scenario 2, (C) Scenario 3 and (D) Scenario 4.

For all simulations conducted, Case 4 (Tulsa Unified Model) estimates a faster rate of pressure increase. It shall be noted that the deviations from a smooth line observed for the Case 4 do not have any physical meaning and might be due to numerical instabilities in Aspen HYSYS V9. The results of Case 1 and Case 3 are overlapping, so both predict a similar PST. Case 2 (Beggs & Brill (1979)) shows that the pressure build-up is considerably slower than for the rest of the cases. Several studies have reported that Beggs & Brill (1979) correlation tends to over-predict the pressure gradient, and this is what might have led to a slower rate of pressure increase (i.e. longer response time).

Comparison of process response time (PST)

The summary of calculated PST for all analyzed mass flows (100,000 kg/h, 150,000 kg/h, 180,000 kg/h, and 200,000 kg/h in each of the well inlets), the 5 pipe models (Case 1–5) and the 4 scenarios (Scenarios 1–4) is given in Table 7.2. A representation of Table 7.2 is illustrated in Figure C.3 of Appendix C. The previously mentioned observations can be supported in terms of PST:

- The higher the well-feed mass inflow, the lower the response time of the HIPPS to overcome the overpressure scenario.
- The further the blockage occurs, the more available time.

Table 7.2: Comparison of PST calculated for different blockage scenarios and well-feed mass flow rates.

Mass flow	**Scenario 1**				
(kg/h)	**case 1**	**case 2**	**case 3**	**case 4**	**case 5**
100,000	3.02	3.03	2.98	2.96	3.05
150,000	2.03	2.09	1.99	1.98	2.11
180,000	1.72	1.84	1.63	1.67	1.87
200,000	1.58	1.79	1.48	1.50	1.83

Mass flow	**Scenario 2**				
(kg/h)	**case 1**	**case 2**	**case 3**	**case 4**	**case 5**
100,000	56.0	57.6	55.1	54.5	59.8
150,000	40.2	43.6	39.4	39.2	46.8
180,000	35.6	40.7	34.8	33.0	44.4
200,000	33.6	40.0	32.8	36.4	43.7

Mass flow	Scenario 3				
(kg/h)	**case 1**	**case 2**	**case 3**	**case 4**	**case 5**
100,000	107.3	110.4	106	104.5	116.0
150,000	77.3	84.3	76.1	74.5	98.3
180,000	69.0	79.3	67.6	64.8	98.1
200,000	65.5	78.5	64.1	59.1	99.7

Mass flow	**Scenario 4**				
(kg/h)	**case 1**	**case 2**	**case 3**	**case 4**	**case 5**
100,000	158.5	164.0	156.8	154.1	176.6
150,000	116.5	130.1	114.5	110.9	167.6
180,000	105.9	126.8	103.9	98.3	182.1
200,000	102.3	127.7	100.3	99.6	210.9

The accuracy in the calculation of PST must be ensured, given that HIPPS is often required to close within a maximum of 2 seconds [49]. For the same conditions (fixed mass flow analysis and scenario), the sensitivity of the results increases as higher system volumes are considered. This means that for the lowest mass flow analysis, the differences between PST are not that significant unlike for the highest load case. With regards to the differences between the selected pipe models:

- Case 1 (Beggs & Brill (1979)) and Case 3 (HTFS Homogeneous flow) predict a similar PST, differing in a maximum of approx. 6% in relative numbers for all considered cases.
- Case 2 (Beggs & Brill (1979)) estimates a higher PST in comparison with the rest of pipe flow correlations (Case 1–4). This is attributed to the over-estimation of the pressure drop given by Case 2, which in turn results in a slower pressure build-up over time, thus predicting a higher PST.
- Case 4 (Tulsa Unified Model) generally predicts a lower PST than the rest of the pipe flow correlations. For Scenario 2 and Scenario 4, the PST increases when considering 180,000 kg/h & 200,000 kg/h. The expected result should have been a reduction in the available response time as a result of the mass flow rate increases. This finding might be a consequence of the numerical instabilities found for this case (see Figure 7.3).

- Case 5 (simplified pipe friction model) estimates a much higher PST than the rest of the pipe flow correlations. This suggests that the simplification made by using a simplified pipe friction model might not give reliable results.

7.2 Evaluation of the piping layout

The results for all cases of piping layout and blockage scenarios have been computed similarly, considering a fixed well-feed inflow of 150,000 kg/h and different vertical to horizontal (V/H) ratios for a 100 meters segment located in the manifold (10"-PIPE-101, refer to Figure 5.2). The results of PST for different V/H ratios, which aim to reflect the influence of specifying elevations and pipe orientations, are given in Table 7.3.

Table 7.3: Comparison of PST calculated for different blockage scenarios and V/H ratios.

V/H	Scenario 1				
(%)	case 1	case 2	case 3	case 4	case 5
0	2.03	2.09	1.99	1.98	2.11
20	2.03	2.08	1.99	1.97	2.09
50	2.02	2.08	1.99	1.97	2.09
80	2.03	2.08	1.99	1.97	2.08

V/H	Scenario 2				
(%)	case 1	case 2	case 3	case 4	case 5
0	40.2	43.6	39.4	39.2	46.8
20	40.2	43.6	39.4	39.2	46.8
50	40.2	43.6	39.4	39.3	46.7
80	40.1	43.6	39.4	39.3	46.9

V/H	Scenario 3				
(%)	case 1	case 2	case 3	case 4	case 5
0	77.3	84.3	76.1	74.5	98.3
20	77.3	84.3	76.1	74.5	98.1
50	77.3	84.3	76.1	74.3	98.0
80	77.3	84.3	76.1	74.2	97.9

V/H	Scenario 4				
(%)	case 1	case 2	case 3	case 4	case 5
0	116.5	130.1	114.5	110.9	167.6
20	116.5	130.0	114.5	111.5	167.3
50	116.6	129.9	114.5	110.2	166.7
80	116.6	130.0	114.5	110.5	166.3

As it can be observed in Table 7.3, almost no variations in PST are found, even though slight differences are found when further distances and more system volume are considered. Pipe flow correlations (Case 1–4) do not show almost any sensitivity to the specifications. However, Case 5 shows more sensitivity with the piping layout choices. This suggest that the selection of a simplified pipe friction model is more subjected to variations the isometrics/elevations.

7.3 Discussion of results

Based on the obtained results, the importance of the choices made when building the simulations, in terms of pipe models and level of detail (i.e. pipe elevations, fittings, etc.) is now discussed.

The use of a simplified pipe friction models (Case 5) is preferred from a modelling point of view, as it is a more simple model that requires less computational time. However, results have shown an over-estimation of the PST outside the ranges of PST calculated for the pipe flow correlations (Case 1–4). This suggests that the use of simplified pipe friction models might not give a reliable result of the PST. With regards to the results for the pipe flow correlations (Case 1–4), little variations are found, even though the dissimilarities between pipe flow correlations increase as larger system volumes and further locations of blockage are considered. However, results for Case 2 show the over-prediction of pressure drop that was reported before by other authors [73]. Therefore, to preserve conservatism, the simulations suggest the selection of the Tulsa Unified Model (Case 4), since it is the one that gives less PST.

With regards to the required level of detail, the simulations results using different pipe flow correlations reveal a little influence of the piping elevations in the PST. Although Case 5 presents slight variations in the PST with the increase in V/H piping ratio, the results might not be accurate, and it is left aside from this discussion. It shall be noted that V/H ratios are only specified in one pipe segment of 100 m. If the whole piping network surrounding HIPPS was considered, perhaps major differences could have been found. Therefore, although not conclusive, the study shows that to specify extra information such as elevation or fittings might not be a requirement, which in turn simplifies the process simulation model. Further investigations shall confirm whether the variations in PST intensify with the addition of more details in other pipelines, or not.

Chapter 8

Conclusions

Safety-related operations and hazardous events are intrinsically dynamic in nature. This Master Thesis investigates if a better process design can be achieved by taking into account the dynamic behaviour of the system, and evaluates the level of detail required in the simulations to achieve a reliable result. Two safety systems within the Oil & Gas industry have been analysed using dynamic simulations: the flare and the HIPPS systems.

Part I. The flare system

The full plant depressurization of three different offshore facilities has been analysed. The results from the dynamic simulations are benchmarked against the steady-state design to investigate the possible hidden debottlenecking potential. The conclusions obtained from this part are listed next:

- A significant reduction in both mass peak flare rate and backpressure in the system, are found by taking into account dynamics. This finding is attributed to the line-packing effects in the flare system hold-up volume, and the fact that the mass flow decreases rapidly as the blowdown segments are depressurized.
- An even higher reduction in mass peak flare rate is found by adding a higher level of complexity in the model through the incorporation of dead-ends (inactive). This is due to the increase of available hold-up volume and also, possible reverse flow effects. Although not conclusive, a higher influence of the addition of dead-ends is observed in smaller facilities. The effect is not the dominating one in terms of contribution to mass peak flow rate reduction, and can be ignored for more conservative results.
- It is observed that the larger the flare system, the larger the hidden potential for debottlenecking, and results can be fitted using a quadratic relationship.

Part II. The HIPPS system

The performance of HIPPS in terms of process response time (PST) when subjected to an overpressure scenario is analyzed. The level of detail and the robustness required in the models to achieve an effective model (simple i.e. less prone to errors) that can ensure reliability in the results is considered. The conclusions obtained for this part are listed next:

- The higher the well-feed mass inflow, the lower the response time of the HIPPS as a result of the higher volume in the system.
- The further the blockage occurs, the more available time. This can be attributed to a buffer volume effect given by the gas phase in the pipeline counter-acting and delaying the reverse flow towards the manifold.
- Even though the use of a simplified pipe friction models (Case 5) is preferred from a modelling point of view, Case 5 does not provide reliable results. The pressure drop is under-estimate, thus a higher PST is predicted (i.e. less conservative).
- The pipe flow correlations (Case 1–4) present little variations in the calculated PST, even though dissimilarities in the results increase as larger system volumes and further locations of blockage are considered. Generally, it is observed that a more conservative prediction can be achieved when using the pipe flow correlation Tulsa Unified Model, since it predicts the lowest PST.
- Although not conclusive, the study shows that to specify extra information such as elevation or fittings might not be a requirement, which in turn, simplifies the process simulation model.

Concluding remarks

The critical relationship between process design and process safety can be connected with the use of dynamic simulations. The conservatism conventionally used in the design through the use of steady state simulations can be revised, since dynamic simulations can provide the required conservatism and reliability to the design, as well as representing the actual behaviour of the system. A model can be built for anything whatsoever, as long as it is consistent in its ability to reproduce the actual behaviour of the system. A relation between robustness of the model and reliability of the results, must be found. For the present study, valuable information has been uncovered, however additional work within this area can improve the quadratic relationship found, and a more detail benchmarking of the PST with and without isometrics, can aid in confirming the findings of this Master Thesis.

Bibliography

[1] Daniel A Crowl and Joseph F Louvar. *Chemical process safety: fundamentals with applications*. Pearson Education, 2001.

[2] Adam S Markowski et al. "Uncertainty aspects in process safety analysis". In: *Journal of Loss Prevention in the Process Industries* 23.3 (2010), pp. 446–454.

[3] Havard Devold. *Oil and gas production handbook: An introduction to oil and gas production, transport, refining and petrochemical industry*. ABB Oil and Gas, 2013.

[4] Yong Bai and Qiang Bai. *Subsea Engineering Handbook*. Gulf Professional Publishing, 2019.

[5] Mark Bothamley. "Offshore processing options vary widely". In: *Oil & gas journal* 102.45 (2004), pp. 47–55.

[6] Alireza Bahadori. *Essentials of oil and gas utilities: process design, equipment, and operations*. Gulf Professional Publishing, 2016.

[7] Ayo Akintoye, Amec Foster Wheeler, and Shinfield Park. "Determination of Alarm Safety Response Time". In: 2016.

[8] Saeid Mokhatab, William A. Poe, and James G. Speight. "Chapter 13 - Dynamic simulation of gas processing plants". In: *Handbook of Natural Gas Transmission and Processing*. Burlington: Gulf Professional Publishing, 2006, pp. 461–483.

[9] David Schumann, Gregory T. Davis, and Piyush Shah. *Application of Simulation Models in Operations – A Success Story*. Available online: `https://pdfs.semanticscholar.org/2d9f/2a7113a42e5db7f3f97e73c973080e2a3a99.pdf`. (Visited on 05/21/2020).

[10] F. Bezzo et al. "Using Process Simulators for Steady-State and Dynamic Plant Analysis: An Industrial Case Study". In: *Chemical Engineering Research and Design* 82.4 (2004). 8th UK National Heat Transfer Conference, pp. 499 –512.

[11] Mo Mohitpour, William Thompson, and Benjamin Asante. "The importance of dynamic simulation on the design and optimization of pipeline transmission systems". In: *1996 1st International Pipeline Conference*. American Society of Mechanical Engineers Digital Collection. 1996, pp. 1183–1188.

[12] Yula Tang, Liang-Biao Ouyang, et al. "A dynamic simulation study of water hammer for offshore injection wells to provide operation guidelines". In: *International Oil and Gas Conference and Exhibition in China*. Society of Petroleum Engineers. 2010.

[13] S Mokhatab and BF Towler. "Dynamic simulation of offshore production plants". In: *Petroleum science and technology* 25.6 (2007), pp. 741–757.

[14] Rune Kjerrumgaard Jensen et al. "Implementation and Validation of a Free Open Source 1D Water Hammer Code". In: *Physics of Fluids* 3.3 (2018), pp. 1–49.

[15] Antonio Critsinelis et al. *Subsea flowline pressure surge relief system*. US Patent 10,215,321. Feb. 2019.

[16] Xiaole Yang and M Sam Mannan. "The development and application of dynamic operational risk assessment in oil/gas and chemical process industry". In: *Reliability Engineering & System Safety* 95.7 (2010), pp. 806–815.

[17] Zhongde Zhang et al. "Dynamic Analysis on the Pressure Relief Process of Hydrocarbon Pressure Vessel With Multi-Components Under External Fire". In: *The 27th International Ocean and Polar Engineering Conference*. International Society of Offshore and Polar Engineers. 2017.

[18] Michael Bjerre et al. "Analysis of pressure safety valves for fire protection on offshore oil and gas installations". In: *Process Safety and Environmental Protection* 105 (2017), pp. 60–68.

[19] Anders Andreasen et al. "On the adequacy of API 521 relief-valve sizing method for gas-filled pressure vessels exposed to fire". In: *Safety* 4.1 (2018), p. 11.

[20] KK Botros, PJ Campbell, and DB Mah. "Dynamic simulation of compressor station operation including centrifugal compressor and gas turbine". In: (1991).

[21] Yeon-pyeong Jo, Yongheon Cho, and Sungwon Hwang. "Dynamic analysis and optimization of flare network system for topside process of offshore plant". In: *Process Safety and Environmental Protection* 134 (2020), pp. 260–269.

[22] FFK Chen, RA Jentz, DG Williams, et al. "Flare System Design: A Case for Dynamic Simulation". In: *Offshore Technology Conference*. Offshore Technology Conference. 1992.

[23] Rakesh Wasnik et al. "De-Bottlenecking of Existing Flare System for Facility Up-Gradation using Dynamic Simulation Approach-Case Study". In: *Abu Dhabi International Petroleum Exhibition & Conference*. Society of Petroleum Engineers. 2018.

[24] Srinivasa Lingireddy, Don J Wood, and Naftali Zloczower. "Pressure surges in pipeline systems resulting from air releases". In: *Journal-American Water Works Association* 96.7 (2004), pp. 88–94.

[25] Robin Smith. *Chemical process: design and integration*. John Wiley & Sons, 2005.

[26] Roberto Bubbico et al. "Dynamic assessment of safety barriers preventing escalation in offshore Oil&Gas". In: *Safety Science* 121 (2020), pp. 319 –330.

[27] Ron Johnson Luis M. Duran. "Independent layers of protection with integrated safety systems". In: *ABB Value Paper* (2016).

[28] Ronald J. Willey. "Layer of Protection Analysis". In: *Procedia Engineering* 84 (2014). 2014 International Symposium on Safety Science and Technology, pp. 12 –22.

[29] American Petroleum Institute. Production Dept. *API Recommended Practice 14C: Analysis, Design, Installation, and Testing of Safety Systems for Offshore Production Platforms*. 8th ed. American Petroleum Institute, 2018.

[30] American Petroleum Institute. *API Standard 521: Pressure-relieving and Depressuring Systems*. 6th ed. American Petroleum Institute, 2014.

[31] Arjan Abeynaike and Venkatesh Sourirajan. "Reliability modelling of over-pressure protection systems for oil and gas flowlines". In: *Journal of Loss Prevention in the Process Industries* 50 (2017), pp. 257 –265.

[32] Marc Hellemans. *The safety relief valve handbook: design and use of process safety valves to ASME and International codes and standards*. Elsevier, 2009.

[33] American Petroleum Institute. Production Dept. *API Standard 520: Sizing, Selection, and Installation of Pressure-relieving Devices*. 6th ed. American Petroleum Institute, 2015.

[34] Robert J Stack et al. "High integrity protective system design using a risk-based approach". In: *Process Safety Progress* 30.2 (2011), pp. 115–121.

[35] Yeon-pyeong Jo, Yongheon Cho, and Sungwon Hwang. "Dynamic analysis and optimization of flare network system for topside process of offshore plant". In: *Process Safety and Environmental Protection* 134 (2020), pp. 260–269.

[36] Alireza Bahadori. "Chapter 6 - Blow-Down and Flare Systems". In: *Natural Gas Processing*. Boston: Gulf Professional Publishing, 2014, pp. 275 –312.

[37] Dennis P. Nolan. "Chapter 12 - Depressurization, Blowdown, and Venting". In: *Handbook of Fire and Explosion Protection Engineering Principles*. Oxford: William Andrew Publishing, 2011, pp. 127 –138.

[38] Martin Schoen. "The Joule–Thomson effect in confined fluids". In: *Physica A: Statistical Mechanics and its Applications* 270.3 (1999), pp. 353 –379.

[39] Fadhli Hadana Rahman et al. "High CO2 Blowdown During Emergency Depressurization EDP at Offshore Environment". In: *Offshore Technology Conference Asia*. Offshore Technology Conference. 2018.

[40] Process Systems Enterprise Limited – A Siemens Business. *Vessel and system blowdown*. Available online: `https://www.psenterprise.com/sectors/oil-and-gas/application-areas/blowdown-analysis`. (Visited on 05/27/2020).

[41] Ben Firth. "Unpicking Oversimplification: Relief and Flare Studies for Complex Plant using Dynamic Process Modelling". In: *Hazards 26* (2016), pp. 1–12.

[42] NORSOK. *NORSOK Standard P-002: Process Safety Design*. 1st ed. NORSOK, August 2014.

[43] Process Systems Enterprise Limited – A Siemens Business. *Dynamic flare system analysis*. Available online: `https://www.psenterprise.com/sectors/oil-and-gas/application-areas/dynamic-flare-analysis`. (Visited on 05/27/2020).

[44] Amarnath Singh et al. "Flare minimisation via dynamic simulation". In: *International journal of environment and pollution* 29.1-3 (2007), pp. 19–29.

[45] Anders Andreasen. "Process design - can we change mindset?" In: *Offshore Oil and Gas Seminar*. Department of Energy Technology, Aalborg University Esbjerg. August 2014.

[46] DNV GL. "DNVGL-OS-E201: Oil and Gas Processing Systems". In: *Offshore standards*. July 2017.

[47] IEC. *Functional Safety – Safety Instrumented Systems for the Process Industry Sector – Part 1: Framework, definitions, system, hardware and application programming requirements (IEC 61511-1:2016)*. 1st ed. International Electrotechnical Commissio, 2003.

[48] IEC. *Functional Safety – Safety Instrumented Systems for the Process Industry Sector – Part 2: Guidelines for the application of IEC 61511-1:2016 (IEC 61511-2:2016)*. 2nd ed. International Electrotechnical Commissio, 2016.

[49] Severn Glocon Group. *High Integrity Pressure Protection System: Severn Glocon HIPPS brochure*. Available online: `https://www.severnglocon.com/high-integrity-pressure-protection-system/`. (Visited on 05/27/2020).

[50] Snorre Sklet. "Safety barriers: Definition, classification, and performance". In: *Journal of loss prevention in the process industries* 19.5 (2006), pp. 494–506.

[51] Jacob G Hoseth, Endre Willmann, Paul Roberts, et al. "Implementation Options for the Subsea High Integrity Pipeline Protection System (HIPPS) Solution". In: *Offshore Technology Conference*. Offshore Technology Conference. 1997.

[52] Y Doreen Chin, Zeng-Gang Xu, et al. "Dynamic Processes of Multiphase Flow in Subsea Flowline/Riser Systems During ESD Valve Shut Down". In: *SPE Latin American and Caribbean Petroleum Engineering Conference*. Society of Petroleum Engineers. 2001.

[53] Janardhan Davalath, Harold Brian Skeels, Sverre Corneliussen, et al. "Current state of the art in the design of subsea HIPPS systems". In: *Offshore Technology Conference*. Offshore Technology Conference. 2002.

[54] Amine Meziou et al. "Model-based design and analysis of a subsea high integrity pressure protection system (HIPPS)". In: *2016 IEEE International Conference on Advanced Intelligent Mechatronics (AIM)*. IEEE. 2016, pp. 1216–1221.

[55] Aspen Technology Inc. *Getting Started with Aspen HYSYS Dynamics: Solving safety and operability challenges*. Available online: `https://www.aspentech.com/email/email_archive/getting_started_with_aspen_hysys_dynamics.pdf`. 2012. (Visited on 05/27/2020).

[56] Aspen Technology Inc. *Aspen HYSYS Dynamics: Dynamic Process Simulation Made Easy*. Available online: `https://www.aspentech.com/en/products/pages/aspen-hysys-dynamics`. (Visited on 05/27/2020).

[57] Gunasekar Govindan, Azwan Shaharun, et al. "Overpressure Protection Workflow to Address Pipeline Integrity Using Multiphase Dynamic Simulation". In: *Offshore Technology Conference Asia*. Offshore Technology Conference. 2016.

[58] Ali Danesh. "Chapter 1 - Phase Behaviour Fundamentals". In: *PVT and Phase Behaviour of Petroleum Reservoir Fluids*. Vol. 47. Developments in Petroleum Science. Elsevier, 1998, pp. 1 –31.

[59] Karen Schou Pedersen, Peter Lindskou Christensen, and Jawad Azeem Shaikh. *Phase behavior of petroleum reservoir fluids*. CRC press, 2014.

[60] Abdus Satter and Ghulam M. Iqbal. "Chapter 5 - Phase behavior of hydrocarbon fluids in reservoirs". In: *Reservoir Engineering*. Boston: Gulf Professional Publishing, 2016, pp. 107 –115.

[61] Guanghua Gao et al. “A simple correlation to evaluate binary interaction parameters of the Peng-Robinson equation of state: binary light hydrocarbon systems”. In: *Fluid phase equilibria* 74 (1992), pp. 85–93.

[62] Donald L Katz et al. “Overview of phase behavior in oil and gas production”. In: *Journal of Petroleum Technology* 35.06 (1983), pp. 1–205.

[63] A. Kayode Coker. “Chapter 4 - Thermodynamic Properties of Petroleum and Petroleum Fractions”. In: *Petroleum Refining Design and Applications Handbook*. John Wiley & Sons, Ltd, 2018, pp. 63–110.

[64] Agelia M Abudour et al. “Generalized binary interaction parameters for the Peng–Robinson equation of state”. In: *Fluid Phase Equilibria* 383 (2014), pp. 156–173.

[65] TA Roberts et al. “Design and protection of pressure systems to withstand severe fires”. In: *Process Safety and Environmental Protection* 82.2 (2004), pp. 89–96.

[66] ISA. “Flow Equations for Sizing Control Valves, ANSI/ISA S75.01 Standard, ISA-S75.01-1985”. In: Instrument Society of America. 1995.

[67] Guy Borden Jr and G Paul. “Control Valves - ISA Practical Guides for Measurement and Control”. In: Instrument Society of America. 1998.

[68] Kwizin. *Do's & don'ts in process modelling: Dynamic Modelling of Flare Networks*. Available online: `http://processmodelling.blogspot.com/2015/02/dynamic-modelling-of-flare-networks.html`. (Visited on 05/27/2020).

[69] Aspen Technology Inc. *Top 8 Questions About Pipe Flow Hydraulic Analysis (AT-03835-0218)*. Available online: `https://www.aspentech.com/en/resources/faq-documents/top-8-questions-about-pipe-flow-hydraulic-analysis`. 2018. (Visited on 05/27/2020).

[70] American Petroleum Institute. Production Dept. *API Specification 6A: Specification for Wellhead and Christmas Tree Equipment*. 7th ed. American Petroleum Institute, 1999.

[71] Dale H Beggs, James P Brill, et al. “A study of two-phase flow in inclined pipes”. In: *Journal of Petroleum technology* 25.05 (1973), pp. 607–617.

[72] Iván Darío Gil Chaves et al. “Fluid Handling Equipment”. In: *Process Analysis and Simulation in Chemical Engineering*. Springer, 2016, pp. 103–137.

[73] Aspen Technology Inc. *Multiphase Pipe Flow Modeling in Aspen HYSYS (AT-03829-0218)*. Available online: `https://www.aspentech.com/en/resources/white-papers/multiphase-pipe-flow-modeling-in-aspen-hysys`. 2018. (Visited on 05/27/2020).

[74] GA Payne et al. “Evaluation of inclined-pipe, two-phase liquid holdup and pressure-loss correlation using experimental data (includes associated paper 8782)”. In: *Journal of Petroleum Technology* 31.09 (1979), pp. 1–198.

[75] Hong-Quan Zhang, Cem Sarica, et al. “Unified modeling of gas/oil/water pipe flow-Basic approaches and preliminary validation”. In: *SPE Projects, Facilities & Construction* 1.02 (2006), pp. 1–7.

[76] Stuart W Churchill and CHURCHILL SW. “Friction-factor equation spans all fluid-flow regimes.” In: *Chemical Engineering* 84 (1977), pp. 91–92.

Appendix A

Revealing hidden debottlenecking potential in flare systems on offshore facilities using dynamic simulations – A preliminary investigation

Revealing hidden debottlenecking potential in flare systems on offshore facilities using dynamic simulations – A preliminary investigation

Ana Xiao Outomuro Somozas[a], Rudi P. Nielsen[a], Marco Maschietti[a], Anders Andreasen[b,*],

[a] *Aalborg University, Department of Chemistry and Bioscience, Niels Bohrs Vej 8, DK-6700 Esbjerg, Denmark*
[b] *Ramboll Energy, Field Development, Studies and FEED, Bavnehøjvej 5, DK-6700 Esbjerg, Denmark*

Abstract

Three flare systems are modeled and total plant depressurization is investigated using dynamic simulations in order to access the debottlenecking potential. Usually steady-state simulation of the flare network is used for sizing and rating of the flare system. By using dynamic simulations effects from line packing in the flare system can be studied. The results show that peak flow during a dynamic simulations is significantly lower than the peak flow used in a steady-state case. The three systems investigated span a wide range in flare system size, both in terms of number of process segments disposing into the flare network, in terms of peak design rate and the flare network pipe dimensions and total hold-up volume. Generally, it is observed that the larger the flare system, the larger debottlenecking potential.

Keywords: Emergency depressurization, Flare network, Debottlenecking, Dynamic simulation

*Corresponding author
Email address: anra@ramboll.com (Anders Andreasen)

1. Introduction

The flare system is a pivotal part of the safety system in process plants handling flammable and hazardous substances. In case of an upset condition causing for instance pressure relief or plant depressurization, the flare system collects vented substances and routes the hazardous fluids to the flare stack. At the flare tip incineration takes places, thereby converting the flammable and hazardous substances to less harmful oxidized products such as CO_2 and H_2O. The flare system boundaries are pressure safety valves (PSVs), emergency depressurization valves (EDPs)/blowdown valves (BDVs), spill-over valves/pressure control valves (PCVs), in one end, and the flare stack/tip in the other end. From each source, fluid is collected via tail pipes in a network of sub-headers, and headers, via a flare knock-out (KO) drum, to the flare stack and flare tip.

A typical flare system layout for an offshore production facility is shown in Figure 1. The example shows BDVs and PSVs connected to the flare system. Under normal operation, the BDVs and PSVs act as barriers between the hydrocarbon containing process segments/equipment and the flare/disposal

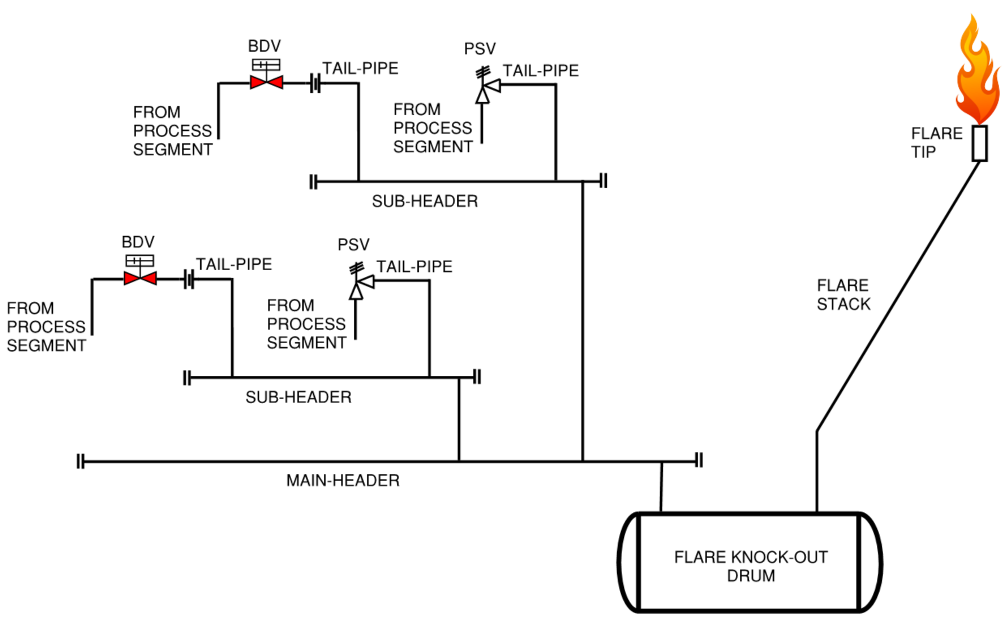

Figure 1: Typical flare system layout on offshore production facility. PCVs/spill-over valves not shown.

Reference	Tail pipe		Sub-header/header	
	Mach. No. (–)	ρv^2 (Pa)	Mach. No. (–)	ρv^2 (Pa)
API (2014)	N/A	N/A	N/A	N/A
NORSOK (2014)	0.7	200,000	0.6	200,000
Total (2012)	0.7	150,000	0.7	150,000
Shell (2010)	<1	N/A	<1/0.7	N/A

Table 1: Typical design criteria used for sizing of flare network piping according to recognized standards and major oil company standards.

system. In real systems, multiple BDVs and PSVs are connected to sub-headers and headers.

The design of the flare system often follows API 521 recommended practice (API, 2014) or similar European standards (ISO, 2006; NORSOK, 2014) or more detailed and/or stringent company guidelines. The flare system is designed for a number of scenarios e.g., pressure relief from one source, or simultaneous reliefs from a number of coincident sources, production flaring and emergency depressurization etc.

Common design criteria for the flare network are summarized in Table 1. Furthermore, during the design of the flare system, it shall also be verified that the backpressure within the flare system does not exceed the design pressure of any part.

API 521 (API, 2014) specifically mentions dynamic simulations as a means for refinement of disposal system design load by e.g., considering that individual relief loads may occur at different times (Nougués et al., 2010) and in general to determine the disposal system hydraulic performance. However, it is common industry practice to determine the flare system hydraulic capacity with a steady-state network solver. Typically, initial peak flows are used for hydraulic sizing of all tail pipes, sub-headers, flare KO drum and flare stack/tip using a commercial steady-state network solver. When evaluating the backpressure and flow rate/velocity in a steady-state approach, these are determined under the assumption that the entire flare system is subjected to the peak flow at once. Especially considering emergency depressurization, a steady-state approach is conservative. Taking the dynamic nature of the depressurization process into account, it can easily be comprehended that downstream segments in the flare system e.g. main header, flare KO drum and flare tip will never be subjected to the maximum flow (Chakrabarty et al., 2016). In reality, the initial (peak) flow will rapidly decline owing to the reduction in the upstream pressure and the build up of backpressure. The former is caused by the plant segments being depressurized, whereas the latter is caused by the line packing, i.e., the gradual filling of the entire flare system. These combined effects would effectively smoothen out the peak flow.

It is common practice to use dynamic analysis when considering the depressurization of individual process segments for e.g. sizing of the flow capacity of the BDV and/or downstream restriction orifice (Haque et al., 1990; Richardson and Saville, 1992; Haque et al., 1992; Biswas and Fischer, 2017; Leporini et al., 2018). The initial rate is used as input to a steady-state flare network simulation. Even individual relief loads from various relief scenarios are analyzed using dynamic simulations (Singh et al., 2007; Firth, 2016; Bjerre et al., 2017; Andreasen et al., 2018). On the other hand, the analysis of the flare system as a whole is typically not subjected to dynamic analysis (Chen et al., 1992).

Andreasen (2014) modeled a sub-part of a flare system on an existing offshore oil and gas production facility. By comparing the system load from steady-state and dynamic simulations, it was found that taking line packing into account via dynamic simulation, the simulated flare tip mass flow rate was 12% lower than the corresponding steady-state simulation.

Wasnik et al. (2018) studied the depressurization of 14 blowdown segments into an offshore complex flare system. The initial flow from the BDV segments was 545 MMSCFD. The result of a dynamic simulation was that the maximum rate into the flare KO drum was 532 MMSCFD and the maximum load at the flare tip (located 1.8 km away and connected to the process facility via a 42" pipeline) was reduced to 447 MMSCFD (18% reduction from initial BDV rate). In the same study, an extension of an existing facility was also investigated. Dynamic simulations showed that the maximum backpressure calculated during a full plant depressurization was reduced by approx. 17% compared to steady-state simulation results.

Jo et al. (2020) studied a separator blocked-outlet scenario with multiple PSVs discharging into the flare system of an offshore process facility using dynamic simulations. They found that substantial line sizing optimization could be obtained for most lines compared to a traditional steady-state approach, thereby reducing CAPEX. However, it was also discovered that a few lines had to be increased in size when analyzed in dynamics due to high

Mach numbers.

Although the literature on dynamic flare system modeling for full plant emergency depressurization is sparse, there are clear indications that existing flare systems designed using a steady-state approach have additional ullage which can be revealed by dynamic simulations. This is especially useful when considering brownfield modifications to existing processing facilities adding equipment that needs to be accommodated within an existing flare system when depressurized. Following a steady-state approach, adding additional flare system load will probably result in bottlenecks in the flare system requiring expensive upgrades. On the other hand, a dynamic modeling approach may elucidate hidden debottlenecking potential by an inherent over-capacity of the original flare system, thereby avoiding expensive flare system upgrades. Dynamic modeling analysis have to be done case by case, since flare systems on different facilities are unique

In this paper, the hidden debottlenecking potential in flare systems on offshore processing facilities is studied using dynamic simulations of the emergency depressurization event.

Three facilities in different sizes in terms of flare system design load and number of segments being depressurized are studied in an attempt to quantify expected built-in ullage. To the authours knowledge, this is the first study reported, which systematically investigates the potential of applying dynamic simulations for revealing hidden debottlenecking potential in existing flare systems.

2. Methods

2.1. Tools and modeling

All simulations in the present study are conducted with Aspen HYSYS Dynamics ver. 9 (AspenTech, Bedford, Massachusetts, USA). The process fluids are modeled using the Peng-Robinson equation of state (Peng and Robinson, 1976) and the COSTALD method is applied for liquid density (Hankinson and Thomson, 1979). Heavy hydrocarbon fractions are modeled as hypotheticals/pseudo-components.

The blowdown segment is modeled as a vessel in HYSYS with a volume equivalent to the blowdown segment modeled. Heat transfer is not considered in the present study, which means that the dimensions of the vessels used for modeling the blowdown segments are irrelevant, as long as the volume is matched. The BDV for each blowdown segment is modeled as a control valve,

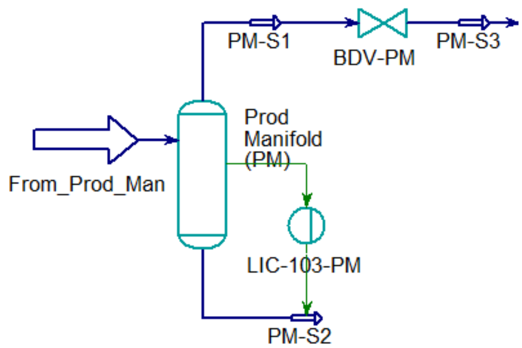

Figure 2: Example of blowdown segment modeling in HYSYS.

with a C_V calibrated to the initial flow rate through the restriction orifice downstream the BDV. The C_V is determined by the ANSI/ISA method (ISA, 1995; Borden, 1998) using a semi-ideal C_p/C_v. The modeling of the blowdown segments as a vessel and downstream BDV including restriction orifice (valve and orifice modeled as a control valve) is illustrated in Figure 2. The fluid composition for each blowdown segment is sourced from a corresponding steady-state process simulation of the plant. The initial conditions are set according to the plant's flare, blowdown and relief report. For blowdown segments which extends over pressure change e.g. an entire compressor loop, the initial pressure before start of depressurization is found from a settle-out analysis (Andreasen et al., 2015).

Although the blowdown segments may contain liquids the relief through the BDV is in the vapor upstream the BDV. Downstream the BDV, smaller amounts of condensation may occur due to Joule-Thomson cooling over the valve.

The flare network is modeled using details from existing Flare System Analyser (FSA) (AspenTech, Bedford, Massachusetts, USA), which includes piping information about length an internal diameter. This information is sourced and used for specifying equivalent HYSYS pipe segments. Fittings data from the equivalent FSA model is included in the HYSYS pipe segments except for swages. Based on the data sourced from FSA, the dynamic model in HYSYS is benchmarked against the steady-state model by running it to a steady-state using the depressurization flow rates from the FSA model as boundary conditions. In the result section of this study the comparison between dynamic simulation results and steady state will be based on the

Facility	Design load (MMSCFD)	(kg/h)	No. BDVs (#)
A	73	88,000	13
B	341	350,000	24
C	714	684,000	43

Table 2: Summary of facilities flare systems investigated with dynamic simulations.

same dynamic model.

The pipe segment in HYSYS has some shortcomings in its modeling rigor e.g., acceleration pressure drop is not included for pure gas flow, which uses Darcy-Weisbach for pressure drop calculation. Darcy-Weisbach is better suited for incompreesible flow with constant density. For compressible flow with varying density it is notoriously inaccurate. Still, we will use it for simplicity. Each of the tail pipes, sub-headers, and headers modelled are broken down into a vast number of individual segments, providing a discretization and updating mechanism of the fluid density. This will to a large extent mitigate the modeling deficiencies. Compared to more rigorous compressible flow modeling, it is the authors experience that this may lead to a slight underestimation of backpressure with a resulting underestimation of line-packing effect. Hence, the results derived in the present study can be considered conservative. The building of large networks with more rigorous tools, such as e.g. Aspen Hydraulics (AspenTech, Bedford, Massachusetts, USA), is very tedious.

Elevations of tail-pipes, sub-headers and headers are ignored, which is considered to have neglible influence ion the results. Only the contribution to static pressure drop from the elevation of the flare tip is included in the model. The flare tip is modeled as a control valve with a C_V calibrated to the actual pressure drop at the design rate from vendor data.

2.2. System description

Three different flare systems on different offshore facilities are analyzed in the present study. A summary of key data describing the three systems is provided in Table 2. All three systems are dimensioned for full plant depressurization/emergency depressurization as the governing relief scenario. All BDV's are actuated at once, i.e. no delays or staggered blowdown is applied. No relief from PSVs are included to occur concurrently with the plant depressurization.

2.3. Facility A

The first facility is an integrated platform designed for light crude with associated gas, which has separation of oil, gas and water in a two-stage separation train with final polishing of crude export in an electrostatic coalescer (final dewatering and desalting). A compression system boosts the gas pressure from the separators for wet gas export/reinjection and gas lift.

The system comprises a combined HP and LP flare system. The governing gas rate design capacity of the flare system is emergency depressurization. The main flare header is 16" and is routed to the Flare KO Drum. The size of the header is increased to 18" just upstream of the KO drum. A 14" flare line is routed from the KO drum (ID 3 m by T/T 10 m) to the flare tip. The flare system has 13 BDVs discharging into the flare system upon depressurization. The flare system as modeled in the process simulator is visualized in Figure 3. The details for the blowdown segments are summarised in Table 3.

	Pressure	Temperature	Total volume	Liquid Volume	Initial BDV rate		Gas MW
BDV No.	(bar)	(°C)	(m^3)	(m^3)	(kg/h)	(MMSCFD)	(kg/kmole)
1	36.0	93.4	101.0	70.9	26,836	22.36	23.8
2	63.4	64.8	1.8	0.7	4,610	3.97	21.8
3	68.6	64.8	4.6	1.8	9,140	7.87	21.8
4	2.5	80.0	113.1	67.7	11,656	5.85	40.0
5	36.0	93.4	49.8	31.3	19,578	16.48	23.8
6	180.0	111.9	0.4	0.0	1,391	1.14	24.5
7	4.9	38.0	15.2	1.9	3,996	1.74	38.0
8	13.2	45.0	5.6	0.9	3,319	0.96	34.0
9	34.0	93.4	3.6	0.2	1,561	1.35	24.0
10	125.0	115.0	1.9	0.0	3,044	2.49	24.5
11	40.6	40.0	1.3	0.0	6,544	5.16	24.3
12	130.9	75.0	3.7	1.1	10,209	8.34	24.5
13	31	93.4	3.6	0.2	500	0.43	24.0

Table 3: Summary of specifications for blowdown segments of Facility A. The conditions are for the initial system state prior to depressurization.

2.4. Facility B

Facility B is a gas-condensate integrated processing platform, with two-stage condensate knock-out and booster compression of flash-gas from the

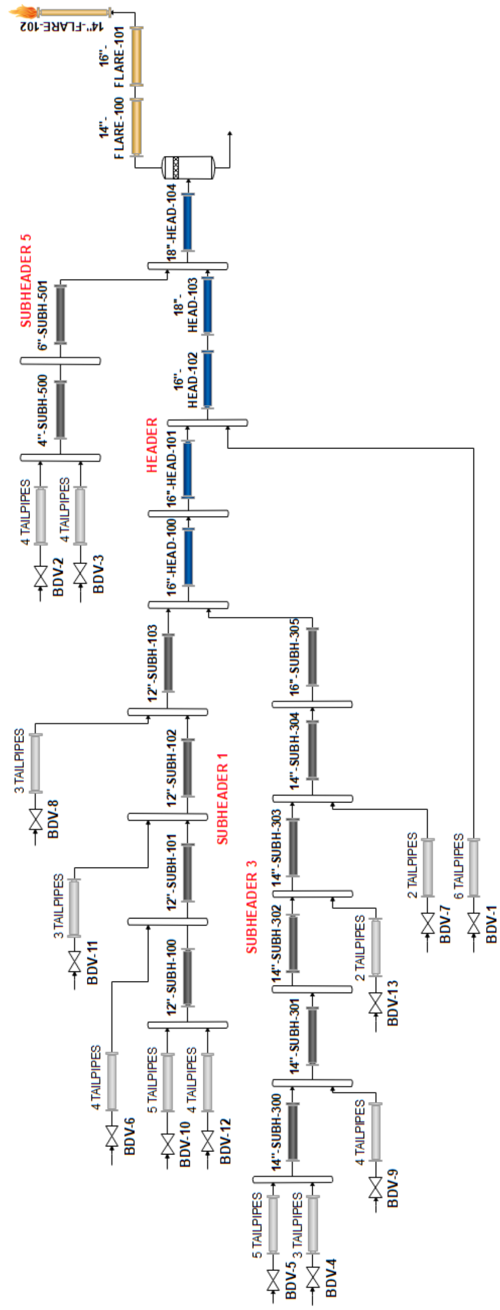

Figure 3: Flare system model for facility A. Dead ends from PSVs and PCVs not disposing into the flare system during emergency depressurization have not been included.

2nd stage separator. Before export, the gas is dehydrated and dew point controlled (hydrocarbons).

The platform has separate LP and HP flare systems, but only the HP flare is modeled in the present study. The main flare header is 20" and is routed to the flare KO drum. A 20" flare line is routed from the KO drum (ID 3 m by T/T 7.2 m) to the flare stack/tip. The flare system has 24 BDVs disposing into the flare system upon depressurization. The flare system as modeled in the process simulator is visualized in Figure **??**. The details for the blowdown segments are summarised in Table 4.

	Pressure	Temperature	Total volume	Liquid Volume	Initial BDV rate		Gas MW
BDV No.	(bar)	(°C)	(m^3)	(m^3)	(kg/h)	(MMSCFD)	(kg/kmole)
1	87.9	68.2	0.3	0.1	627	0.6	20.3
2	55.0	88.1	0.3	0.1	375	0.4	20.6
3	41.5	47.7	0.6	0.1	524	0.5	20.4
4	41.2	69.0	0.5	0.1	537	0.5	20.7
5	42.4	85.7	0.6	0.0	528	0.5	20.8
6	41.6	72.8	0.9	0.0	531	0.5	20.7
7	40.9	67.7	30.9	1.4	15,943	15.5	21.7
8	40.0	58.1	3.7	2.5	1.797	1.8	20.4
9	89.9	84.8	22.3	3.6	26,717	25.2	21.2
10	24.0	30.7	105.7	58.5	23,721	22.5	21.0
11	56.2	35.0	7.4	0.0	4,674	4.7	19.7
12	22.3	30.6	7.9	7.4	20,035	18.8	21.8
13	56.4	35.0	8.5	0.0	9,609	9.8	19.7
14	76.5	39.5	82.3	34.9	99,998	95.9	20.2
15	40.7	52.1	6.7	0.1	2,207	2.1	21.0
16	75.0	19.0	41.3	7.3	41,878	40.4	20.5
17	56.6	-9.1	59.6	17.7	51,306	54.1	20.0
18	65.4	39.2	5.3	0.0	3,872	3.9	19.7
19	14.0	45.4	2.4	0.0	235	0.2	19.7
20	95.2	49.5	10.9	3.4	13,520	13.2	20.5
21	101.4	75.7	0.4	0.1	1,642	1.6	21.1
22	58.7	33.8	1.1	0.0	1,039	1.0	20.9
23	67.0	45.4	3.9	0.0	8,617	8.3	20.9
24	25.9	30.7	1.5	1.5	19,901	18.9	21.3

Table 4: Summary of specifications for blowdown segments of Facility B. The conditions are for the initial system state prior to depressurization.

2.5. Facility C

The last facility modeled is a central processing facility handling production from a number of bridge-connected platforms including tie-backs from remote facilities. Mainly gas condensate is handled and oil/water/gas separation is performed including gas compression dehydration and hydrocarbon

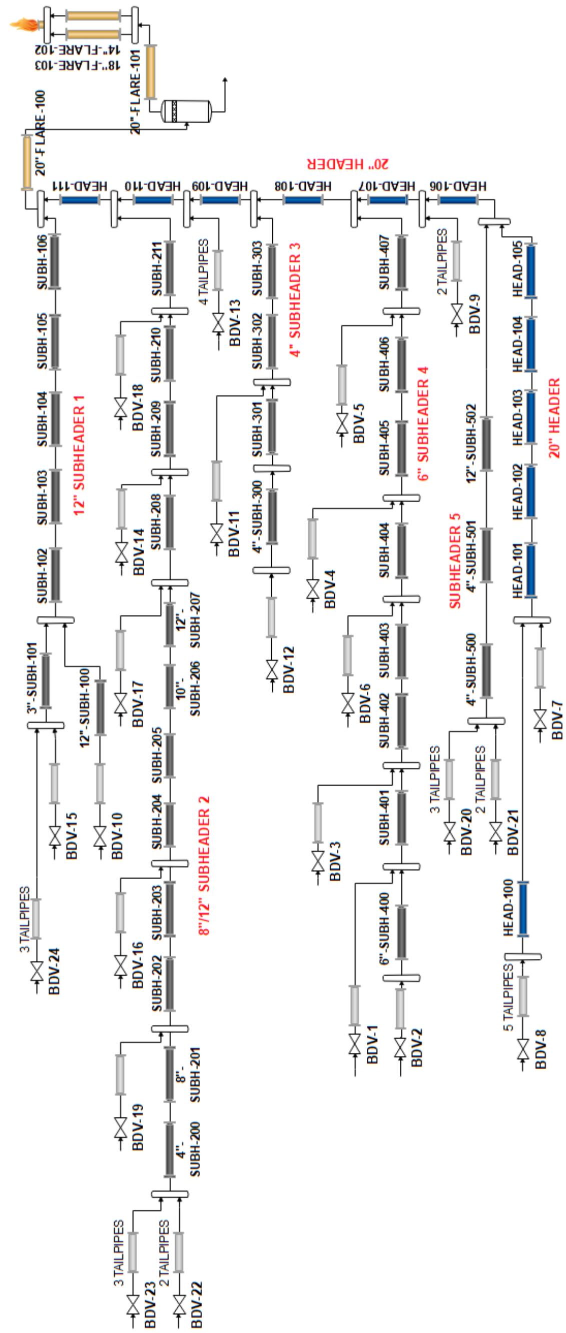

Figure 4: Flare system model for facility B. Dead ends from PSVs and PCVs not disposing into the flare system during emergency depressurization have not been included.

dew-pointing. The CPF exports gas to shore as well as it provides gas lift to wells requiring artificial lift.

The flare system includes both an LP and HP flare system, but only the HP flare system is modeled. The HP flare system has separate 18" main headers for cold and warm (wet) flare terminating at the flare KO drum (ID 3.55 m x T/T 10.6 m). A 24" flare line is routed from the KO drum to the flare stack/tip. The flare system has 43 BDVs disposing into the flare system upon depressurization. The flare system as modeled in the process simulator is visualized in Figure 5. The details for the blowdown segments are summarised in Table 5.

3. Results and Discussion

3.1. Facility A

For facility A, the emergency depressurization process is simulated using the dynamic process model depicted in Figure 3. Two simulations are conducted; The first uses a fixed pressure boundary upstream all BDVs at the value of the initial pressure prior to blowdown and the dynamic simulation is run until steady-state is reached. This relates to the approach applied when using a steady-state network solver, where the peak flow is used. The second applies a zero flow boundary at the inlet of the blowdown segments i.e. the pressure decreases with time in the blowdown segments concurrently with the mass flow out of the blowdown valve/orifice. This simulates the real dynamic behavior of the system with mass flow from blowdown segment decreasing with time as the pressure upstream decreases.

In Figure 6, the backpressure in various places in the flare system, calculated using the steady-state approach and the full dynamic approach, are depicted. As seen from the results, the peak backpressure with the dynamic approach is lower than the corresponding steady-state value. This behavior is similar to the one observed by Wasnik et al. (2018).

The mass flow reaching the flare tip is also compared for the steady-state and dynamic simulations. This is shown in Figure 7. Included is also a simulation run with a model with increased complexity, referred to as a dead ends model In this more complex model, all tail pipes and sub-headers from non-flow sources such as PSVs and PCVs which normally do not dispose into the flare system during emergency depressurization have been included. The can be compared back-to-back in the Suplpemetary Material.

BDV No.	Pressure (bar)	Temperature (°C)	Total volume (m^3)	Liquid Volume (m^3)	Initial BDV rate (kg/h)	Gas MW kg/kmole
1	50.0	31.0	41.0	13.3	16,260	18.9
2	23.8	48.2	56.6	3.6	10,230	19.2
3	55.0	55.0	47.2	2.6	18,507	19.3
4	72.0	30.0	67.2	9.1	41,714	19.3
5	62.6	6.5	17.5	1.7	13,375	18.9
6	62.6	6.5	17.5	1.7	13,375	18.9
7	137.6	49.0	8.5	0.0	14,075	19.2
8	114.6	48.8	15.8	0.0	19,137	18.5
9	50.0	15.9	4.1	1.9	13,798	20.0
10	138.0	45.0	16.7	0.0	27,107	18.5
11	15.0	55.0	155.5	155.5	15,329	23.1
12	9.7	75.1	9.0	0.5	0	34.5
13	9.7	75.1	9.0	0.5	0	34.5
14	72.0	26.0	9.5	0.0	6,893	19.2
15	50.0	28.2	8.6	0.1	4,087	19.3
16	63.0	24.2	20.8	0.0	11,488	18.5
17	72.0	25.0	67.5	6.1	58,678	19.7
18	50.0	31.7	62.3	37.8	101,354	18.6
19	50.0	31.7	14.3	9.3	22,285	18.6
20	50.0	31.7	5.4	5.4	104,121	26.4
21	50.0	31.7	32.4	32.4	8,466	26.4
22	50.0	28.2	74.2	0.7	29,908	18.8
23	50.0	28.2	3.7	0.0	1,476	18.8
24	50.0	28.2	3.7	0.0	1,373	18.8
25	50.0	28.2	10.7	0.1	4,325	18.8
26	50.0	36.1	51.6	1.3	21,989	18.6
27	50.0	36.1	4.4	0.1	2,008	18.6
28	138.0	44.7	28.9	0.0	47,256	18.5
29	138.0	44.7	17.3	0.0	28,254	18.5
30	72.0	-7.8	0.2	0.2	3,914	20.0
31	72.0	-7.8	1.3	1.3	12,185	18.5
32	72.0	1.4	61.2	6.1	59,171	18.4
33	125.0	1.4	1.8	0.0	4,096	19.1
34	80.0	1.4	0.9	0.0	954	18.5
35	170.0	28.5	9.1	0.0	24,445	19.2
36	192.0	36.9	0.6	0.0	1,793	19.2
37	138.0	44.7	26.5	0.0	48,273	18.5
38	138.0	44.7	13.3	0.0	24,304	18.5
39	138.0	44.7	35.6	0.0	70,405	18.5
40	192.0	36.9	9.5	0.0	29,933	19.2
41	192.0	36.9	0.7	0.0	2,121	19.2
42	192.0	36.9	0.7	0.0	2,274	19.2
43	97.1	52.6	7.9	0.0	7,956	18.5

Table 5: Summary of specifications for blowdown segments of Facility C.

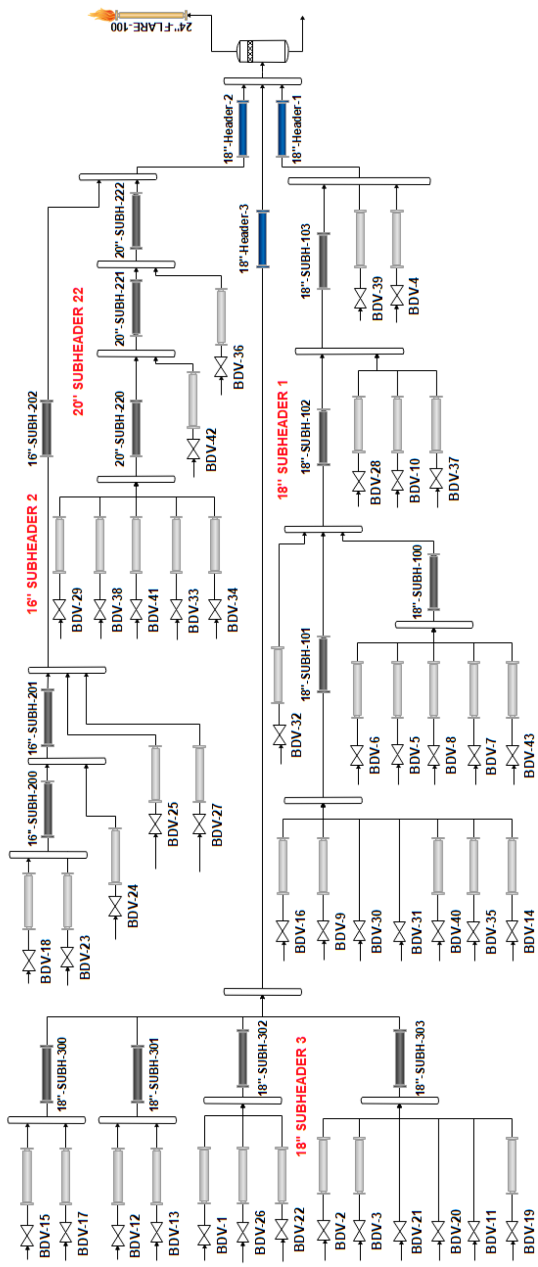

Figure 5: Flare system model for facility C. Dead ends from PSVs and PCVs not disposing into the flare system during emergency depressurization have not been included.

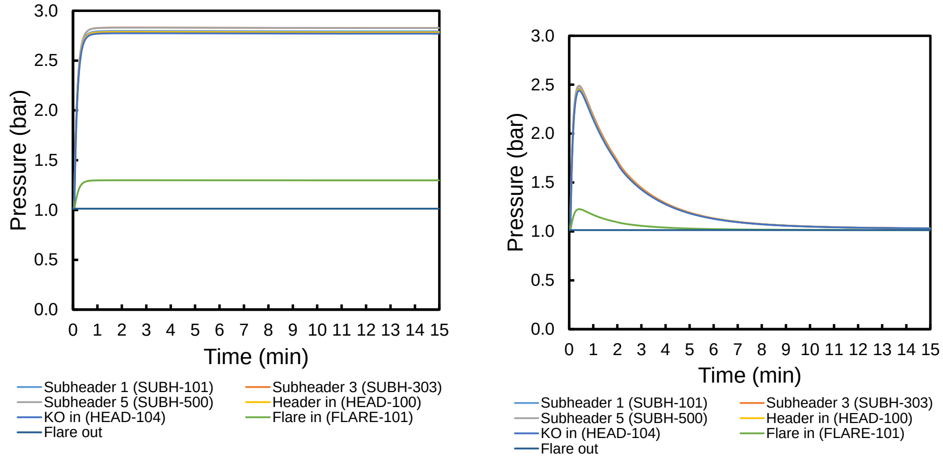

(A) (B)

Figure 6: Comparison between calculated backpressure in selected flare lines, flare KO drum for (A) steady-state and (B) dynamic simulations for facility A.

As seen from Figure 7, the mass flow rate in the dynamic simulations, both the with and without dead ends increases rapidly to a maximum value at a time between 0.5-1 min. after start of the depressurization. The maximum mass flow rate is at a lower value than the steady-state value due to line-packing in the flare system in agreement with previous findings (Andreasen, 2014; Wasnik et al., 2018). It is also noted that the peak mass flow is reduced by including the dead ends in the dynamic simulation model. The dead ends contribute with increased hold-up volume and hence a bigger line-packing potential. The reduction in peak flare rate is 11,370 kg/h and 13,994 kg/h for the dynamic model without and with dead ends, respectively. In relative numbers, the reduction is 13% and 16%.

3.2. Facility B

For facility B, the emergency depressurization process is simulated using the dynamic process model depicted in Figure 4 in **??**. Again, two simulations are conducted; a dynamic simulation run to a steady-state using the initial peak flow from blowdown segments and the full dynamic simulation.

In Figure 8 the backpressures in various places in the flare system calculated using the steady-state and the full dynamic approach are depicted. As seen from the results, the peak backpressure with the dynamic approach is

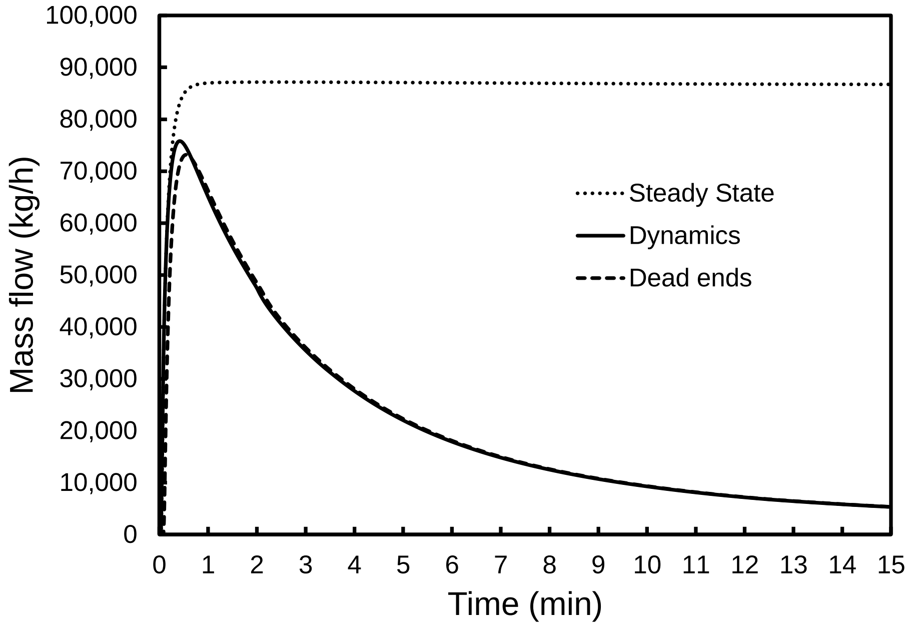

(A)

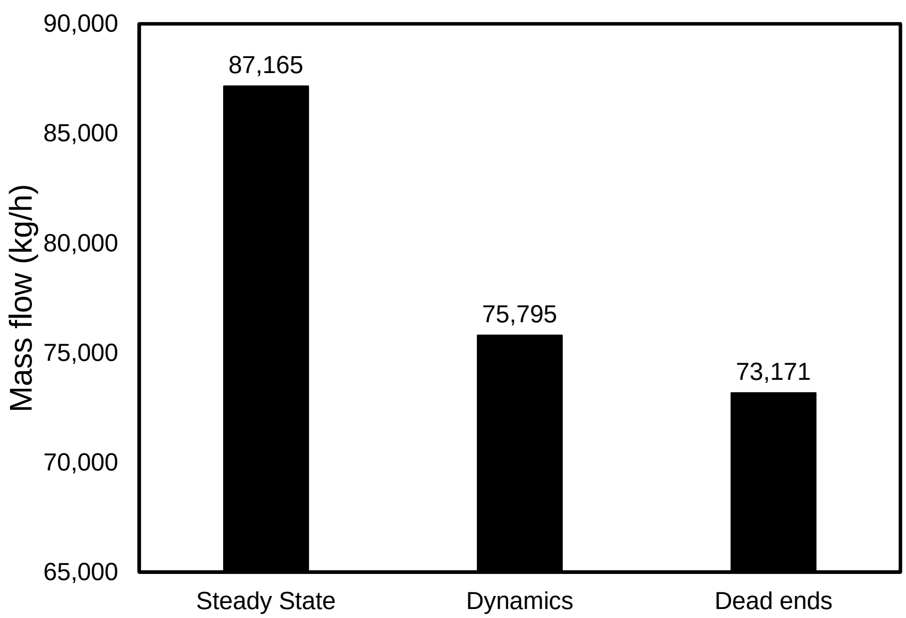

(B)

Figure 7: Comparison between calculated flare-tip mass flow for facility A for steady-state, dynamic simulations without dead ends, and dynamic simulations including dead ends.

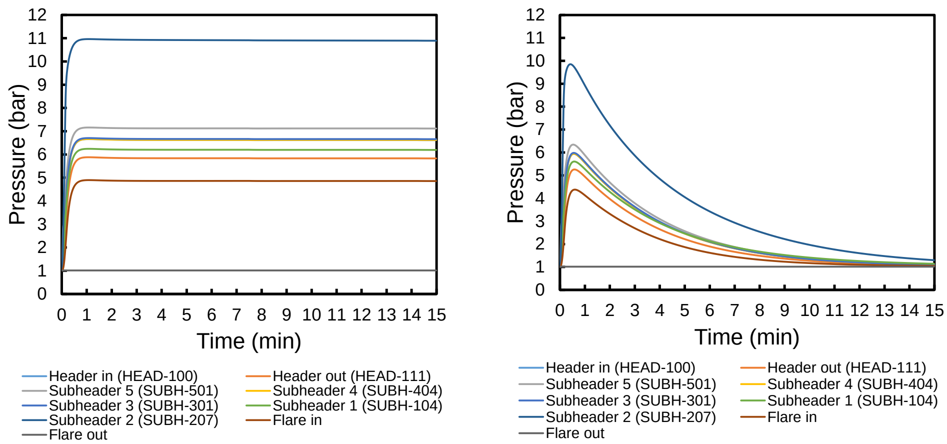

(A) (B)

Figure 8: Comparison between calculated backpressure in selected flare lines, flare KO drum for (A) steady-state and (B) dynamic simulations for facility B.

lower than the corresponding steady-state value as also demonstrated for the facility A model.

The mass flow reaching the flare tip is also compared for the steady-state and dynamic simulations. This is shown in Figure 9. The results also include a more complex model which includes all dead ends as described for facility A. The flowsheets with and without dead ends for facilty B can be compared back-to-back in the Supplementary Material.

As seen from Figure 9, the mass flow in the dynamic simulations both the one with and the one without dead ends increase rapidly to a maximum value at a time between 0.5-1 min. after start of depressurization. The maximum mass rate is at a lower value than the steady-state value as also shown for facility A. Again, it is noted that the peak mass flow is reduced by including the dead ends in the dynamic simulation model. The reduction in peak flare rate is 41,670 kg/h and 44,329 kg/h for the dynamic model without and with dead ends, respectively. In relative numbers, the reduction is 13.5% and 14.4%. Compared to facility A, the reduction in flare rate is higher in absolute numbers for facility B, whereas the relative reduction is comparable. In absolute numbers, the inclusion of dead ends is very similar to Facility A, but less significant in relative numbers.

Combined with findings from facility A, the simulation results for facility B suggest that it can be beneficial to build a simulation model including all

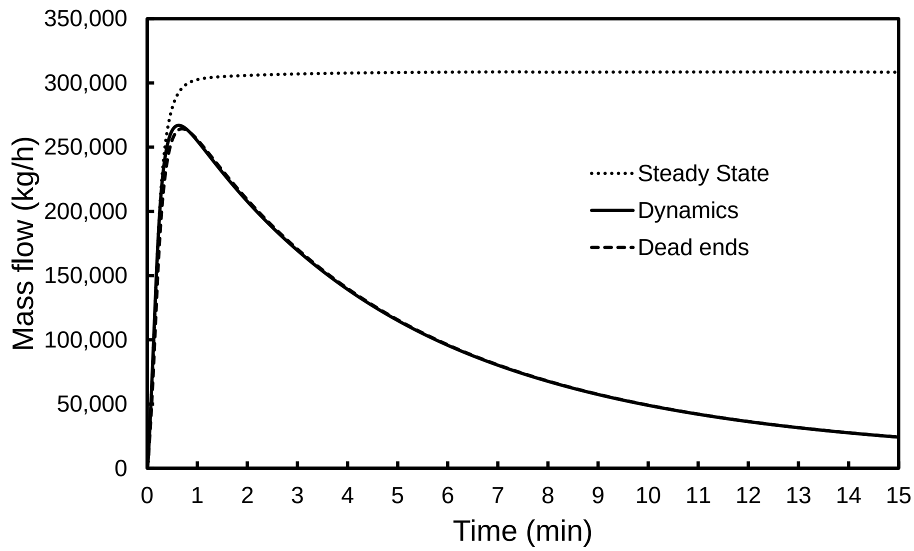

(A)

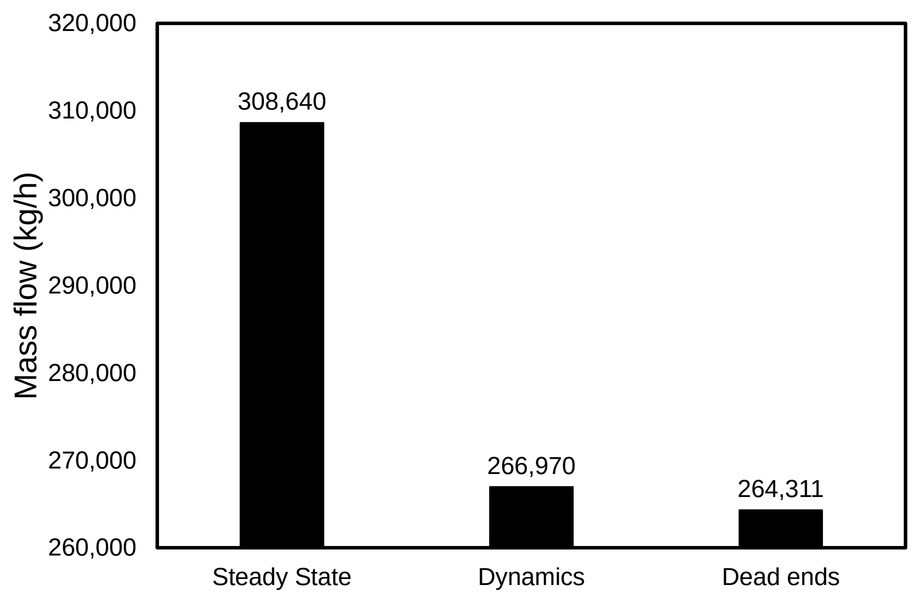

(B)

Figure 9: Comparison between calculated flare-tip mass flow for facility B for steady-state, dynamic simulations without dead ends and dynamic simulations including dead ends.

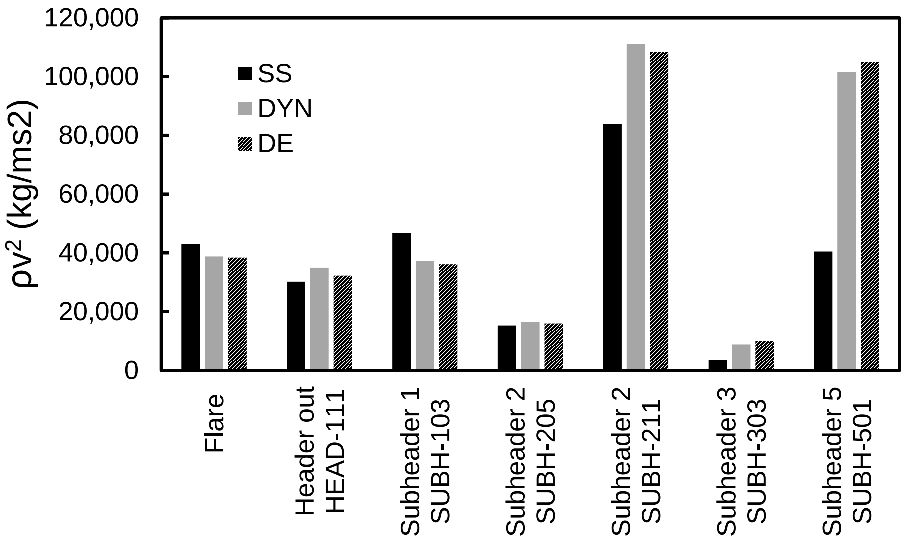

Figure 10: Comparison between calculated peak ρv^2 Facility B for steady-state, dynamic simulations without dead ends, and dynamic simulations including dead ends.

system volumes. On the other hand, using a less complex model is conservative. Apparently, the larger facility B shows less reduction in flare rate by including dead ends as facility A. Although, not conclusive, this might suggest that a more accurate and detailed model is more important for a smaller facility.

In order to also assess the consequence of a dynamic simulation analysis of a flare system, on ρv^2, one of the key design parameters, this is compared between the steady-state model and the dynamic models without and with dead ends. Comparison is made between the peak values during dynamic simulations and corresponding steady-state values for the main sub-headers, headers and main line to the flare tip in Figure 10.

As seen from Figure 10, the calculated peak ρv^2 using the dynamic simulations is higher than the corresponding steady-state value for some of the investigated sub-headers and headers e.g. *Subheader 5* and *Subheader 2 out*. This phenomenon may be rationalized in terms of a lower peak backpressure as illustrated in Figure 8 for the dynamic simulations. A lower pressure results in lower density and hence larger actual value flows, which translates to higher velocity. Although a lower density counterbalances a higher velocity, the velocity dominates since it is a squared term. Jo et al. (2020) also observed that in some flare lines, the Mach numbers calculated in a dynamic simulation exceeded those from a steady-state simulation. In some locations the ρv^2 for the dynamic model is lower that the steady-state model as shown for the flare.

This is an important takeaway when analyzing dynamic flare models, and while lower mass flow rates and lower backpressure are important for identifying spare capacity in the flare system, it is important also to analyze other key design factors such as ρv^2 and Mach number.

3.3. Facility C

For facility C, the mass flow reaching the flare tip is compared for the steady-state and dynamic simulations. This is shown in Figure 11. The details available for facility C has not allowed an analysis of the effect of dead-ends.

As seen from Figure 11, the peak mass flow in the dynamic simulations is at a lower value than the steady-state value as also shown for facility A and B. The dynamic simulations results in a peak flare rate of 511,989 kg/h at the flare tip compared to a steady-state value of 676,473 kg/h. The reduction in peak flare rate is 164,484 kg/h for the dynamic model which corresponds to a reduction of 24.3%. Compared to both facility A and B, the reduction in flare rate for facility C is higher in both absolute numbers and in relative numbers. In absolute numbers, the order of reduction in peak flare rate is the following A $<$ B $<$ C.

3.4. Synthesis

The results from the analysis of all three facilities are summarized in Table 6. The main results are the steady-state design rate and the corresponding peak flare rate at the flare tip as found from a dynamic simulation of the emergency depressurization process. More specifically the difference between the steady-state and dynamic analysis, also termed the *hidden potential* for debottlenecking is included. Further, included are also details about the flare system in terms of hold-up volumes, flare network length and average flare piping diameter.

It is seen from Table 6, that generally the total system volume of the flare system including both piping and the flare KO drum scales with the steady-state design rate, which is partly due the average piping diameter being larger and partly due to longer piping in the flare system. This can be rationalized by the fact that a larger design rate typically comes from a

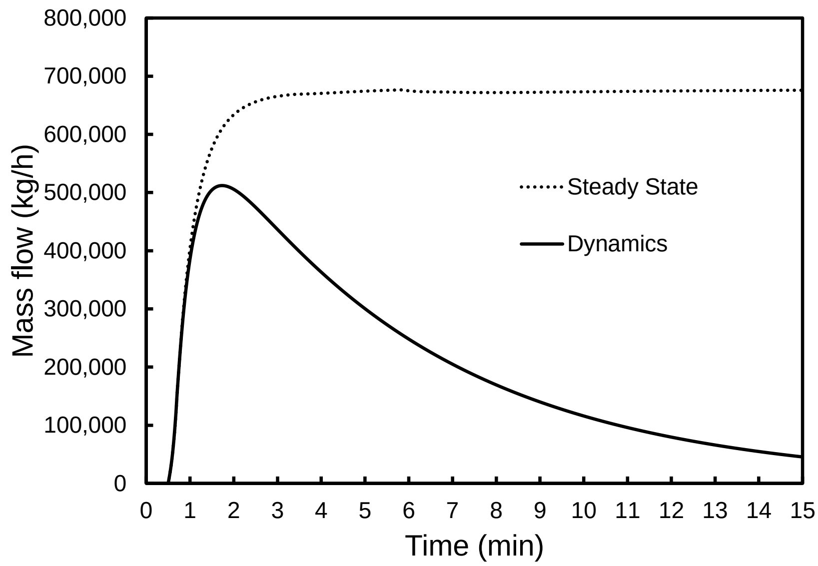

(A)

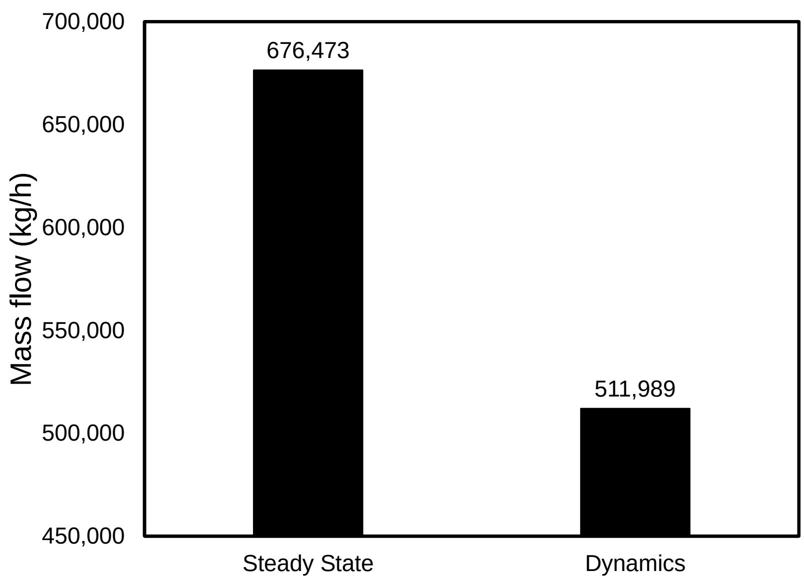

(B)

Figure 11: Comparison between calculated flare-tip mass flow for facility C for steady-state and dynamic simulations without dead ends.

Facility	Dead end	L_{net} (m)	V_{pipe} (m^3)	V_{KO} (m^3)	V_{tot} (m^3)	D_{mean} (inch)	Peak flare rate SS (MMSCFD)	Peak flare rate Dyn. (MMSCFD)	Hidden potential (MMSCFD)	Hidden potential (%)
A	no	288	19.2	79.4	98.6	10.5	72.8	63.2	9.5	13.0
	yes	497	27.0	79.4	106.4	9.3	72.8	61.1	11.7	16.1
B	no	1,457	126	50.5	176.6	11.7	303.1	262.2	40.9	13.5
	yes	2,034	150	50.5	200.5	10.7	303.1	259.5	43.5	14.4
C	no	2,686	359.6	103.3	462.9	15.3	733.2	555.0	178.2	24.3

Table 6: Summary of model details and modeling results for all three investigated facilities. Results included for models without and with dead ends included. L_{net}: Total length of piping included in the flare network model, V_{pipe}: Hold-up volume of modeled piping, V_{KO}: Hold-up volume of flare Knock-out drum, V_{tot}: Total hold-up volume of flare system, D_{mean}: Average diameter of flare network piping, found from a weighted average with individual piping diameters weighted by their corresponding pipe length.

higher number of blowdown segments, which in turn also comes from a larger facility and hence longer piping.

It is also seen that a larger design rate also results in a higher potential for debottlenecking, especially considering the absolute value of the hidden potential. In relative terms, facility A and B are quite similar, with facility C displaying a higher relative reduction in flare rate from dynamic analysis.

The difference between the steady-state design rate and the peak rate found from dynamic simulations of the emergency depressurization for all investigated facilities is depicted as a function of the steady-state design rate in Figure 12.

In Figure 12, a second-order polynomial regression with a forced intercept at zero is also included which seems to fit the data from the present study quite well. The quadratic dependence of the hidden potential on the steady-state design rate is required to explain the progressively increasing relative reduction in flare tip rate with increasing system design rate. Data on the flare rate reduction potential from Andreasen (2014) and Wasnik et al. (2018) is included for benchmarking of the proposed relationship (not included in the regression analysis). While the data material is relatively sparse, the included results seem to fit the picture of a near-quadratic relationship. The quadratic relationship is to a large extent driven by the results from facility C, and in future investigations more data on large scale facilities shall be analyzed to confirm this relationship.

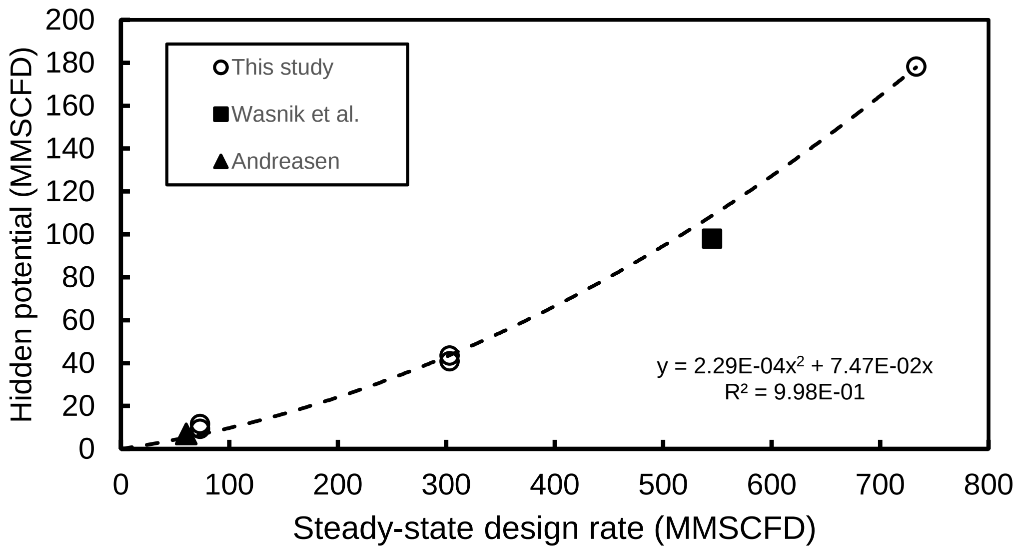

Figure 12: The hidden potential for debottlenecking i.e. difference between the steady-state design flare rate and the peak dynamic simulation rate at the flare tip as a function of steady-state design rate. Comparison with other reported flare rate reductions from dynamic analysis is included for Andreasen (2014) and Wasnik et al. (2018).

4. Conclusion

In this paper, the possible hidden debottlenecking potential in existing flare systems is analyzed employing dynamic process simulations of an emergency depressurization event. Three different offshore facilities are analyzed, and a comparison is made between steady-state and dynamic simulations. It is generally found that the system backpressure and maximum mass flow rate at the flare tip is significantly reduced compared to the steady-state value. This is due to line-packing effects in the flare system hold-up volume and the fact that the mass flow decreases rapidly as the blowdown segments are depressurized.

By comparing different model complexities, it is also shown that a higher debottlenecking potential can be revealed, if dead ends from non-flow sources are included, since this increases the available hold-up volume. However, the effect is not the dominating one, and can be ignored for more conservative results, especially when fast screening studies are required.

While both mass rates and back pressure decrease, it is observed that in some locations in the flare system the ρv^2 may actually increase in a dynamic simulation. This can be explained by lower backpressure and hence higher peak velocity due to a lower gas density.

By compiling and analyzing the results for all three facilities, apparently it is found that the larger the facility, the larger the debottlenecking potential. A quadratic relationship between the flare system design rate and the corresponding debottlenecking potential fits the data well.

Abbreviations and symbols

$\mathrm{D_{mean}}$	Average diameter of flare network piping
$\mathrm{L_{net}}$	Total length of piping included in the flare network model
$\mathrm{V_{KO}}$	Hold-up volume of flare Knock-out drum
$\mathrm{V_{pipe}}$	Hold-up volume of modeled piping
$\mathrm{V_{tot}}$	Total hold-up volume of flare system
C_p	Specific heat capacity at constant pressure
C_v	Specific heat capacity at constant volume
API	American Petroleum Institute
BDV	Blowdown Valve
$\mathrm{C_V}$	Valve flow coefficient
CPF	Central Processing Facility
DE	Dead end
Dyn.	Dynamic (simulation)
EDP	Emergency Depressurization
FSA	Flare System Analyzer
HP	High-Pressure
ID	Internal diameter

KO Knock-out

LP Low-Pressure

MW Molecular Weight

NORSOK NORsk SOkkels Konkurranseposisjon

PCV Pressure Control Valve/Spill-over valve

PSV Pressure Safety Valve

SS Steady-state

T/T Tan-to-tan

References

Andreasen, A., 2014. Process design – can we change mindset?, in: Offshore Oil and Gas seminar, 18-22 August 2014, Department of Energy Technology, Aalborg University Esbjerg. doi:10.13140/RG.2.2.13310.33606. oral presentation.

Andreasen, A., Borroni, F., Zan Nieto, M., Stegelmann, C., P. Nielsen, R., 2018. On the Adequacy of API 521 Relief-Valve Sizing Method for Gas-Filled Pressure Vessels Exposed to Fire. Safety 4, 11. doi:10.3390/safety4010011.

Andreasen, A., Eriksen, J.G.I., Stegelmann, C., Lynggaard, H., 2015. Method improves high-pressure settle-out calculations. Oil & Gas Journal 113, 88–96.

API, 2014. Pressure-relieving and Depressuring Systems, API Standard 521. Technical Report API Standard 521, Sixth Edition, January. American Petroleum Institute.

Biswas, S., Fischer, B.J., 2017. Application and validation of the api analytical fire method in pressure-relieving and depressuring systems. Journal of Loss Prevention in the Process Industries 50, 154 – 164. doi:10.1016/j.jlp.2017.09.008.

Bjerre, M., Eriksen, J.G.I., Andreasen, A., Stegelmann, C., Mandø, M., 2017. Analysis of pressure safety valves for fire protection on offshore oil and gas installations. Process Safety and Environmental Protection 105, 60–68. doi:10.1016/j.psep.2016.10.008.

Borden, G. (Ed.), 1998. Control Valves – Practical Guides for Measurement and Control. Instrument Society of America.

Chakrabarty, A., Mannan, S., Cagin, T., 2016. Multiscale Modeling for Process Safety Applications. Butterworth-Heinemann, Boston. doi:10.1016/B978-0-12-396975-0.05001-4.

Chen, F.F.K., Jentz, R.A., Williams, D.G., 1992. Flare System Design: A Case for Dynamic Simulation, in: Offshore Technology Conference, pp. 421–430. doi:10.4043/6919-MS.

Firth, B., 2016. Unpicking Oversimplification: Relief and Flare Studies for Complex Plant using Dynamic Process Modelling, in: Hazards 26, Institution of Chemical Engineers Symposium Series, pp. 1–12.

Hankinson, R.W., Thomson, G.H., 1979. A new correlation for saturated densities of liquids and their mixtures. AIChE Journal 25, 653–663. doi:10.1002/aic.690250412.

Haque, A., Richardson, S., Saville, G., Chamberlain, G., 1990. Rapid depressurization of pressure vessels. Journal of Loss Prevention in the Process Industries 3, 4 – 7. doi:10.1016/0950-4230(90)85015-2.

Haque, M.A., Richardson, M., Saville, G., 1992. Blowdown of pressure vessels. Pt. I: Computer model. Trans. IChemE B 70, 3–9.

ISA, 1995. Flow Equations for Sizing Control Valves, ANSI/ISA S75.01 Standard, ISA-S75.01-1985 (R 1995). Instrument Society of America.

ISO, 2006. Petroleum, petrochemical and natural gas industries — Pressure-relieving and depressuring systems . Technical Report ISO 23251:2006(E). International Organization for Standardization.

Jo, Y.P., Cho, Y., Hwang, S., 2020. Dynamic analysis and optimization of flare network system for topside process of offshore plant. Process Safety and Environmental Protection 134, 260 – 269. doi:10.1016/j.psep.2019.12.008.

Leporini, M., D'Alessandro, V., Mancini, E., Terenzi, A., Marchetti, B., Giacchetta, G., Grifoni, R.C., 2018. A new integrated approach to study the thermal and mechanical response of vessels subject to a safe blowdown process. Journal of Loss Prevention in the Process Industries 53, 103 – 114. doi:10.1016/j.jlp.2017.06.003. risk Analysis in Process Industries: State-of-the-art and the Future.

NORSOK, 2014. Process System Design, NORSOK Standard, P-002, Edition 1, August 2014. Technical Report. NORSOK. URL: `www.standard.no/petroleum`.

Nougués, J., Gruber, D., Leipnitz, D.U., Sethuraman, P., Alos, M., Brodkorb, M., 2010. Are there alternatives to an expensive overhaul of a bottlenecked flare system? Petroluem Technology Quarterly Q1, 94.

Peng, D.Y., Robinson, D.B., 1976. A new two-constant equation of state. Industrial & Engineering Chemistry Fundamentals 15, 59–64. doi:10.1021/i160057a011.

Richardson, S.M., Saville, G., 1992. Blowdown of vessels and pipelines, in: Institution of Chemical Engineers Symposium Series, pp. 195–209.

Shell, 2010. Design of pressure relief, flare and vent systems, Shell DEP 80.45.10.10. Shell.

Singh, A., Li, K., Lou, H.H., Hopper, J., Golwala, H., Ghumare, S., Kelly, T., 2007. Flare minimisation via dynamic simulation. International Journal of Environment and Pollution 29, 19–29. doi:10.1504/IJEP.2007.012794.

Total, 2012. GENERAL SPECIFICATION, PROCESS GS EP EP 103, Process Sizing Criteria, rev. 7. TOTAL.

Wasnik, R., Singh, H., Kamal, F.R., Takieddine, O.H., 2018. Debottlenecking of existing flare system for facility up-gradation using dynamic simulation approach - case study, in: Abu Dhabi International Petroleum Exhibition & Conference, 12-15 November, Abu Dhabi, UAE, Society of Petroleum Engineers. pp. 1–12. doi:10.2118/192750-MS. paper SPE-192750-MS.

Appendix B

Aspen HYSYS Simulation Models

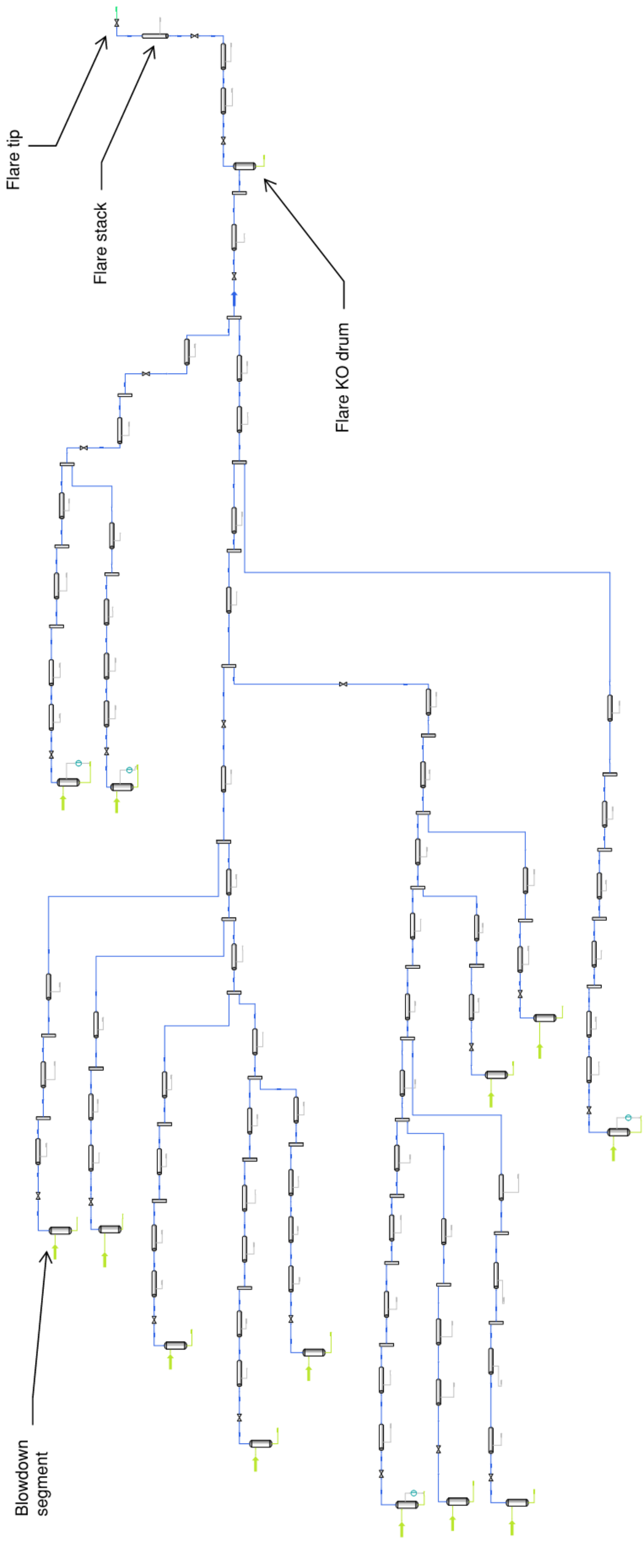

Figure B.1: Process simulation flowsheet for the flare system of Facility A as modelled in Aspen HYSYS (dead-ends not included).

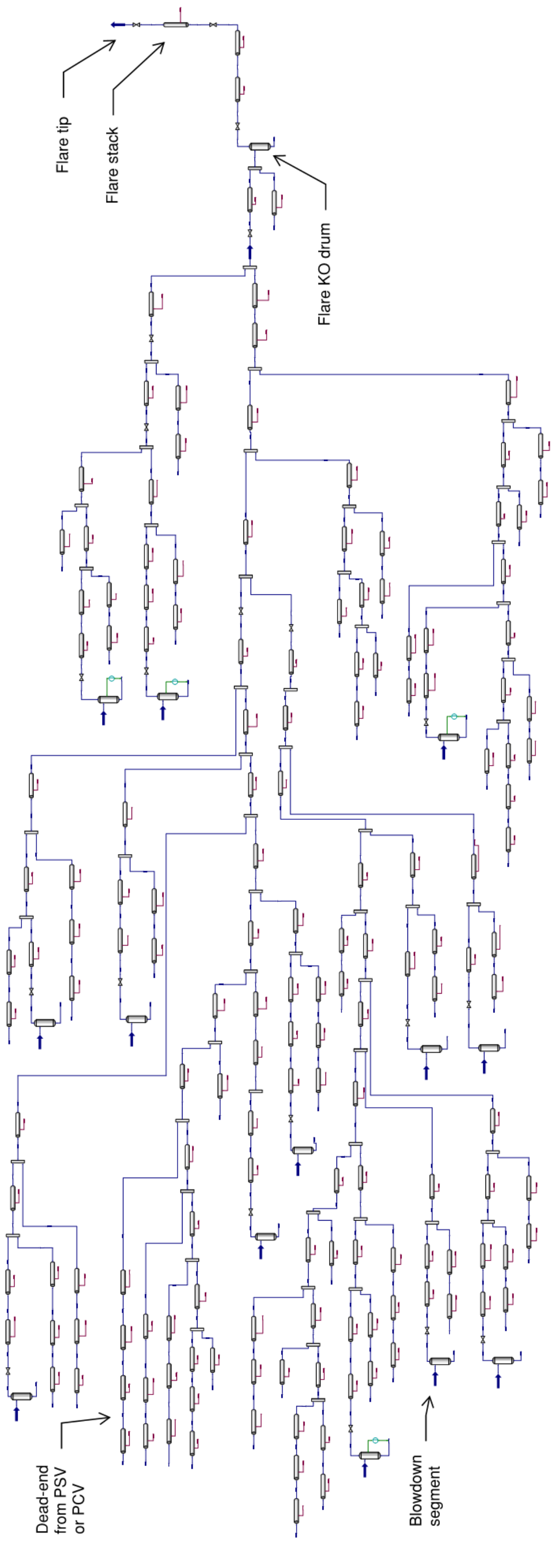

Figure B.2: Process simulation flowsheet for the flare system of Facility A as modelled in Aspen HYSYS (dead-ends included).

Figure B.3: Process simulation flowsheet for the flare system of Facility B as modelled in Aspen HYSYS (dead-ends not included).

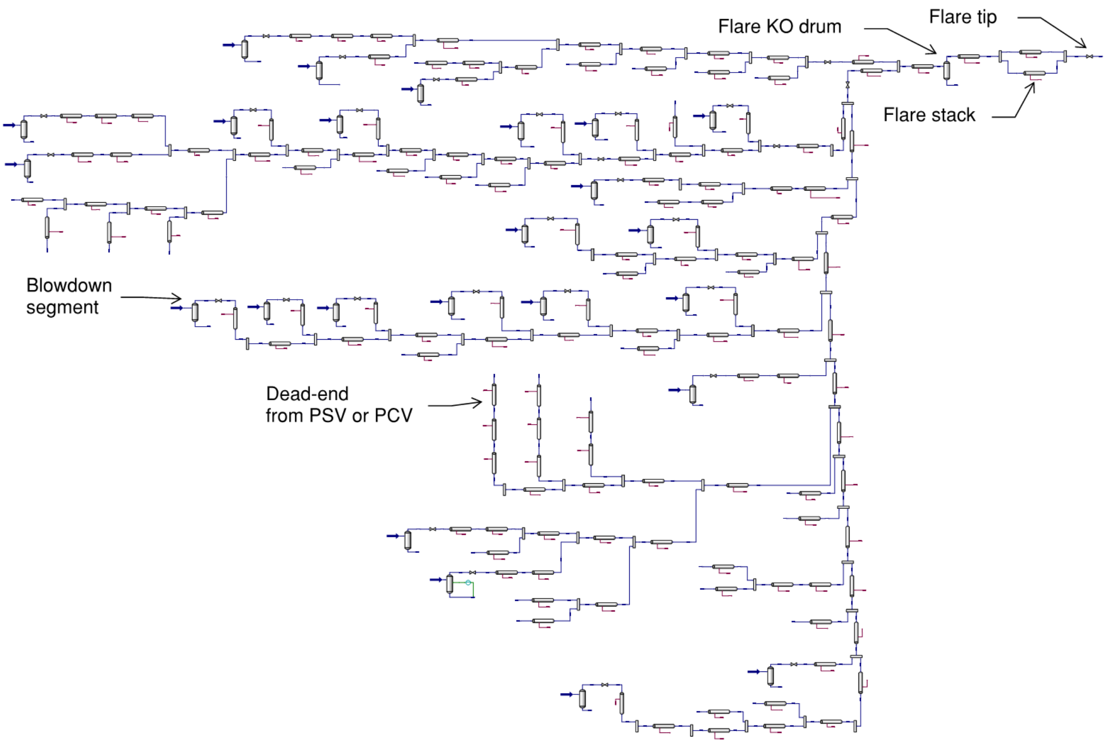

Figure B.4: Process simulation flowsheet for the flare system of Facility B as modelled in Aspen HYSYS (dead-ends included).

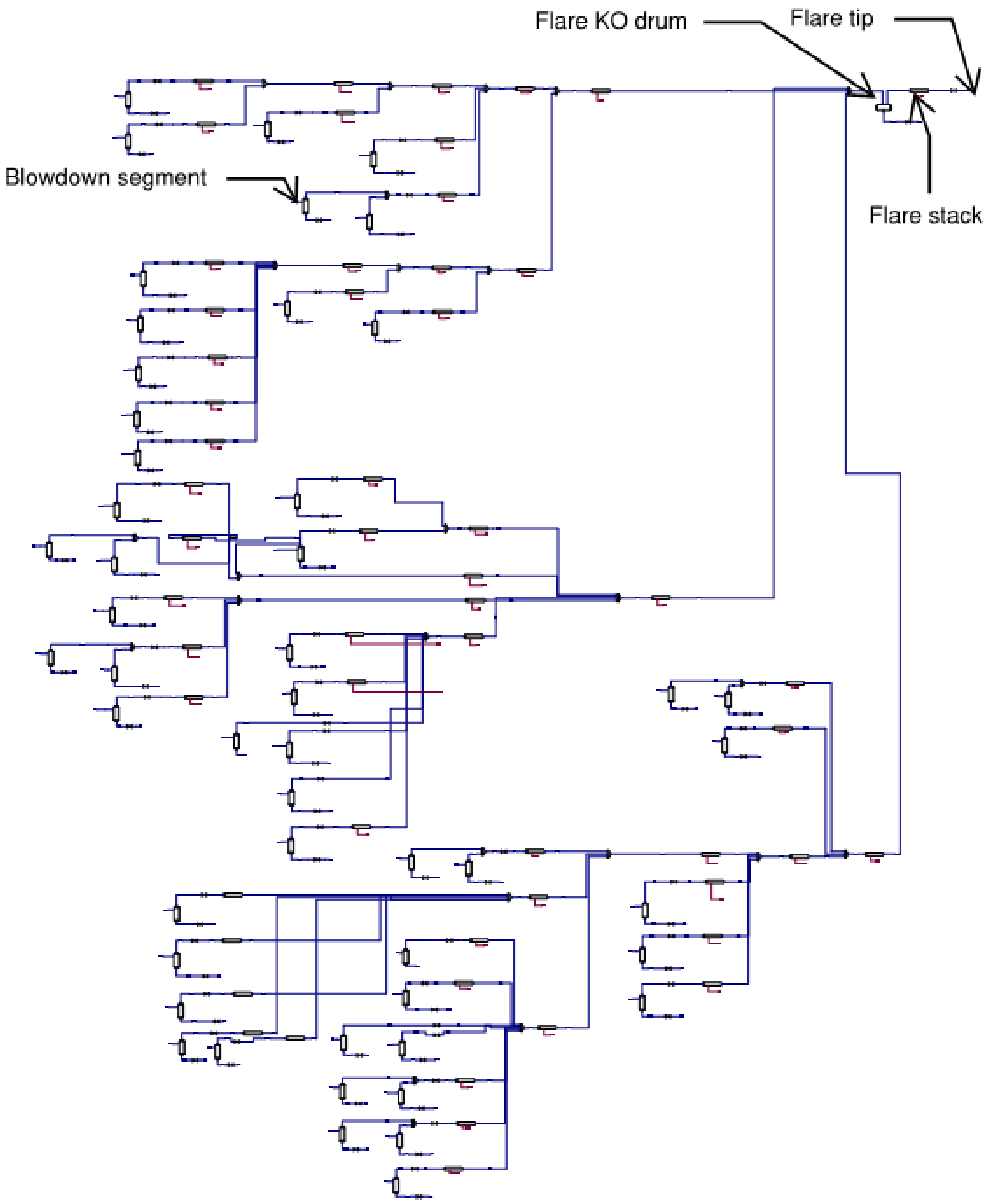

Figure B.5: Process simulation flowsheet for the flare system of Facility C as modelled in Aspen HYSYS (dead-ends not included).

Appendix C

Additional graphs to support HIPPS results

C.1 150,000 kg/h

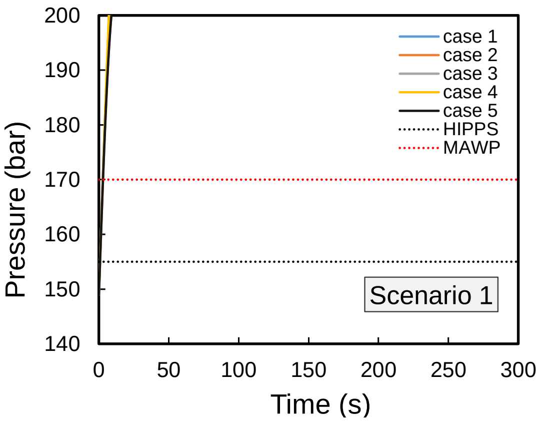

(A)

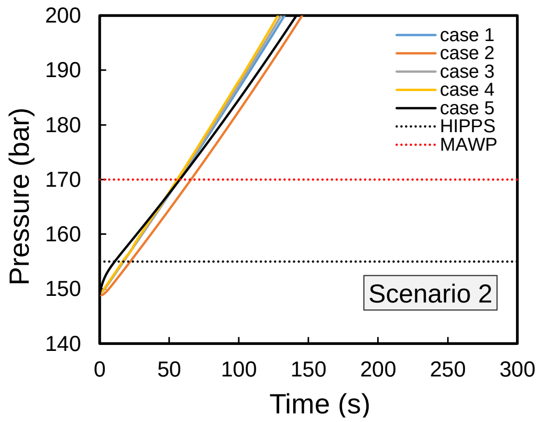

(B)

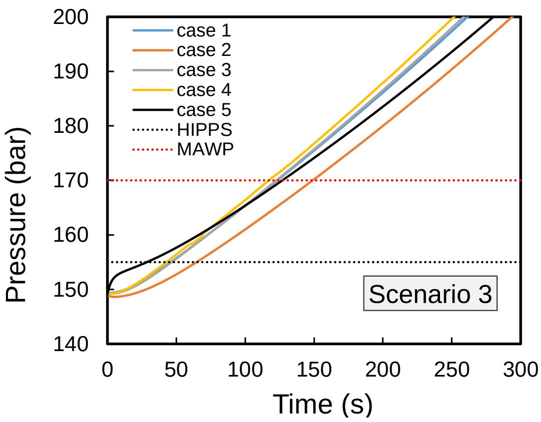

(C)

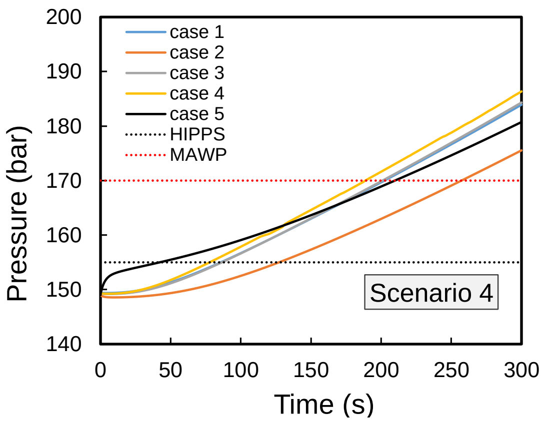

(D)

Figure C.1: Comparison of pressure development in the manifold considering well feed of 150,000 kg/h for (A) Scenario 1, (B) Scenario 2, (C) Scenario 3 and (D) Scenario 4.

C.2 180,000 kg/h

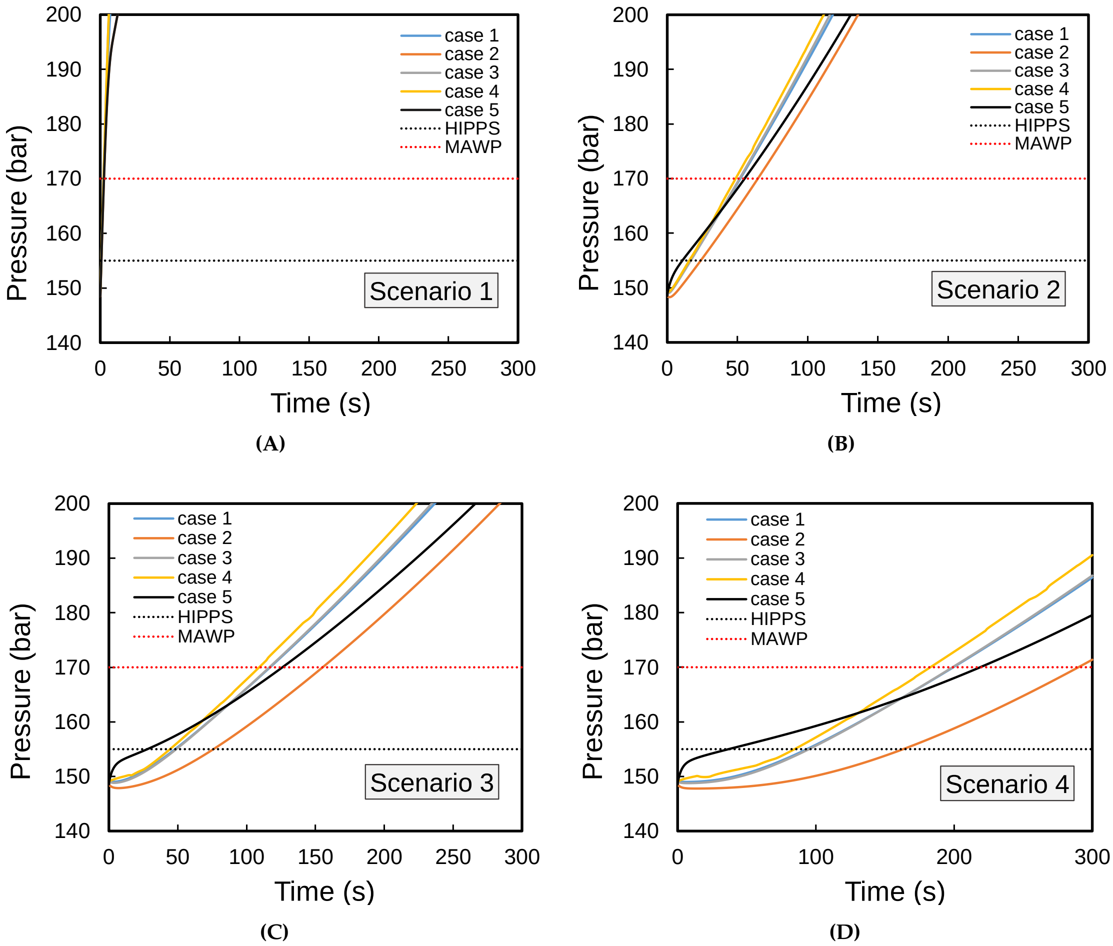

Figure C.2: Comparison of pressure development in the manifold considering well feed of 180,000 kg/h for (A) Scenario 1, (B) Scenario 2, (C) Scenario 3 and (D) Scenario 4.

C.3 PST calculated for different mass flows

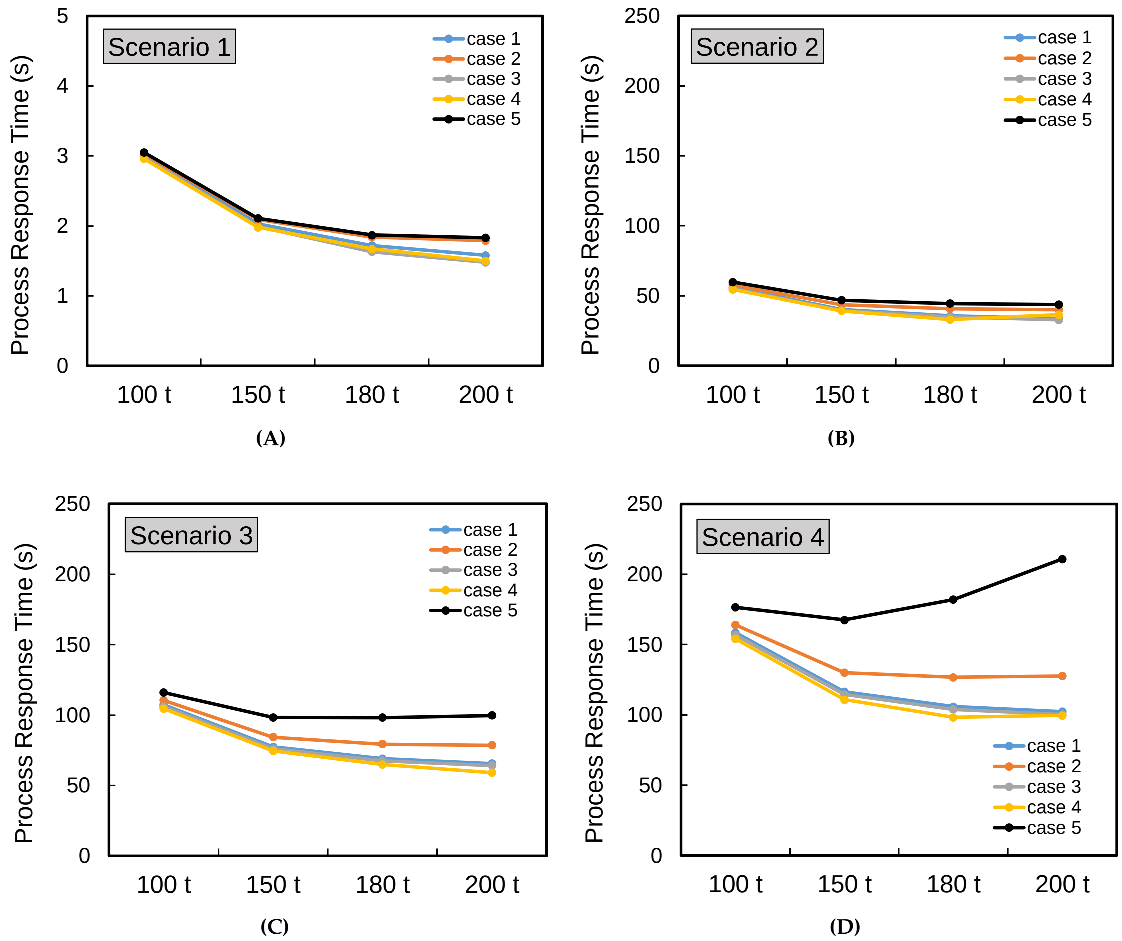

Figure C.3: Comparison of PST for (A) Scenario 1, (B) Scenario 2, (C) Scenario 3 and (D) Scenario 4.